THE PERFORMANCE OF HOLLOW FIBER GAS SEPARATION MEMBRANES IN THE PRESENCE OF AN AGGRESSIVE FEED STREAM

A Dissertation
Presented to
The Academic Faculty

By

William Clark Madden

In Partial Fulfillment
Of the Requirements for the Degree
Doctor of Philosophy in
Chemical Engineering

Georgia Institute of Technology
December, 2005

THE PERFORMANCE OF HOLLOW FIBER GAS SEPARATION MEMBRANES IN THE PRESENCE OF AN AGGRESSIVE FEED STREAM

Approved by:

Dr. William J. Koros, Advisor
School of Chemical & Biomolecular Engineering
Georgia Institute of Technology

Dr. Peter J. Ludovice
School of Chemical & Biomolecular Engineering
Georgia Institute of Technology

Dr. Charles A. Eckert
School of Chemical & Biomolecular Engineering
Georgia Institute of Technology

Dr. Satish Kumar
School of Polymer, Textile, & Fiber Engineering
Georgia Institute of Technology

Dr. Clifford L. Henderson
School of Chemical & Biomolecular Engineering
Georgia Institute of Technology

Date Approved: November 14, 2005

ACKNOWLEDGEMENTS

I would first like to acknowledge my advisor, Professor Bill Koros, for his support through out my graduate school experience. He is an exceptional mentor, a tireless investigator, and an outstanding person. He is, in short, everything one could ever ask for in a graduate research advisor, and I am honored to be his student.

I would like to acknowledge all of the members of the Koros research group for being friends as well as coworkers. The older students, Ted Moore, David Wallace, and Shilpa Damle-Mogri, helped to get me started in the right direction. The members of my class, Alexis Hillock, Shabbir Husain, Hensley Sejour, and Jason Williams, were always available for support, advice, or a beer. Finally, the younger members of the group, specifically, Preeti Chandra, Raymond Chafin, and John Perry have all been great friends.

Finally, I would like to acknowledge my parents who are simply amazing people. I know it is a cliché, but without them I would not be the person that I am today.

TABLE OF CONTENTS

LIST OF TABLES

LIST OF FIGURES

SUMMARY

Industrial utilization of polymeric gas separation membranes is predicted to increase significantly over the next 20 years. This growth will be driven by application of membrane based separations to increasingly aggressive feed streams. In this work, the performance of defect-free Matrimid® asymmetric hollow fiber membranes in the presence of high pressure carbon dioxide and trace levels of toluene and n-heptane in the feed stream are studied.

Specifically, this work shows a significant decrease in the carbon dioxide plasticization pressure and the carbon dioxide permeance prior to plasticization as a result of accelerated physical aging at ambient temperature. Interestingly, sub-T_g thermal annealing at 220 ^oC reverses the effects of physical aging by increasing the plasticization pressure and the carbon dioxide permeance prior to plasticization for a typical polyimide commonly used in membranes. The counterintuitive effects of thermal annealing are believed to be the result of charge transfer complex formation. This work highlights the difference between physical aging at ambient temperature where charge transfer complexes are not formed and above ambient thermal annealing where charge transfer complexes are free to form.

The performance of Matrimid® asymmetric hollow fiber membranes in feed streams contaminated with up to 1200 ppm toluene and 2000 ppm n-heptane is investigated. In the presence of both feed stream contaminants, the productivity and efficiency of the membrane are observed to significantly decrease in this work. However, exposure to toluene contamination affects the performance of the

membrane much more than exposure to n-heptane contamination. These decreases in performance are shown to be the result of antiplasticization, and a free volume based model is developed to correlate the effect of feed stream contamination on membrane performance.

CHAPTER 1

INTRODUCTION

1.1 Background

Membrane based separations of gaseous feed streams have been performed industrially for the past 25 years [1]. Despite this lengthy history, industrial utilization of membranes for gas separations is expected to grow dramatically in the future. Baker published an analysis of the membrane market which predicts the overall gas separation membrane market to grow from a $150 million/year business in 2000 to a 760 million/year business in 2020 [2]. This growth is driven by the introduction of membranes to separate condensable feed streams such as paraffin/olefin separations [2, 3]. To this point in time, membranes have traditionally been used to separate non-condensable feed streams (e.g. oxygen/nitrogen). A breakdown of the percentage of each particular membrane separation to the total membrane market as of 2000 and as predicted in 2020 is given in Figures 1.1 and 1.2.

The desire to separate condensable feed streams using membranes presents a large challenge for current generation membrane materials. These current generation materials often experience substantial performance reductions when contacted with highly-interacting, condensable feed stream components, even at relatively low concentrations. For this reason, in most current applications the feed stream is pre-treated using a number of secondary separations to minimize the amount of condensable components that actually contact the membrane. In order to use

membranes for separation of condensable streams in the future, next generation membranes must be much less susceptible to this form of performance degradation.

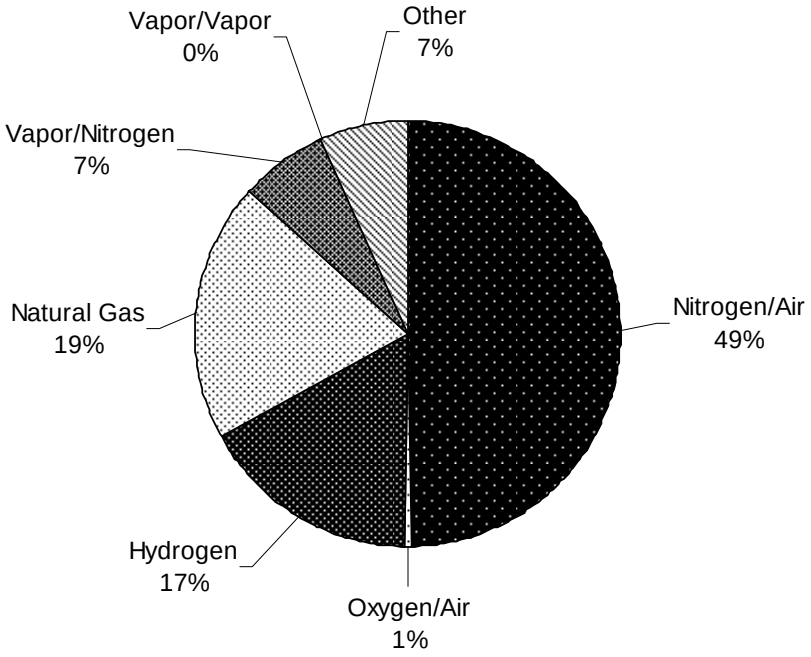

Figure 1.1: Distribution of membrane market in 2000 [2]

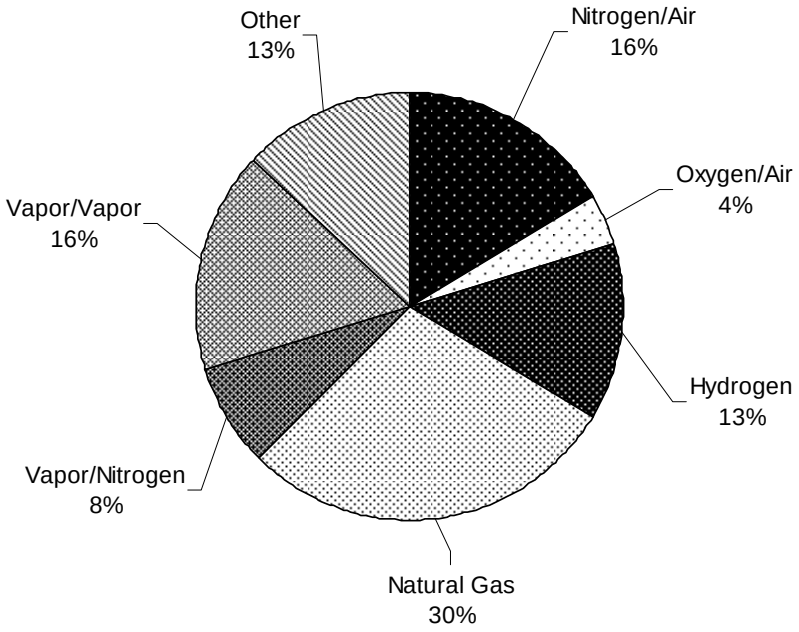

Figure 1.2: Predicted distribution of membrane market in 2020 [2]

A complete understanding of the mechanism of membrane performance degradation of current generation materials in the presence of aggressive feed streams is not available. With this fact in mind, an investigation was conducted to understand the effects of aggressive feed stream conditions on the performance of hollow fiber gas separation membranes used for natural gas sweetening, the removal of carbon dioxide from methane. Natural gas sweetening is an emerging area for membrane application, where industrial adoption has been hindered by poor membrane performance in the often aggressive feed streams that are encountered. These aggressive feed streams often contain high partial-pressures of carbon dioxide and highly sorbing trace contaminants, both of which are conditions where membranes have historically performed poorly.

Unprocessed natural gas typically contains 75-90% methane. The remainder of the gas is composed of carbon dioxide, hydrogen sulfide, nitrogen, water, and various higher hydrocarbons. The precise composition of the feed stream varies from well to well, and the composition of natural gas can vary dramatically across different geographic regions [4]. In the continental United States alone there are proven reserves of 60,698 billion cubic-feet of sub-quality natural gas [5]. This so-called "sub-quality" natural gas has a particularly high concentration of carbon dioxide or some other contaminant, which makes production uneconomical with current technology. Next generation membranes that perform better in aggressive streams have the potential to shift the economics of producing sub-quality natural gas thereby harnessing a new source of domestic energy.

Regardless of the unprocessed natural gas composition, the natural gas must be processed to meet the sales specification, given in Table 1.1, for use in the United States. The sales specification calls for the removal of carbon dioxide to less than 2% is required to limit corrosion of carbon steel pipe and increase the heating value of the natural gas. Traditionally, this separation is performed using amine absorption. Membranes offer many potential advantages over amine absorption including reduced footprint, modular design, increased reliability, environmental advantages, and decreased capital investment [6]. Despite these advantages, membranes have not been fully adopted commercially for natural gas sweetening primarily because of their degraded performance in aggressive feed streams. From industrial experience, with proper pre-treatment current generation membrane materials perform

adequately; however, the amount of academic literature available for quantifying membrane performance under these conditions is sparse.

Table 1.1: Sales specification of natural gas [7]

Component	Specification
Carbon dioxide	<2%
Water	<120 ppm
Hydrogen sulfide	<4 ppm
C_{3+} content	950-1050 Btu/scf -20°C dew point
Inert gases (N_2, CO_2, He, etc.)	<4%

The primary objectives of this dissertation are as follows:

- To investigate the performance of membranes in the presence of carbon dioxide. Specifically, to study the effect of physical aging on transport plasticization.
- To quantify the performance degradation of membranes operating with feed streams containing trace concentrations of highly sorbing contaminants.
- To develop a model to correlate and provide fundamental insight of the impact on gas transport when membranes are exposed to highly sorbing contaminants.

This work is conducted on asymmetric hollow fiber membranes formed from Matrimid®. These membranes represent the current state-of-the-art in commercially available membrane material and morphology.

1.2 Organization of Dissertation

This dissertation is divided into eight chapters including this introduction:

Chapter 2 provides a general theoretical framework for interpretation of the data presented in subsequent chapters.

Chapter 3 provides information on the materials used, membrane formation process, and experimental procedures.

Chapter 4 discusses age dependent membrane performance in the presence of carbon dioxide.

Chapter 5 contains experimental data for sorption of methane, carbon dioxide, toluene, and n-heptane in Matrimid®.

Chapter 6 contains experimental data for the productivity and efficiency of the carbon dioxide/methane separation in varying levels of feed stream contamination by n-heptane and toluene.

Chapter 7 develops a model to interpret the experimental data presented in Chapter 6.

Chapter 8 presents the conclusions of this dissertation and recommendations for future research.

1.3 References

1. Koros, W.J. and G.K. Fleming, "Membrane-based gas separation," *Journal of Membrane Science*, **83**(1), 1 (1993).

2. Baker, R.W., "Future Directions of Membrane Gas Separation Technology," *Industrial & Engineering Chemistry Research*, **41**(6), 1393 (2002).

3. Burns, R.L. and W.J. Koros, "Defining the challenges for C3H6/C3H8 separation using polymeric membranes," *Journal of Membrane Science*, **211**(2), 299 (2003).

4. Meyer, H.S., D. Leppin, and J.L. Savidge, "Gas Research Institute's Gas Processing Research and Development Program," *Proceedings of the 68th GPA Annual Convention*, **69**, 149 (1990).

5. Meyer, H.S., "Volume and distribution of subquality natural gas in the United States," *GasTips*, **6**(1), 10 (2000).

6. Bhide, B.D., A. Voskericyan, and S.A. Stern, "Hybrid processes for the removal of acid gases from natural gas," *Journal of Membrane Science*, **140**(1), 27 (1998).

7. Lee, A.L., et al., "Field tests of membrane modules for the separation of carbon dioxide from low-quality natural gas," *Gas Separation & Purification*, **9**(1), 35 (1995).

CHAPTER 2

THEORY

This chapter provides a general overview of background material relevant to the research presented in subsequent chapters. An overview of the classical theories of gas and vapor sorption and permeation in glassy polymers will be given. Furthermore, glassy polymers are non-equilibrium materials whose transport properties are history-dependent. The effects of physical aging, plasticization, antiplasticization, and conditioning will be discussed.

2.1 Gas Transport

In this section, the basic solution-diffusion mechanism of gas transport through nonporous polymers will be discussed. The transient sorption model of Berens-Hopfenberg and the dual mode model of equilibrium sorption will be described to account for gas sorption into glassy polymers. Furthermore, the dual mode transport model and free-volume based models will be described to account for gas transport through glassy polymers.

2.1.1 Solution-Diffusion

Small molecule transport through nonporous polymers proceeds by the solution-diffusion mechanism [1]. This a three step mechanism where penetrant molecules: 1. sorb into the polymer phase from a high activity external gas or liquid phase, 2. diffuse across the polymer driven by a chemical potential gradient, and 3.

desorb from the polymer phase to a low activity gas or liquid external phase. While these three general steps of the solution diffusion mechanism are agreed upon, the specifics of sorption into and out of the polymer phase and diffusion across it are still active areas of research.

Regardless of how one conceptualizes the sorption and diffusion processes, the solution-diffusion mechanism states that the flux through the polymer is proportional to a chemical potential gradient. If a chemical potential gradient does not exist, in the absence of an imposed bulk flow, no net transport of penetrant occurs through the polymer. This proportionality is stated mathematically as:

$$J_A = -\kappa \frac{d\mu_A}{dx} \ , \tag{2.1}$$

where J_A is the flux of penetrant 'A' through the polymer, μ_A is the penetrant chemical potential of penetrant 'A' in the polymer phase, and κ is a proportionality factor.

In the absence of electromotive forces, the chemical potential of a dissolved penetrant in the polymer phase can be written as [2]:

$$\mu_A = \mu_A^0 + RT \ln(\gamma_A c_A) + V_A(p_A - p_A^0), \tag{2.2}$$

where μ_A^0 is the chemical potential of the pure penetrant at the reference pressure, p_A^0. γ_A is the activity coefficient at concentration, c_A, and the partial molar volume of the penetrant is V_A. The reference pressure is usually set as the pure component vapor pressure. With the knowledge that a chemical potential gradient must exist through the polymer, from inspection of Equation 2.2 one can imagine three possible ways to

effect such a gradient: 1. a concentration gradient across the polymer, 2. a pressure gradient across the polymer, or 3. the coexistence of both pressure and concentration gradients across the polymer. In an elegant series of papers [3-5], Paul and coworkers showed that a concentration gradient solely affects the gradient in chemical potential. The fact that no pressure gradient exists through the membrane interior can be proved using a simple mechanical argument. In the common laboratory setup for gas separations, the membrane is supported on the low pressure side by a porous metal support. If a pressure is exerted on the upstream side of the membrane by the gas, the metal support must exert an equal and opposite pressure on the downstream side of the membrane. For this reason, the pressure inside the membrane is equal to the upstream pressure [5]. By using a constant pressure through the membrane, Paul was able to rationalize the observed dependence of flux on the external pressure difference for both hydraulic permeation and pervaporation systems [3]. Furthermore, Paul conducted a series of experiments using a composite membrane consisting of a stack of 3 to 4 rubber membranes to measure the concentration gradient through the membrane. It was shown that the concentration gradient determined from these measurements alone accounted for the entire chemical potential gradient [4]. This result excluded the possibility of a pressure gradient inside the membrane for solution-diffusion transport processes.

Since only a concentration gradient exists in the membrane, it is a simple exercise to derive Fick's Law based on a chemical potential driving force,

$$J_A = -\kappa \frac{d\mu_A}{dx} = -\kappa \frac{d\mu_A}{dc_A} \frac{dc_A}{dx} \quad . \tag{2.3}$$

With the knowledge that a pressure gradient does not exist through the membrane, the derivative of chemical potential with respect to penetrant concentration is calculated from Equations 2.2 and 2.3 yielding Fick's law [6]:

$$J_A = \left(\frac{-\kappa RT}{c_A}\right)\left(1+\frac{d\ln\gamma_A}{d\ln c_A}\right)\frac{dc_A}{dx} = -D_A\frac{dc_A}{dx} \tag{2.4}$$

2.1.2 Membrane Permeability and Selectivity

In membrane applications the flux is usually reported in the form of permeability, the flux normalized by the external transmembrane partial pressure difference, Δp_A, and the membrane thickness, L, as given in Equation 2.5 [7].

$$P_A = \frac{J_A}{\Delta p_A / L} \tag{2.5}$$

The units of permeability are commonly reported in Barrers, where 1Ba = 10^{-10} (cm^3[STP]*cm)/(cm^2*sec*cmHg). More recently, permeability has been reported in the SI units of moles/(m*sec*Pa). In asymmetric membranes, where the active membrane thickness is not precisely known, the flux is often reported in terms of permeance as given by Equation 2.6.

$$P_A \big/ L = \frac{J_A}{\Delta p_A} \tag{2.6}$$

The units of permeance are the GPU, where 1 GPU = 10^{-6} cm^3[STP]/(cm^2*sec*cmHg).

A value commonly used to characterize the efficiency of the membrane separation is the ideal selectivity, $\alpha^*_{A/B}$. The ideal selectivity is simply the ratio of permeability or permeance from Equation 2.5 or 2.6 for a given gas pair as shown in

Equation 2.7. A value of the ideal selectivity above unity means that penetrant 'A' is preferentially transported through the membrane relative to penetrant 'B'.

$$\alpha^*_{A/B} = \frac{P_A}{P_B} = \frac{P_A / L}{P_B / L} \tag{2.7}$$

The permeability can also be expressed as the product of a diffusivity and solubility coefficient:

$$P_A = \overline{D}_A \cdot \overline{S}_A . \tag{2.8}$$

The diffusivity and solubility coefficients in the above expression are effective averages applied across the membrane between its upstream and downstream faces. The average mutual diffusion coefficient $\overline{D}_A$ is given below for penetrant A in the membrane:

$$\overline{D}_A = \frac{\int_{c_{A1}}^{c_{A2}} D_A dc_A}{c_{A2} - c_{A1}}, \tag{2.9}$$

where c_{A1} and c_{A2} are the concentration of component 'A' sorbed into the membrane at the downstream and upstream faces, respectively. Under ideal conditions of fixed upstream pressure and negligible downstream pressure, the $\overline{S}_A$ parameter is equal to the secant slope of the sorption concentration versus pressure isotherm evaluated at the upstream partial pressure p_{A2} of the component:

$$\overline{S}_A = \frac{c_{A2}}{p_{A2}} . \tag{2.10}$$

2.1.3 Gas and Vapor Sorption in Glassy Polymers

The sorption of gases and vapors into glassy polymers is a highly active area of investigation due to the impact of sorption on a wide-ranging number of commercial applications. There are a large number of equilibrium sorption models presented in the literature; however, the most commonly used model is the dual mode sorption model [8]. The dual mode model is commonly used because of its proven performance in a number of penetrant/polymer systems, its mathematical simplicity, and its well-founded fundamental basis. There are also a large number of models of transient sorption kinetics presented in the literature. The behavior of transient sorption kinetics is very diverse in glassy polymers, ranging from diffusion-controlled Fickian uptake to entirely relaxation-controlled uptake [9-14].

2.1.3.1 Dual Mode Sorption

The physical basis of the dual mode model rests on the concept of unrelaxed free volume, which is unique to the glassy state. The *unrelaxed* free volume is defined as $\hat{V}_g - \hat{V}_l$, where $\hat{V}_g$ is the specific volume of the glass and $\hat{V}_l$ is the extrapolated specific volume of the polymer in a hypothetical liquid state. The concept of unrelaxed free volume in the glassy state is shown on a volume-temperature diagram in Figure 2.1 [15]. Below the glass transition of a material, the relaxation time for segmental motion becomes extremely long, which upon quenching from the rubbery state allows for the trapping of nonequilibrium chain conformations in glasses. This results in the inclusion of unrelaxed free volume, which causes the

specific volume of a glass to be higher than the extrapolation for a hypothetical liquid.

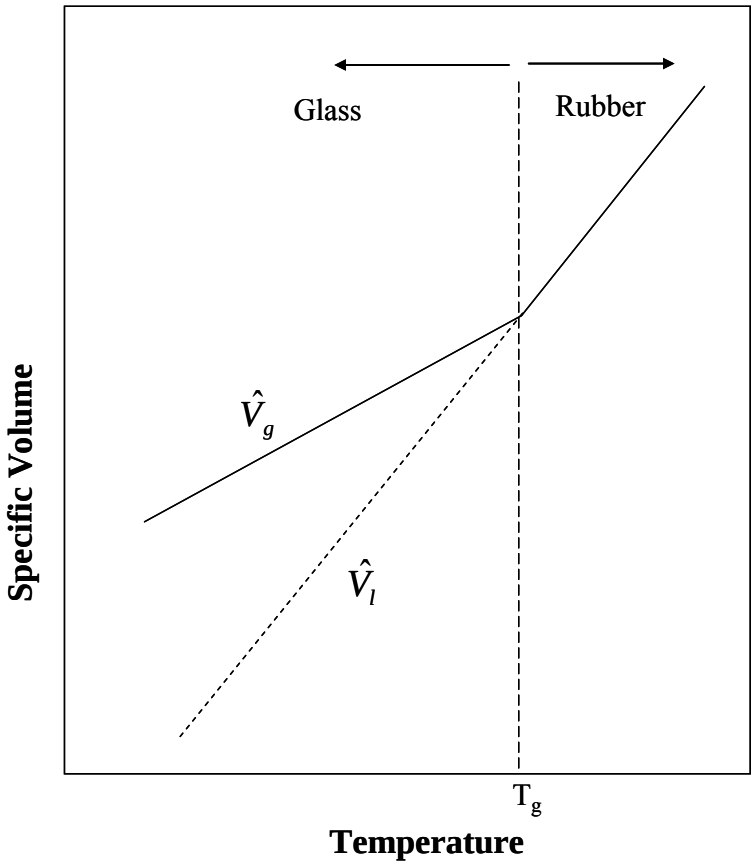

Figure 2.1: Schematic representation of the unrelaxed free volume [15]

The dual-mode sorption model considers the glassy solid to consist primarily of an equilibrium densified matrix with a small volume fraction of uniformly distributed nonequilibrium, molecular-scale gaps throughout the matrix. This model has proved to be very useful for interpreting a wide spectrum of phenomena including pure component and multi-component permeation and sorption and penetrant-induced

dilation in gas–glassy polymer systems. The development of the dual mode model has been reviewed [8, 16].

If a hypothetical equilibrium-densified glass, $\hat{V}_l$ in Figure 2.1, is exposed to a given pressure of a penetrant, a sorption concentration C_D, characteristic of true molecular dissolution, occurs as it does in rubbery polymers or liquids. In a nonequilibrium glass, the additional volume (i.e. the unrelaxed free volume) present in the form of inter-segmental gaps, provides for additional low energy berths for penetrants. In this case, an additional sorption population with concentration C_H can occupy these sites in local equilibrium with the dissolved mode population, C_D. This hole-filling population, C_H, is described by a Langmuir isotherm. The dual mode model can be written analytically for a penetrant indicated by subscript A, in terms of the sum of a Henry's law expression for C_D and a Langmuir expression for C_H:

$$c_A = C_{D_A} + C_{H_A} = k_{D_A} p_A + \frac{C'_{H_A} b_A p_A}{1 + b_A p_A}, \tag{2.11}$$

where k_{D_A} is the coefficient that characterizes sorption of the penetrant in the densified regions of the matrix and p_A is the penetrant partial pressure. The b_A and C'_{H_A} parameters are the Langmuir affinity and capacity constants, respectively.

The dual mode model is easily extended to include gas mixtures [17]. In terms of partial pressures, the expressions for mixed gas sorption are usually written as

$$c_A = k_{D_A} p_A + \frac{C'_{H_A} b_A p_A}{1 + b_A p_A + b_B p_B} \tag{2.12}$$

$$c_B = k_{D_B} p_B + \frac{C'_{H_B} b_B p_B}{1 + b_A p_A + b_B p_B}. \tag{2.13}$$

Due to competition for the available sorption sites, the dual mode model predicts a reduction in sorption of any gas, at a fixed partial pressure, as the partial pressure of a second gas is increased. Figure 2.2 shows pure and mixed gas data [18] for the sorption of CO_2 and CH_4 in polya (PPO). The solid lines represent dual mode model predictions for a partial pressure of 0.5 MPa (5 atm) for each component using parameters from the pure gas isotherm. The dual mode sorption model provides an accurate description of the solubility of both pure and mixed gases for these polymers over the range of partial pressures studied.

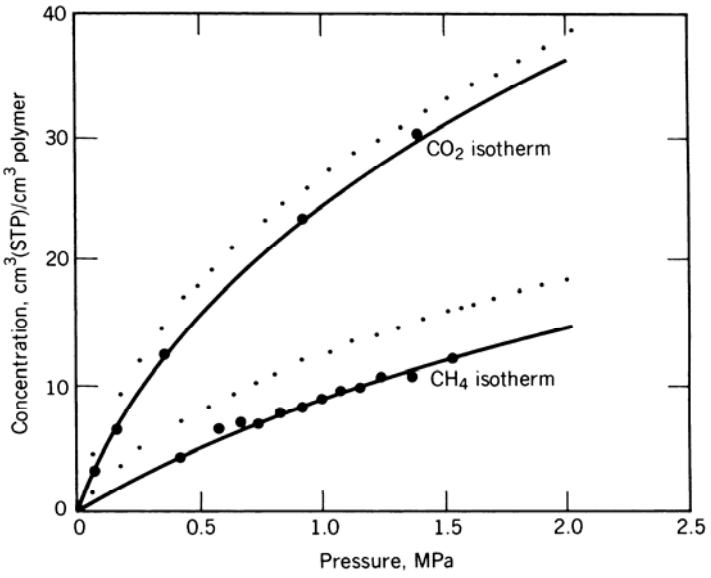

Figure 2.2: Mixed gas sorption for the $PPO/CO_2/CH_4$ system at $35^{\circ}C$. Dotted lines are pure gas sorption and solid lines show model predictions for $p_{CO_2} = p_{CH_4} = 0.5$ MPa (5 atm) [18].

2.1.3.2 Transient Sorption

The time-dependent uptake of gas into a glassy polymer exhibits a rich palette of possible behaviors [9-14]. The simplest of these behaviors is Fickian diffusion controlled uptake of gas into the glassy polymer matrix. In this case, the time-dependent uptake into a sheet of thickness *L* can be determined by solving the diffusion equation with constant boundary conditions and uniform initial concentration of penetrant in the polymer. Crank et al. [6] have given a solution for this case:

$$\left(\frac{M_t}{M_\infty}\right)_A = 1 - \sum_{n=0}^{\infty} \frac{8}{\pi^2 (2n+1)^2} \exp\left(\frac{-D_A (2n+1)^2 \pi^2 t}{L^2}\right), \tag{2.14}$$

where D_A is the diffusion coefficient of gas 'A' in the polymer, M_t and M_∞ are the masses of the penetrant sorbed at times t and ∞. The mathematics of Fickian diffusion are often complicated by the highly concentration dependent diffusion coefficients which occur in glassy polymers.

In addition to the added complexity of concentration dependent diffusion, glassy polymers can also experience relaxation-controlled uptake of penetrant. As penetrant sorbs into the polymer matrix, the segmental mobility of polymer chains may increase, thereby allowing for relaxation. As the polymer matrix relaxes, more room becomes available for penetration occupation. The time-scale of these relaxation processes is usually much longer than that of diffusion. Berens and Hopfenberg [19] proposed a model to account for the simultaneous processes of Fickian and relaxation driven uptake occurring in glassy polymers. In this model the mass uptake M_t is given as:

$$\left(\frac{M_t}{M_\infty}\right)_A = \left[(1-\alpha_R)\left\{1-\sum_{n=0}^{\infty}\frac{8}{\pi^2(2n+1)^2}\exp\left(\frac{-D_A(2n+1)^2\pi^2 t}{L^2}\right)\right\}\right] + \left[\alpha_R\left\{1-\exp\left(\frac{-t}{\tau_R}\right)\right\}\right], \quad (2.15)$$

where α_R is the fraction of mass uptake occurring via a relaxation-controlled process, $(1-\alpha_R)$ is the fraction of mass uptake occurring via a diffusion-controlled process, and τ_R is the time constant of the relaxation process. Although the Berens-Hopefenberg models accounts for the simultaneous occurrence of diffusion-controlled and relaxation-controlled uptake; it is often possible to divide the mass uptake into two distinct stages where the initial, fast uptake is associated with the Fickian response and the longer, slower approach to equilibrium is controlled by the relaxation process.

2.1.4 Gas Permeation in Glassy Polymers

The two most common models of gas transport in glassy polymers are based on the dual mode model of sorption and on free volume theory. Both of these models have been continually developed and refined over the last twenty-five years to account for many of the unique phenomena observed in gas transport through polymers [20-27]. A basic description of each model is given in this section.

2.1.4.1 Dual Mode Transport

As a direct extension of the dual mode sorption model, it is convenient to treat pure gas permeability as the sum of two terms, which are characteristic of the two

sorbed penetrant populations C_D and C_H [20]. For the case where there is a vacuum downstream and a pressure p_{A_2} of component 'A' upstream the following expression results:

$$J_A = -D_{D_A} \frac{dC_{D_A}}{dx} - D_{H_A} \frac{dC_{H_A}}{dx}, \tag{2.16}$$

where D_{D_A} and D_{H_A} are diffusion coefficients characteristic of the Henry's law and the Langmuir populations of sorbed gas molecules. After substitution of Equation 2.11 into Equation 2.16, the flux expression can be integrated analytically to give the equation for pure gas permeability, again for the condition of zero downstream pressure and an upstream pressure of p_{A_2}:

$$P_A = k_{D_A} D_{D_A} \left\{ 1 + \frac{F_A K_A}{1 + b_A p_{A_2}} \right\}, \tag{2.17}$$

where $F_A = D_{H_A} / D_{D_A}, K_A = C'_{H_A} b_A / k_{D_A}$. By plotting pure gas permeability data for component A, values of F_A, D_{D_A}, and D_{H_A} can be determined. The sorption parameters, k_{D_A}, C'_{H_A}, and b_A can be determined independently by equilibrium sorption measurements, so the parameters in Equation 2.17 can be easily determined.

Assuming that the diffusion coefficients D_{D_i} and D_{H_i} for components in a gas mixture are unchanged from their pure gas values, the simple expression represented above can be extended to gas mixtures. After substitution of Equation 2.12 into Equation 2.16, the flux equation can be analytically integrated to give the following expression for the permeability of component A in a binary mixture of gases A and B [28]:

$$P_{\mathrm{A}} = k_{D_{\mathrm{A}}} D_{D_{\mathrm{A}}} \left\{ 1 + \frac{F_{\mathrm{A}} K_{\mathrm{A}}}{1 + b_{\mathrm{A}} p_{\mathrm{A}_2} + b_{\mathrm{B}} p_{\mathrm{B}_2}} \right\}. \tag{2.18}$$

Similarly, for component B,

$$P_{\mathrm{B}} = k_{D_{\mathrm{B}}} D_{D_{\mathrm{B}}} \left\{ 1 + \frac{F_{\mathrm{B}} K_{\mathrm{B}}}{1 + b_{\mathrm{A}} p_{\mathrm{A}_2} + b_{\mathrm{B}} p_{\mathrm{B}_2}} \right\}. \tag{2.19}$$

2.1.4.2 Free Volume Theory

From examination of Equation 2.8, it is apparent that the overall permeability of a gas in a given polymer is the product of both diffusion and solubility based contributions. Both the diffusion coefficient and the solubility coefficient are known to be dependent upon the fractional free volume of the material [24, 29-31]. In glassy polymers, the diffusion coefficient shows a much greater variation from one polymer to another than that seen for the solubility coefficient. The permeability is often correlated using the expression [32, 33]:

$$P_A = A_A \exp\left(\frac{-B_A}{FFV} \right), \tag{2.20}$$

where A_A and B_A are constant for a particular gas. The fractional free volume is defined as:

$$FFV = \frac{\hat{V}_g - \hat{V}_0}{\hat{V}_0}. \tag{2.21}$$

$\hat{V}_g$ is the experimentally determined specific volume of the glass at a specific temperature, and $\hat{V}_0$ is the occupied specific volume of the polymer chains. $\hat{V}_0$ is

often determined from group contribution methods such as those given by van Krevelen [34].

From examination of Figure 2.3 it is apparent that Equation 2.20 does not exactly correlate the observed behavior due to the degree of data scatter in evidence. The degree of scatter indicates that other factors besides of fractional free volume influence permeability. Despite the degree of scatter present in the data, it is obvious that fractional free volume has a strong correlation to the permeability, and Equation 2.20 is capable of quickly providing a rough estimate of the permeability of a given gas in a glassy polymer.

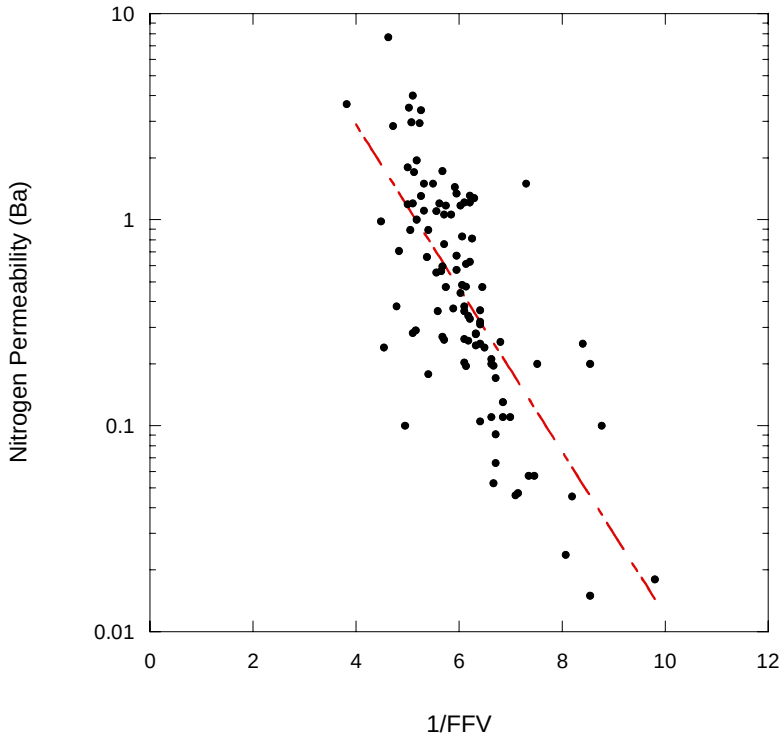

Figure 2.3: Correlation of permeability to fractional free volume. Data compiled for 105 polymers at 35 ^{o}C and 2 atm. [32].

2.2 History Dependent Behavior in Glassy Polymers

Due to the nonequilibrium nature of glassy polymers, gas transport through these materials show history dependent effects. Processing, thermal, and previous gas exposure history have all been shown to affect gas transport in glassy polymers [35-39]. Furthermore, the process of physical aging is always underway in glassy polymers, and the effect of physical aging on gas transport can be quite significant in thin films and asymmetric membranes.

2.2.1 Physical Aging

Recently, it has been noted that the permeability of glassy polymers decreases with time, and the selectivity increases with time. Interestingly, the decreases in permeability and increases in selectivity are accelerated for thin films, on the order of a micron in thickness. The study of the gas transport properties in thin films is of commercial importance because film thicknesses of this order are often used in semiconductors, adhesives, and packaging. It is important to note that the skin thicknesses of asymmetric hollow fibers, studied in this work, are usually one micron or less.

The work of Pinnau et al. with asymmetric films was the first to show dramatic time dependent gas transport properties [40, 41]. Later, Pfromm et al. showed similar behavior in free-standing, polyimide and polysulfone films [42]. Figure 2.4 shows that for a half-micron thick polyimide film the N_2 permeability decreases by approximately 50% over a 6000 hour period, while the He/N_2 selectivity increases by approximately 25% in the same time period. The decrease in

permeability is not nearly as dramatic for the thick films. Rezac et al. [43] and McCaig et al. [44] saw similar effects in polyimide/ceramic and polycarbonate/ceramic composite membranes, respectively. Chung et al. has also recently observed the same effects in asymmetric hollow fiber gas separation membranes [45].

The time dependent gas transport properties illustrated above are a result of physical aging. Physical aging is a well known phenomenon in glassy polymers that results from their nonequilibrium nature. As already mentioned, the segmental motions of the polymer chains are severely hindered in the glassy state, but these motions are not completely excluded. The hindered segmental motions allow for the recovery of unrelaxed free volume, $\hat{V}_g - \hat{V}_l$ (see Figure 2.1). The gradual approach to the equilibrium volume, $\hat{V}_l$, is called physical aging [46]

Two mechanisms are often used to describe physical aging: lattice contraction and diffusion of free volume. In the lattice contraction mechanism, the polymer chains are pictured as uniformly moving closer together, as if the lattice spacing throughout the polymer has decreased. The kinetics of the lattice contraction are not dependent on the sample dimensions. The diffusion of free volume or holes was first proposed by Alfrey [47]. In this mechanism, packets of free volume are pictured as diffusing from the interior to the surface of the sample where they are eliminated. Since the diffusion of free volume process is assumed to be Fickian, the loss of free volume becomes dependent on the sample dimensions.

(a)

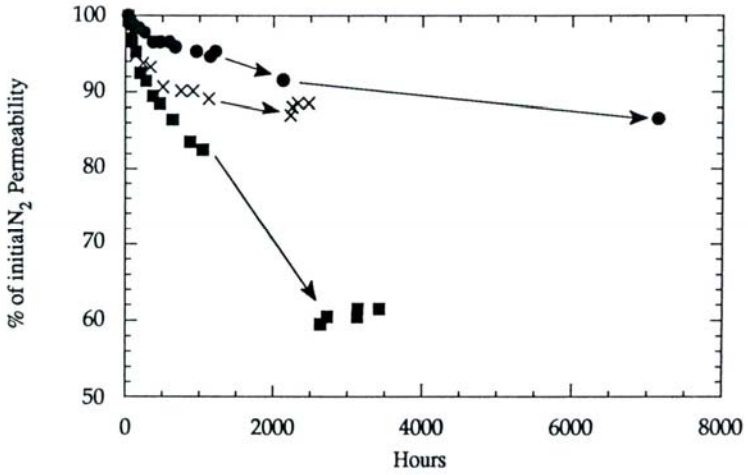

(b)

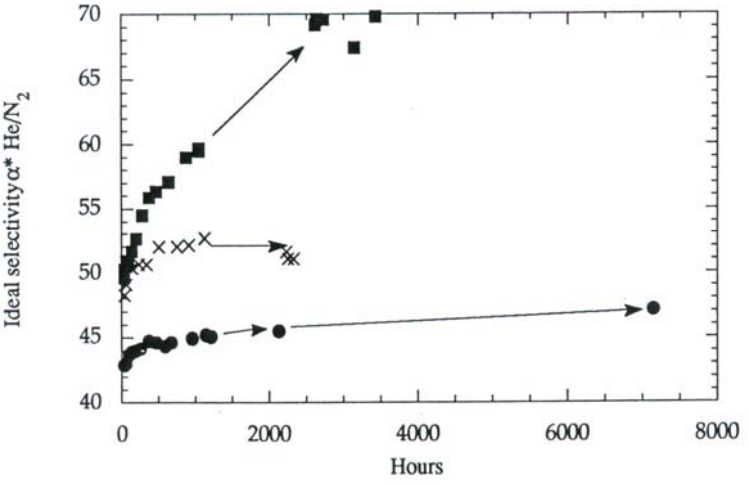

Figure 2.4: **(a)** Decrease in N_2 permeability and **(b)** increase in He/N_2 selectivity for polyimide films of varying film thickness: (•) 28.45, (×) 2.54, and (■) 0.5-microns. Arrows indicate storage in dry air at $35^{\circ}C$. Figures taken from [48].

Curro et al. [49] proposed that contributions from both the lattice contraction and diffusion of free volume mechanisms represented the overall volume recovery in the glass. McCaig et al. extended this idea to capture the effect the free volume recovery had on the permeability of the glass [50]. In this model, the free volume is related to the permeability using Equation 2.20. The time dependence of the free volume loss from the lattice contract mechanism was modeled as a first order exponential with time constant, τ. The time dependence of the free volume loss from the free volume diffusion mechanism was calculated by solving the diffusion equation with a concentration dependent diffusion coefficient. The concentration dependence of the free volume diffusion coefficient was assumed to be of the form:

$$D = D_g \exp\left[-Z\left(\frac{1}{v_f(t)} - \frac{1}{v_f^g}\right)\right], \tag{2.22}$$

where v_f^g is the fractional free volume of the slowly cooled glassy polymer, D_g is the diffusion coefficient when $v_f = v_f^g$, and Z is a material parameter. The concentration dependence of the diffusion coefficient captures the experimentally observed self-retarding nature of physical aging. The diffusion coefficient of free volume decreases as free volume is eliminated from the sample. This is the same concentration dependence seen for the diffusion coefficient with many small penetrants.

The dual mechanism approach of McCaig et al. described above was able to describe the oxygen permeability decay in bisphenol-A benzophenone-dicarboxylic acid (BPA-BnzDCA) films of varying thickness remarkably well. All films,

regardless of thickness, experience an initial sharp decline in permeability. This drop is due to the lattice contraction mechanism which is independent of sample dimension. Only in the thin films where the half thickness, *L/2*, was less than 2.5-microns was a contribution from the free volume diffusion mechanism observed.

2.2.2 Plasticization and Antiplasticization

Transport plasticization occurs in the presence of highly sorbing penetrants, which are capable of swelling the polymer matrix, essentially introducing additional free volume for penetrant diffusion. The introduction of this added free volume increases the permeability of the material but greatly reduces the selectivity. From a macroscopic viewpoint, plasticization increases the softness and ductility of the material and reduces the glass transition temperature. Microscopically, plasticization results in an increase in the segmental mobility [51]. Despite these observations of the end results of plasticization, a truly fundamental understanding of the plasticization phenomena is not available at this time. Furthermore, methods do not currently exist to determine if a penetrant will plasticize a given polymer.

Empirically, Bos and coworkers [52] have introduced the concept of the "plasticization pressure", the pressure at which plasticization first occurs. For glassy polymers, a plot of permeability versus the upstream penetrant pressure typically shows an initial decrease in permeability at lower pressures, which reaches an asymptotic value as the upstream pressure is increased. This behavior is a direct effect of the saturation of Langmuir sorption sites according to the dual mode model of gas transport. In the case of a *plasticizing* penetrant, continued pressurization will

result in an increase in the permeability. The point at which the upturn in permeability occurs is the so-called plasticization pressure of the material. This behavior is shown in Figure 2.5.

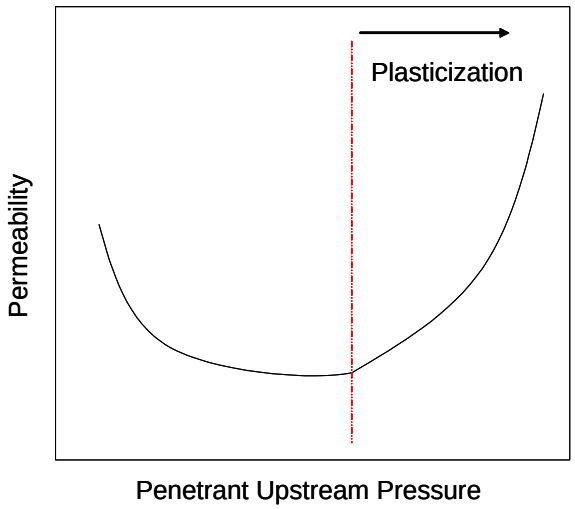

Figure 2.5: Diagram of typical permeability versus pressure response with a plasticizing penetrant

Recent work indicates that the plasticization pressure may not be strictly a material property, but that it may depend on morphology. Wessling et al. studied the effect of carbon dioxide plasticization in polyimide/PDMS composite membranes [53]. The polyimide separation layer ranged in thickness from 1.5 to 4 microns, and the PDMS support layer thickness ranged from 20 to 50 microns. The composite membranes with the thickest selective layers showed traditional permeation behavior with an easily identifiable plasticization pressure. The membranes with the thinnest selective layers showed an immediate increase in permeability even at low carbon

dioxide pressures. A similar early onset of plasticization was observed by Kapantaidakis in Matrimid® asymmetric hollow fibers [54].

At low concentrations, some plasticizers act as antiplasticizers in glassy polymers [55]. In this antiplasticization regime, the addition of penetrant to the polymer matrix is believed to actually retard the segmental mobility of the polymer. Evidence of this effect has been seen in mechanical testing where low concentrations of low molecular weight compounds mixed into the polymer matrix lead to increases in modulus and strength at rapid testing rates [56]. These effects are the opposite of what is expected at high concentrations where plasticization occurs. More importantly, Maeda and Paul have observed the effect of antiplasticization on gas transport in polysulfone and poly(phenylene oxide) [57, 58]. The introduction of low concentrations of non-reactive, low molecular weight additives to the polymer matrix led to reductions in the permeability to gases because of reduced segmental mobility.

The effects of plasticization and antiplasticization may most easily be understood using a specific volume-temperature plot, Figure 2.6 [25]. In this diagram, the pure polymer is indicated as the curve labeled "c_{A0}", which is identical to the volume-temperature behavior described previously in Figure 2.1. Assuming ideal mixing in the rubbery state, when a penetrant with concentration $c_A>0$ is added to the polymer, the specific volume of the penetrant/polymer mixture is greater in the rubbery state than that of the pure polymer. However, since the glass transition temperature of the penetrant/polymer mixture is less than the glass transition temperature of the pure polymer, $T_g\left(c_{A0}\right)$; it is possible for the specific volume of the penetrant/polymer mixture in the glassy state, $\hat{V}_g\left(c_{A1},T\right)$, to be *less* than the specific

volume of the pure polymer in the glassy state, $\hat{V}_g(c_{A0},T)$, at a given temperature. When this situation occurs an antiplasticization type response is observed. At higher penetrant concentration, the more traditional plasticization response occurs when the specific volume of the penetrant/polymer mixture in the glassy state, $\hat{V}_g(c_{A2},T)$, is *greater* than the specific volume of the pure polymer in the glassy state, $\hat{V}_g(c_{A0},T)$, at a given temperature.

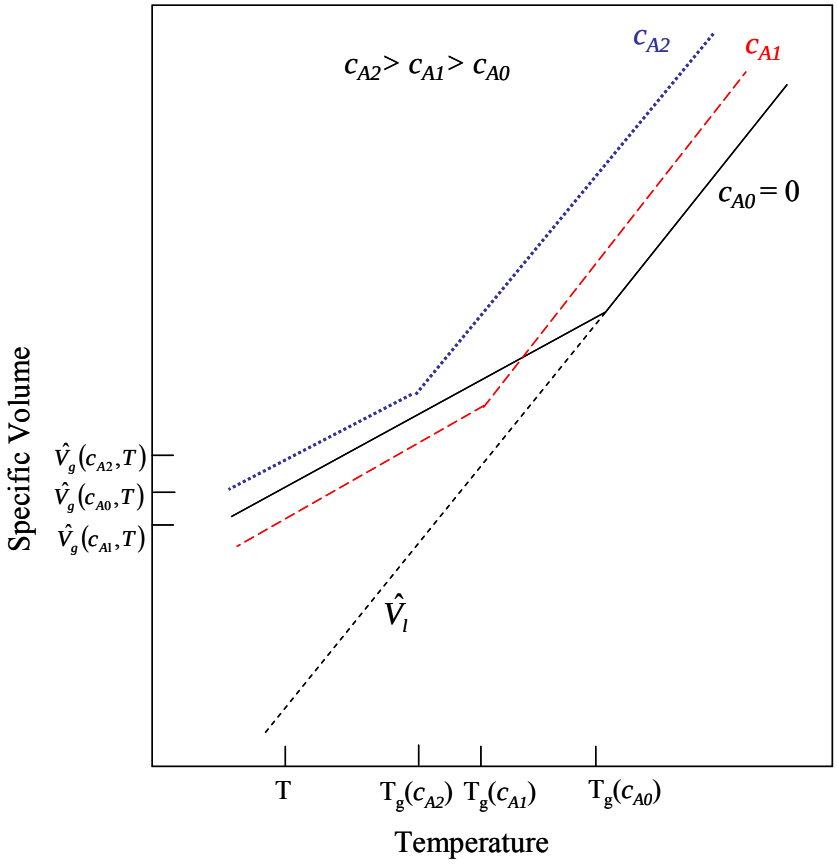

Figure 2.6: Specific volume-temperature description of plasticization and antiplasticization

Models are available to determine the specific volume of a penetrant/polymer pair in the glassy state, which then can be readily applied for use with free volume theories of permeation [23, 55, 59, 60]. These models and their applicability to explain gas transport behavior will be discussed in detail in Chapter 7.

2.2.3 Conditioning

Many studies have reported conditioning effects for gas and vapor sorption and transport properties in glassy polymers. It is important to understand the subtle difference between plasticization and conditioning. A highly sorbing penetrant plasticizes the polymer matrix by introducing additional free volume. Upon removal of the plasticizer, some of this additional free volume remains in the polymer matrix [38, 61]. The free volume induced by the plasticizer is only relaxed over long periods of time through mechanisms believed to be analogous to those of standard physical aging. During the period of time when the additional free volume induced by the plasticizer is still present in the polymer matrix, but after removal of all sorbed plasticizer, the material is said to be "conditioned". Only highly sorbing penetrants such as carbon dioxide and organic vapors are capable of plasticization [62-64]; however, the sorption of low solubility gases such as nitrogen after removal of the plasticizer can probe and maintain the nonequilibrium polymer matrix in a conditioned state indefinitely [61].

The conditioning effect in glassy polymers gives rise to hystereses in sorption, dilation, and permeation properties. Figure 2.7 shows hystereses in the sorption and dilation of carbon dioxide in bisphenol-A polycarbonate [65]. Since dilation

measures the macroscopic volume change of polymer upon sorption of a penetrant, it is the most direct method for observing the inclusion of additional free volume due to conditioning by the plasticizer. On total removal of carbon dioxide, the nonzero intercept on the volume dilation axis represents the additional volume introduced during sorption–desorption cycles.

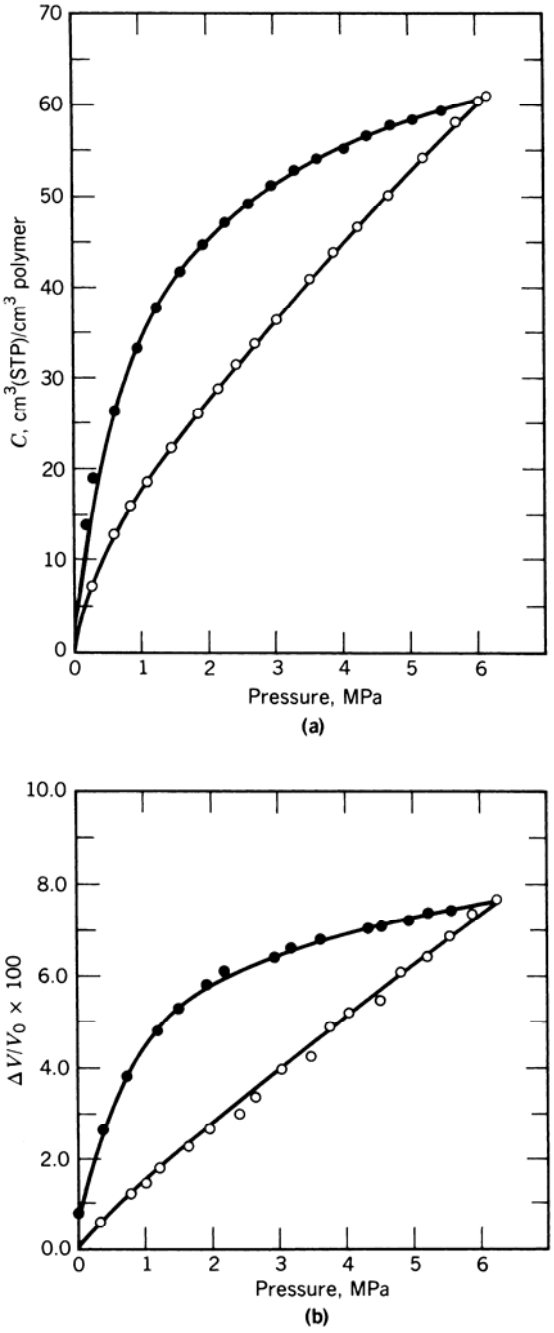

Figure 2.7: (a) Sorption and (b) dilation isotherms for CO_2 in bisphenol-A polycarbonate at $35^{\circ}C$. ∘, sorption; •, desorption [65].

As one would expect from the observed hysteresis in solubility, a hysteresis effect was seen for carbon dioxide permeation through bisphenol-A polycarbonate. The carbon dioxide permeability shown in Figure 2.8 [38] displays the behavior typical of a dual-mode response at low pressures, followed by plasticization at high pressures during pressurization. Upon depressurization, the permeability increases steadily as the pressure is reduced. At low pressures, the permeabilities upon depressurization are about 100% larger than the permeabilities during pressurization. The increase in the permeability upon depressurization can be explained in terms of the enhanced solubility and diffusivity in the conditioned matrix.

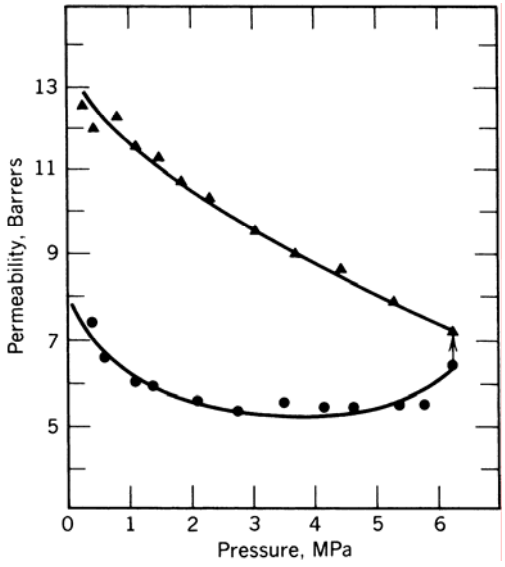

Figure 2.8: Permeability of CO_2 through bisphenol-A polycarbonate at $35^{\circ}C$ illustrating the hysteretic behavior due to conditioning; •, pressure increasing, ▲, pressure decreasing [38].

2.3 References

1. Wijmans, J.G. and R.W. Baker, "The solution-diffusion model: a review," *Journal of Membrane Science*, **107**(1-2), 1 (1995).

2. Koros, W. and W. Madden, "Comments on "Gas permeation through a glassy polymer membrane: Chemical potential gradient or dual mobility model?" by M.A. Islam and H. Buschatz [Chemical Engineering Science 57 (2002) 2089-2099]," *Chemical Engineering Science*, **58**(11), 2461 (2003).

3. Paul, D.R. and O.M. Ebra-Lima, "Pressure-induced diffusion of organic liquids through highly swollen polymer membranes," *Journal of Applied Polymer Science*, **14**(9), 2201 (1970).

4. Paul, D.R. and O.M. Ebra-Lima, "Mechanism of liquid transport through swollen polymer membranes," *Journal of Applied Polymer Science*, **15**(9), 2199 (1971).

5. Paul, D.R., "Role of membrane pressure in reverse osmosis," *Journal of Applied Polymer Science*, **16**(3), 771 (1972).

6. Crank, J., *The Mathematics of Diffusion*. 2nd ed. 1975, New York: Oxford University Press.

7. Kesting, R.E. and A.K. Fritzsche, *Polymeric Gas Separation Membranes*. 1993, New York: John Wiley & Sons, Inc.

8. Vieth, W.R., J.M. Howell, and J.H. Hsieh, "Dual sorption theory," *Journal of Membrane Science*, **1**(2), 177 (1976).

9. Frisch, H.L. and S.A. Stern, "Diffusion of small molecules in polymers," *Critical Reviews in Solid State and Materials Sciences*, **11**(2), 123 (1983).

10. Frisch, H.L., "Diffusion of penetrants in polymers," *Journal of Polymer Science, Part C: Polymer Symposia*, **No. 10**, 11 (1965).

11. Frisch, H.L., "Anomalous polymer-penetrant permeation," *Journal of Chemical Physics*, **37**, 2408 (1962).

12. Vrentas, J.S. and C.M. Vrentas, "Differential sorption in glassy polymers," *Journal of Applied Polymer Science*, **71**(9), 1431 (1999).

13. Vrentas, J.S., J.L. Duda, and W.J. Huang, "Regions of Fickian diffusion in polymer-solvent systems," *Macromolecules*, **19**(6), 1718 (1986).

14. Vrentas, J.S., J.L. Duda, and A.C. Hou, "Anomalous sorption in poly(ethyl methacrylate)," *Journal of Applied Polymer Science*, **29**(1), 399 (1984).

15. Chern, R.T., et al., "Implications of the dual-mode sorption and transport models for mixed gas permeation," *ACS Symposium Series*, **223**(Ind. Gas Sep.), 47 (1983).

16. Hopfenberg, H.B. and V. Stannett, in *The Physics of the Glassy State*, R.N. Haward, Editor. 1973, Applied Science Publishers, Ltd.: London.

17. Koros, W.J., "Model for sorption of mixed gases in glassy polymers," *Journal of Polymer Science, Polymer Physics Edition*, **18**(5), 981 (1980).

18. Story, B.J. and W.J. Koros, "Sorption of carbon dioxide/methane mixtures in poly(phenylene oxide) and a carboxylated derivative," *Journal of Applied Polymer Science*, **42**(9), 2613 (1991).

19. Berens, A.R. and H.B. Hopfenberg, "Diffusion and relaxation in glassy polymer powders. 2. Separation of diffusion and relaxation parameters," *Polymer*, **19**(5), 489 (1978).

20. Paul, D.R. and W.J. Koros, "Effect of partially immobilizing sorption on permeability and the diffusion time lag," *Journal of Polymer Science, Polymer Physics Edition*, **14**(4), 675 (1976).

21. Barrer, R.M., "Diffusivities in glassy polymers for the dual mode sorption model," *Journal of Membrane Science*, **18**, 25 (1984).

22. Petropoulos, J.H., "Plasticization effects on the gas permeability and permselectivity of polymer membranes," *Journal of Membrane Science*, **75**(1-2), 47 (1992).

23. Vrentas, J.S. and C.M. Vrentas, "Fickian diffusion in glassy polymer-solvent systems," *Journal of Polymer Science, Part B: Polymer Physics*, **30**(9), 1005 (1992).

24. Thran, A., G. Kroll, and F. Faupel, "Correlation between fractional free volume and diffusivity of gas molecules in glassy polymers," *Journal of Polymer Science, Part B: Polymer Physics*, **37**(23), 3344 (1999).

25. Duda, J.L., I.H. Romdhane, and R.P. Danner, "Diffusion in glassy polymers - relaxation and antiplasticization," *Journal of Non-Crystalline Solids*, **172-174**(Pt. 2), 715 (1994).

26. Vrentas, J.S. and J.L. Duda, "Diffusion in polymer-solvent systems. I. Reexamination of the free-volume theory," *Journal of Polymer Science, Polymer Physics Edition*, **15**(3), 403 (1977).

27. Vrentas, J.S. and J.L. Duda, "Diffusion of small molecules in amorphous polymers," *Macromolecules*, **9**(5), 785 (1976).

28. Koros, W.J., et al., "A model for permeation of mixed gases and vapors in glassy polymers," *Journal of Polymer Science, Polymer Physics Edition*, **19**(10), 1513 (1981).

29. Pixton, M.R. and D.R. Paul, "Gas transport properties of polyarylates. Part II. Tetrabromination of the bisphenol," *Journal of Polymer Science, Part B: Polymer Physics*, **33**(9), 1353 (1995).

30. Pixton, M.R. and D.R. Paul, "Gas transport properties of adamantane-based polysulfones," *Polymer*, **36**(16), 3165 (1995).

31. Aitken, C.L., W.J. Koros, and D.R. Paul, "Effect of structural symmetry on gas transport properties of polysulfones," *Macromolecules*, **25**(13), 3424 (1992).

32. Park, J.Y. and D.R. Paul, "Correlation and prediction of gas permeability in glassy polymer membrane materials via modified free volume based group contribution method," *Journal of Membrane Science*, **125**(1), 23 (1997).

33. Pixton, M.R. and D.R. Paul, *Relationships between structure and transport properties for polymers with aromatic backbones*, in *Polymeric Gas Separation Membranes*, Y. Yampolskii, Editor. 1994, CRC Press: Boca Raton.

34. van Krevelen, D.W. and P.J. Hoftyzer, *Properties of Polymers*. 2nd ed, New York: Elsevier.

35. Moe, M.B., W.J. Koros, and D.R. Paul, "Effects of molecular structure and thermal annealing on gas transport in two tetramethylbisphenol A polymers," *Journal of Polymer Science, Part B: Polymer Physics*, **26**(9), 1931 (1988).

36. Fuhrman, C., et al., "Effect of thermal hysteresis on the gas permeation properties of 6FDA-based polyimides," *Journal of Applied Polymer Science*, **91**(2), 1174 (2004).

37. Pope, D.S., G.K. Fleming, and W.J. Koros, "Effect of various exposure histories on sorption and dilation in a family of polycarbonates," *Macromolecules*, **23**(11), 2988 (1990).

38. Jordan, S.M., W.J. Koros, and G.K. Fleming, "The effects of carbon dioxide exposure on pure and mixed gas permeation behavior: comparison of glassy polycarbonate and silicone rubber," *Journal of Membrane Science*, **30**(2), 191 (1987).

39. Moe, M., et al., "Effects of film history on gas transport in a fluorinated aromatic polyimide," *Journal of Applied Polymer Science*, **36**(8), 1833 (1988).

40. Pinnau, I., M.W. Hellums, and W.J. Koros, "Gas transport through homogeneous and asymmetric poly(ester carbonate) membranes," *Polymer*, **32**(14), 2612 (1991).

41. Pfromm, P.H., I. Pinnau, and W.J. Koros, "Gas transport through integral-asymmetric membranes: a comparison to isotropic film transport properties," *Journal of Applied Polymer Science*, **48**(12), 2161 (1993).

42. Pfromm, P.H. and W.J. Koros, "Accelerated physical aging of thin glassy polymer films: evidence from gas transport measurements," *Polymer*, **36**(12), 2379 (1995).

43. Rezac, M.E., et al., "Aging of thin polyimide-ceramic and polycarbonate-ceramic composite membranes," *Industrial & Engineering Chemistry Research*, **32**(9), 1921 (1993).

44. McCaig, M.S. and D.R. Paul, "Effect of film thickness on the changes in gas permeability of a glassy polyarylate due to physical aging. Part I. Experimental observations," *Polymer*, **41**(2), 629 (1999).

45. Lin, W.-H. and T.-S. Chung, "The physical aging phenomenon of 6FDA-durene polyimide hollow fiber membranes," *Journal of Polymer Science, Part B: Polymer Physics*, **38**(5), 765 (2000).

46. Struik, L.C.E., "Physical aging in plastics and other glassy materials," *Polymer Engineering and Science*, **17**(3), 165 (1977).

47. Alfrey, T., G. Goldfinger, and H. Mark, "Apparent second-order transition point of polystyrene," *Journal of Applied Physics*, **14**, 700 (1943).

48. Pfromm, P.H., *Gas Transport Properties and Aging of Thin and Thick Films Made From Amorphous Glassy Polymers*, in *Chemical Engineering*. 1994, The University of Texas at Austin: Austin, TX. p. 170.

49. Curro, J.G., R.R. Lagasse, and R. Simha, "Diffusion model for volume recovery in glasses," *Macromolecules*, **15**(6), 1621 (1982).

50. McCaig, M.S., D.R. Paul, and J.W. Barlow, "Effect of film thickness on the changes in gas permeability of a glassy polyarylate due to physical aging part II. Mathematical model," *Polymer*, **41**(2), 639 (1999).

51. Ismail, A.F. and W. Lorna, "Penetrant-induced plasticization phenomenon in glassy polymers for gas separation membrane," *Separation and Purification Technology*, **27**(3), 173 (2002).

52. Bos, A., et al., "CO2-induced plasticization phenomena in glassy polymers," *Journal of Membrane Science*, **155**(1), 67 (1999).

53. Wessling, M., M.L. Lopez, and H. Strathmann, "Accelerated plasticization of thin-film composite membranes used in gas separation," *Separation and Purification Technology*, **24**(1-2), 223 (2001).

54. Kapantaidakis, G.C., et al., "CO2 plasticization of polyethersulfone/polyimide gas-separation membranes," *AIChE Journal*, **49**(7), 1702 (2003).

55. Maeda, Y. and D.R. Paul, "Effect of antiplasticization on gas sorption and transport. III. Free volume interpretation," *Journal of Polymer Science, Part B: Polymer Physics*, **25**(5), 1005 (1987).

56. Jackson, W.J., Jr. and J.R. Caldwell, "Antiplasticizers for bisphenol polycarbonates," *Advances in Chemistry Series*, **No. 48**, 185 (1965).

57. Maeda, Y. and D.R. Paul, "Effect of antiplasticization on gas sorption and transport. II. Poly(phenylene oxide)," *Journal of Polymer Science, Part B: Polymer Physics*, **25**(5), 981 (1987).

58. Maeda, Y. and D.R. Paul, "Effect of antiplasticization on gas sorption and transport. I. Polysulfone," *Journal of Polymer Science, Part B: Polymer Physics*, **25**(5), 957 (1987).

59. Ruiz-Trevino, F.A. and D.R. Paul, "A quantitative model for the specific volume of polymer-diluent mixtures in the glassy state," *Journal of Polymer Science, Part B: Polymer Physics*, **36**(6), 1037 (1998).

60. Vrentas, J.S., J.L. Duda, and H.C. Ling, "Antiplasticization and volumetric behavior in glassy polymers," *Macromolecules*, **21**(5), 1470 (1988).

61. Jordan, S.M., W.J. Koros, and J.K. Beasley, "Characterization of carbon dioxide-induced conditioning of polycarbonate films using penetrants with different solubilities," *Journal of Membrane Science*, **43**(1), 103 (1989).

62. Connelly, R.W., et al., "The effect of sorbed penetrants on the aging of previously dilated glassy polymer powders. I. Lower alcohol and water sorption in poly(methyl methacrylate)," *Journal of Applied Polymer Science*, **34**(2), 703 (1987).

63. Stewart, M.E., et al., "The effect of sorbed penetrants on the aging of previously dilated glassy polymer powders. II. n-Propane sorption in polystyrene," *Journal of Applied Polymer Science*, **34**(2), 721 (1987).

64. Stewart, M.E., et al., "The effect of sorbed penetrants on the aging of previously dilated glassy polymer powders. Part III. The effect of exposure to lower alcohols on enthalpy relaxations in poly(methyl methacrylate)," *Journal of Applied Polymer Science*, **34**(7), 2493 (1987).

65. Fleming, G.K., in *Chemical Engineering*. 1987, The University of Texas at Austin: Austin, TX.

CHAPTER 3

MATERIALS AND EXPERIMENTAL METHODS

3.1 Materials

3.1.1 Polymer

The membranes studied in this work are all formed from Matrimid® 5218. Matrimid® is a wholly amorphous polyimide that is manufactured and marketed by Huntsman LLC. Matrimid® was chosen as the focus of this study because it is currently used to form commercially available, high-performance gas separation membranes. The backbone repeat structure of Matrimid® is shown in Figure 3.1, and Table 3.1 provides material and gas transport properties for Matrimid®.

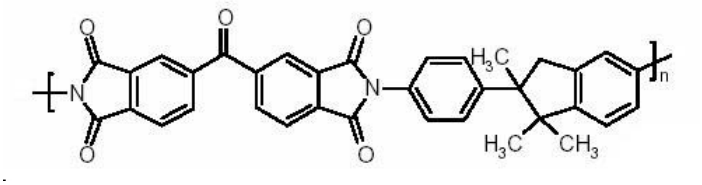

Figure 3.1: Matrimid® repeat structure

Table 3.1: Matrimid® material and gas transport properties at 65 psia and 35 °C [1]

T_g	305 °C
Density	1.2 g/cm^3
O_2 Permeability	2 Ba
CO_2 Permeability	10 Ba
O_2/N_2 Selectivity	6.9
CO_2/CH_4 Selectivity	35.5

3.1.2 Gases

All gases used in this study were obtained from Airgas®. Pure gases of nitrogen, oxygen, helium, carbon dioxide, and methane were all ultra-high purity grade or better. The composition of the gas mixtures used for the conditioning experiments are given in Table 3.2. Due to vapor pressure limitations, higher concentrations of toluene and n-heptane than those listed in Table 3.2 were not available from Airgas®. A bubbler was built to obtain higher loadings of toluene and n-heptane. Gas mixture 1 in Table 3.2 was used as a carrier gas for the bubbler. Details of the design and operation of the bubbler are given in Appendix A.

Table 3.2: Mixed gas compositions from Airgas®

Gas Mixture	Gas Composition (mole %)			
	CH_4	CO_2	n-heptane	toluene
1	90.0	10.0	-	-
2	Balance	9.82	505 ppm	-
3	Balance	9.82	-	293 ppm
4	Balance	9.81	504 ppm	284 ppm

3.2 Membrane Formation

Matrimid® hollow fibers are spun using a dry-jet/wet-quench process [2-5]. In this process, a polymer dope consisting of Matrimid®, N-methyl pyrrolidinone, and ethanol (non-solvent) is extruded through a spinneret. After extrusion, the dope passes through an air gap (approximately 10 cm) before it enters a water quench bath. The fibers are then taken up on a rotating drum. The entire process from extrusion to

fiber take up occurs in less than 1 second. A schematic representation of the spinning process is given in Figure 3.2.

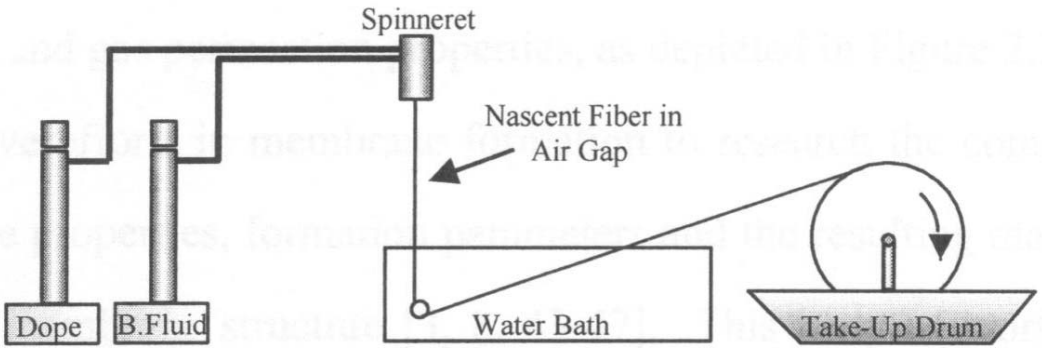

Figure 3.2: Schematic representation of the spinning process

The spinning process is often described with help of a ternary phase diagram such as Figure 3.3 [6]. In these diagrams, the vertices of the triangle represent each of the three pure components, while points on the interior of the triangle represent ternary compositions. Phase diagrams that are relevant to this discussion display a stable one-phase region and an unstable two-phase region where phase separation occurs. Strictly speaking, a metastable two-phase region also exists. In the two-phase region, the polymer solution phase separates into a polymer-lean phase and a polymer-rich phase. The compositions of the polymer-lean and polymer-rich phases are given by equilibrium tie-lines. The spin dope ('*A*' on Figure 3.3) is formulated to lie close to the two-phase region. While the detailed processes during dry-jet/wet-quench spinning that causes the outer region of the spinning dope to transition into a defect-free skin remains unclear, it is believed that the formation of the defect-free skin and the porous substructure follow two separate composition paths on the ternary

phase diagram. When the dope passes through the air gap, solvent evaporates from the outer diameter of the fiber. At this point, the outer region of the fiber is represented by composition 'A'' while the bulk of the fiber still remains at composition 'A'. In both cases, upon immersion in the nonsolvent bath, solvent efflux and nonsolvent influx results in a high nonsolvent composition ('B' and 'B'') which leads to phase separation along equilibrium tie lines to a polymer rich and a polymer lean phase. The complex details of this process determine the morphology of the resulting structure; however, in all cases, the polymer transitions from a polymer solution to a precipitated structure in much less than a second.

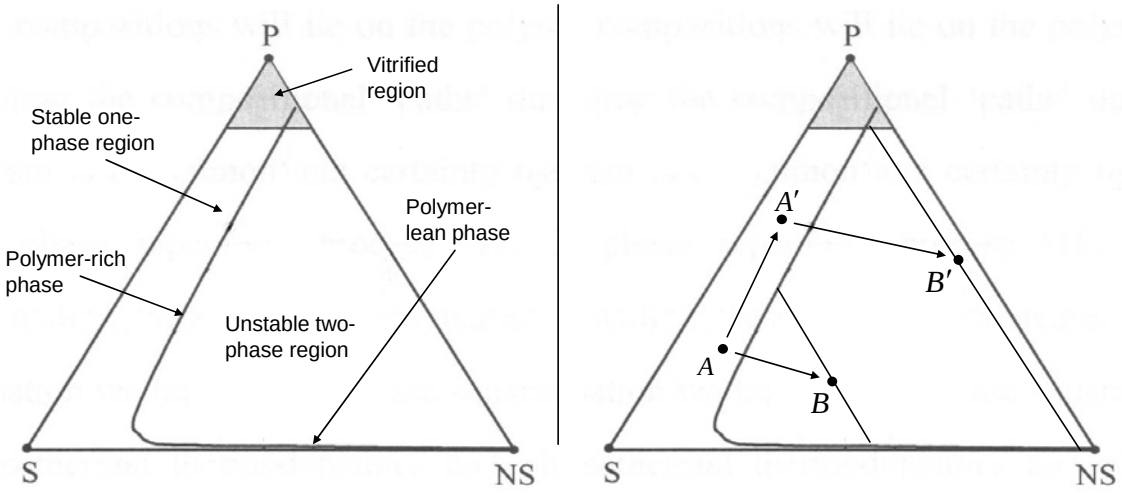

Figure 3.3: Spinning process depicted on a ternary phase diagram

After phase separation the fiber exists in a water saturated state. Simple drying of the fiber from this point results in the collapse of the delicate substructure morphology due to the high surface tension of water [7, 8]. In order to limit substructure collapse, the fibers undergo a solvent exchange procedure where they are washed with methanol and then with hexanes. After replacement of methanol with

hexanes, the fibers can simply be allowed to dry in air without experiencing substructure collapse. A final drying procedure at 120°C under vacuum for one hour is conducted to remove all traces of solvent from the fiber.

The spinning process described above is used to produce defect-free Matrimid® fibers with a skin thickness of approximately 100nm. The nodular or porous support layer of the fiber has characteristic dimensions ranging from 100-400nm. A scanning electron micrograph illustrates the asymmetric hollow fiber morphology in Figure 3.4.

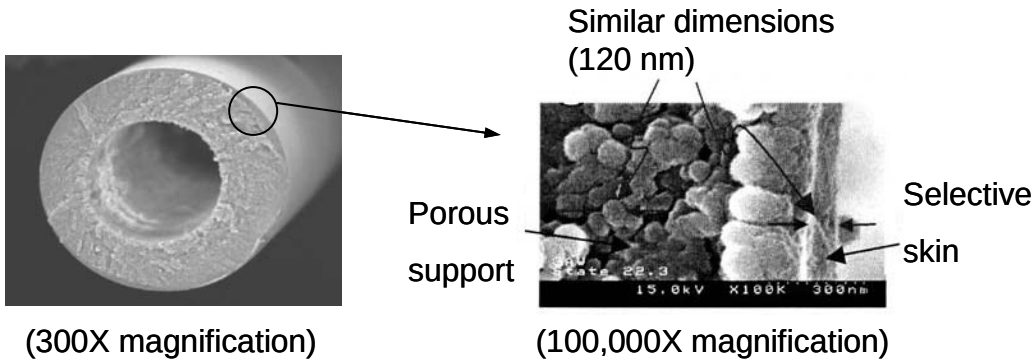

Figure 3.4: SEM images of Matrimid® hollow fibers. Characteristic dimensions of the nodular, porous support layer are similar in size to the skin thickness [9].

3.3 Experimental Methods

3.3.1 Pressure Decay Sorption

The dual volume pressure-decay apparatus is used to measure gas solubility in asymmetric hollow fiber samples. The equipment and operating procedures for this

technique are well documented in the literature [10, 11]. A schematic representation of the dual volume pressure-decay apparatus is given in Figure 3.5.

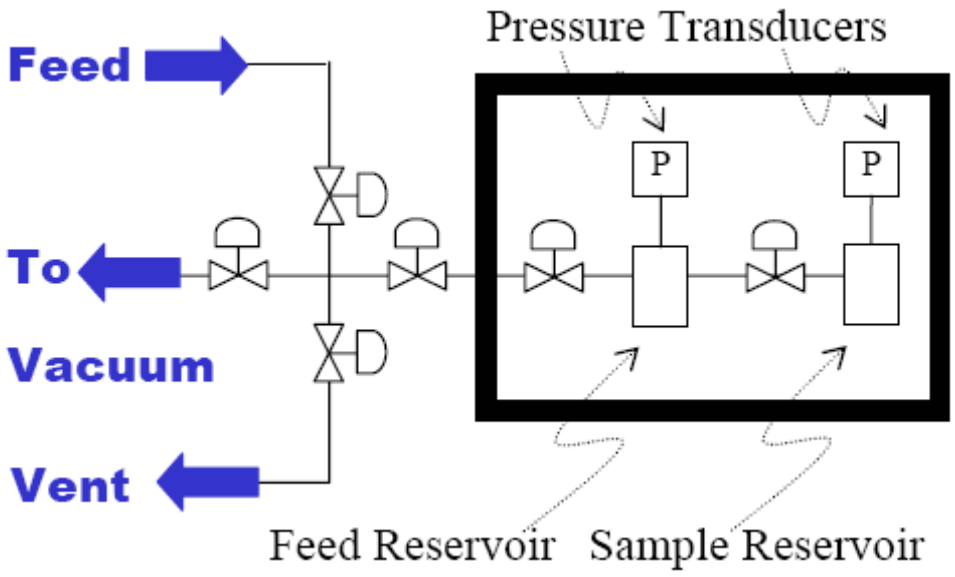

Figure 3.5: Schematic of dual volume pressure-decay apparatus [1]

Following standard procedures, a gas is introduced into a feed reservoir of known volume after complete evacuation of both the feed and sample reservoirs. After allowing the pressure in the feed reservoir to equilibrate, the valve between the feed and sample reservoirs is opened for 3 seconds to allow gas into the sample reservoir. The valve between the feed and sample reservoirs is then closed, and the pressure in both reservoirs is monitored. The pressure in the feed reservoir should almost immediately reach a steady value, while the pressure in the sample reservoir should decay as gas is sorbed into the polymer sample. A mole balance on the system gives the amount of gas sorbed into the polymer sample [9]:

$$n_P = \frac{1}{R_g T}\left[\begin{array}{l}\left(V^{\,Sample\ Res} - V^{\,Sample}\right)\left(\dfrac{p_i^{\,Sample\ Res}}{z_i^{\,Sample\ Res}} - \dfrac{p_f^{\,Sample\ Res}}{z_f^{\,Sample\ Res}}\right) \\ + V^{\,Feed\ Res}\left(\dfrac{p_i^{\,Feed\ Res}}{z_i^{\,Feed\ Res}} - \dfrac{p_f^{\,Feed\ Res}}{z_f^{\,Feed\ Res}}\right)\end{array}\right], \qquad (3.1)$$

where n_P is the number of moles sorbed into the polymer sample, R_g is the ideal gas constant, T is the temperature, and $V^{\,Feed\ Res}$, $V^{\,Sample\ \ Res}$, and $V^{\,Sample}$ are the volumes of the feed reservoir, sample reservoir, and polymer sample, respectively. The externally applied pressure is denoted by p, and z is the compressibility calculated from Table 3.3. The subscripts i and f refer to the initial (before opening of the valve) and final states (after opening of the valve).

Table 3.3: Compressibility factor coefficients where $z = A + Bp + Cp^2 + Dp^3$ and p is pressure in units of psia [12]

Coefficient	Gas	
	CO_2	CH_4
A	1.0006	1.000184
B	-3.375×10^{-4}	-1.112×10^{-4}
C	6.169×10^{-8}	2.147×10^{-8}
D	-1.686×10^{-10}	-6.678×10^{-12}

Statham pressure transducers (Model PA822-1M-16653) are used to measure the pressure and are powered by a Lauda 10 VDC power supply (Model LCS-A-1). The signal is measured with a Keithley Instruments 2700 Multimeter. The multimeter is interfaced with a personal computer using Labview® data acquisition software. The volumes of the feed and sample reservoirs are known to within 0.005 cm^3. For a typical polymer sample volume of 1 cm^3, the concentration of sorbed gas can be determined to within ±0.5%.

3.3.2 Gravimetric Sorption

A McBain balance is used to measure sorption gravimetrically of highly sorbing vapors [13-15]. A schematic representation of the McBain balance is shown in Figure 3.6. The entire apparatus is constructed of glass, which limits measurements to below atmospheric pressure.

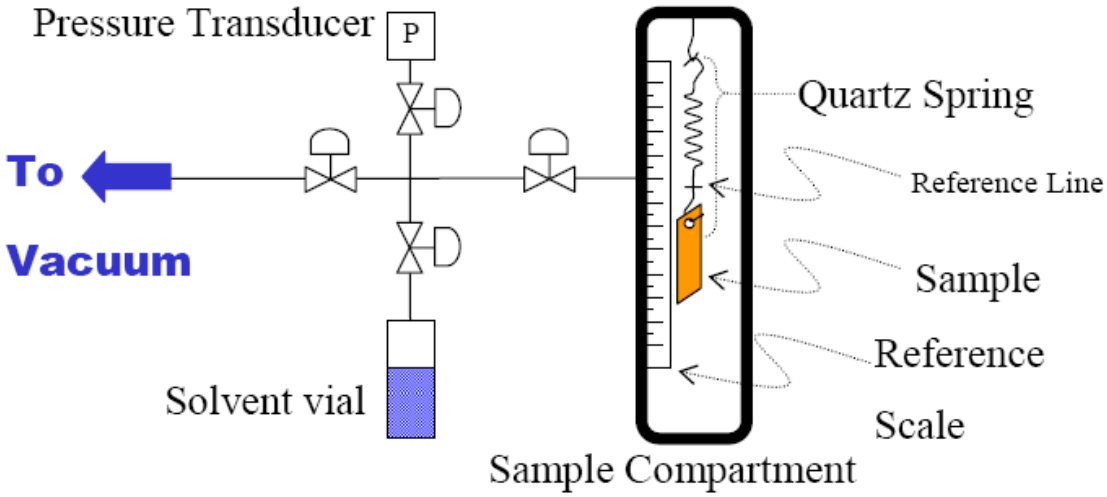

Figure 3.6: Schematic of McBain balance [1]

A measurement is taken by first completely evacuating the apparatus. The valve to the sample compartment is then shut, and the headspace of the solvent vial is evacuated to remove any trapped air. After the solvent vial headspace is evacuated, the valve to the vacuum pump is shut, and solvent vapor is expanded into the sample compartment. As vapor sorbs into the polymer, the quartz spring extends. The extension of the quartz spring is measured using a cathetometer. After equilibrium is reached, the vapor pressure in the sample compartment may be incrementally

increased. Through a succession of sorption measurements at increasing pressures, a complete sorption isotherm may be collected.

The pressure in the sample compartment is measured using a MKS Baratron® 1000 torr pressure transducer (Type 727). The quartz spring, supplied by Ruska Instruments, has a spring constant of 0.251 mg/mm. The extension of the spring can be measured to within 5 μm using the cathetometer. Typical polymer sample weights are approximately 25 mg.

3.3.3 Permeation

The permeance of a given gas and the selectivities for gas pairs are determined using the standard isochoric (constant-volume, variable pressure) technique [16-18]. In this technique the steady-state increase in the permeate pressure is directly proportional to the permeance:

$$P_A/L = 193375\frac{dp/dt\,V_D}{TAP_{up}}, \tag{3.2}$$

where

$$\begin{aligned}
dp/dt &= \text{permeate pressure rise}\,[=]\,\text{torr/sec}\\
V_D &= \text{downstream volume}\,[=]\,\text{cm}^3\\
T &= \text{temperature}\,[=]\,\text{K}\\
A &= \text{membrane surface area}\,[=]\,\text{cm}^2\\
P_{up} &= \text{upstream pressure}\,[=]\,\text{psia}
\end{aligned}$$

Prior to permeation testing, the asymmetric hollow fibers must be potted into a testable module. The details of the module making process are standardized and are

described in Appendix B. The completed membrane module is loaded into the permeation apparatus diagrammed schematically in Figure 3.7. A measurement is taken by first evacuating the upstream and downstream faces of the membrane overnight to remove any sorbed gases from the membrane. After evacuation, the upstream pressure may be increased to the desired pressure with the gas of interest. A period of 30 minutes is given to allow for permeation through the membrane to reach steady state. Due to the thin skin thickness of asymmetric hollow fibers, the diffusive time lag to reach steady state is less than 5 minutes. After steady state is reached, the downstream vacuum valve is closed and the pressure rise in the downstream volume is monitored with a MKS pressure transducer.

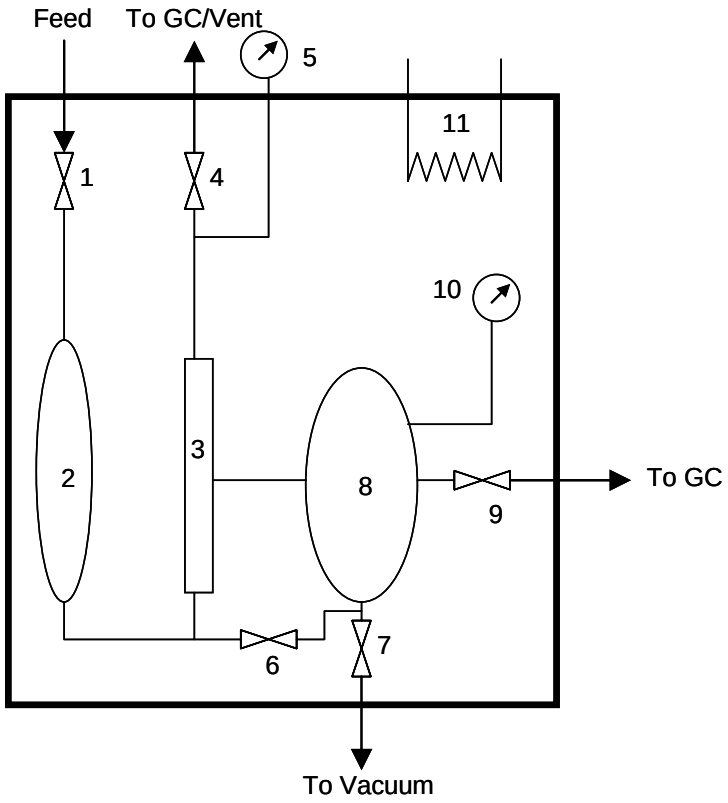

Figure 3.7: Schematic of pressure-rise permeation apparatus. 1. Feed Shutoff Valve, 2. Upstream Ballast, 3. Membrane Module, 4. Retentate Metering Valve, 5. Upstream Pressure Transducer, 6. Bypass Valve, 7. Vacuum Valve, 8. Downstream Volume, 9. GC Valve, 10. Downstream Pressure Transducer, 11. Thermostated Heat Tape

The upstream pressure is monitored using a 1000 psia Sensotec SC Series pressure transducer. The pressure in the downstream volume is measured using a 1000 torr MKS Baratron® (Type 127) pressure transducer. The output from the downstream pressure transducer is interfaced with a personal computer using LabView® data acquisition software to allow for real-time data recording. The entire permeation system is maintained to within ±0.1 ^{o}C using a proportional controller (Cole Parmer Catalog No. BA-2155-54).

When a multicomponent mixture is used as a feed gas, the membrane selectivity is determined by sampling of the permeate with a gas chromatograph. In a multicomponent system, it is important to limit the effects of concentration polarization. Concentration polarization occurs when the "fast" gas is depleted on the upstream side of the membrane. It has been shown that by setting the stage cut to less than 1%, the effects of concentration polarization on the membrane performance are negligible [19]. The stage cut of the process is defined as:

$$stage\,cut = \frac{permeate\,molar\ \ flow\,rate}{feed\ molar\ \ flow\,rate} \tag{3.3}$$

The feed molar flow rate is measured using a 0-100 sccm MKS (Type 02588-0100SV) mass flow meter.

A Hewlett-Packard 5890 gas chromatograph with a thermal conductivity detector and a HayeSep® Q packed porous polymer column is used to separate mixtures of carbon dioxide and methane. The membrane permeate is typically injected into the gas chromatograph at a pressure of approximately 10 torr. The response of the gas chromatograph at this low pressure was calibrated using 4 standard mixtures of carbon dioxide and methane, purchased from AirGas®, ranging in composition from 10 to 90 mole-percent carbon dioxide. The response factor for carbon dioxide, λ_{CO_2}, is defined as [20]:

$$\lambda_{CO_2} = \frac{actual\,mole\%\,CO_2}{detector\,response\,(area\%)}\ . \tag{3.4}$$

The response factor for carbon dioxide as a function of detector response is shown in Figure 3.8.

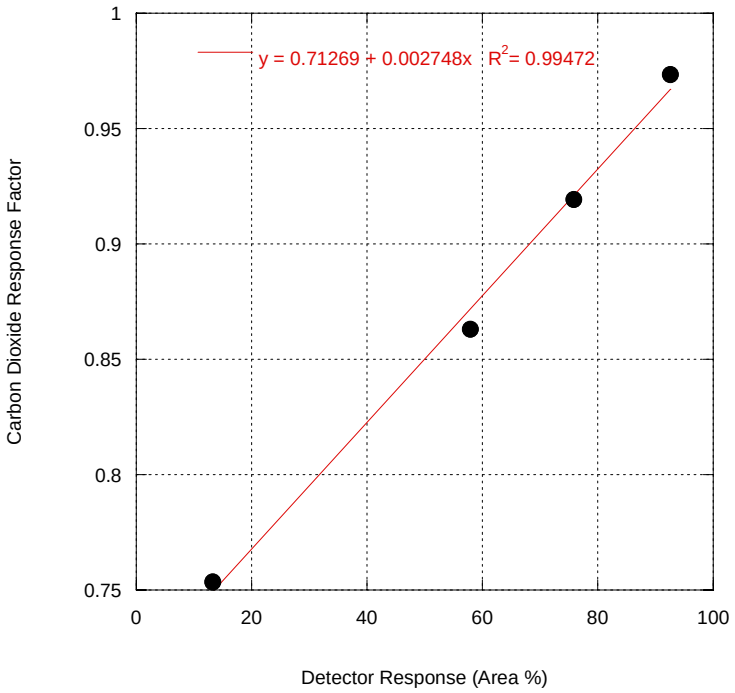

Figure 3.8: Gas chromatograph calibration

3.4 References

1. Moore, T., *Effects of Materials, Processing, and Operating Conditions on the Morphology and Gas Transport Properties of Mixed Matrix Membranes*, in *Chemical Engineering*. 2004, The University of Texas: Austin, TX.

2. Clausi, D.T. and W.J. Koros, "Formation of defect-free polyimide hollow fiber membranes for gas separations," *Journal of Membrane Science*, **167**(1), 79 (2000).

3. Carruthers, S.B., G.L. Ramos, and W.J. Koros, "Morphology of integral-skin layers in hollow-fiber gas-separation membranes," *Journal of Applied Polymer Science*, **90**(2), 399 (2003).

4. Pinnau, I. and W.J. Koros, "Structures and gas separation properties of asymmetric polysulfone membranes made by dry, wet, and dry/wet phase inversion," *Journal of Applied Polymer Science*, **43**(8), 1491 (1991).

5. Chung, T.S., E.R. Kafchinski, and P. Foley, "Development of asymmetric hollow fibers from polyimides for air separation," *Journal of Membrane Science*, **75**(1-2), 181 (1992).

6. Ismail, A.F. and L.P. Yean, "Review on the development of defect-free and ultrathin-skinned asymmetric membranes for gas separation through manipulation of phase inversion and rheological factors," *Journal of Applied Polymer Science*, **88**(2), 442 (2003).

7. Kurdi, J. and A.Y. Tremblay, "Preparation of defect-free Asymmetric membranes for gas separations," *Journal of Applied Polymer Science*, **73**(8), 1471 (1999).

8. Park, H.C., et al., "Effect of solvent exchange on the morphology of asymmetric membranes," *Polymeric Materials Science and Engineering*, **77**, 238 (1997).

9. Punsalan, D.T., *A sorption and dilation investigation of amorphous glassy polymers and physical aging*, in *Chemical Engineering*. 2001, The University of Texas: Austin, TX.

10. Koros, W.J. and D.R. Paul, "Design considerations for measurement of gas sorption in polymers by pressure decay," *Journal of Polymer Science, Polymer Physics Edition*, **14**(10), 1903 (1976).

11. Costello, L.M. and W.J. Koros, "Temperature dependence of gas sorption and transport properties in polymers: measurement and applications," *Industrial & Engineering Chemistry Research*, **31**(12), 2708 (1992).

12. Fleming, G.K., *Dilation of silicone rubber and glassy polycarbonates due to high pressure gas sorption*, in *Chemical Engineering*. 1988, The University of Texas: Austin, TX.

13. McBain, J.W., H.P. Lucas, and P.F. Chapman, "The sorption of organic vapors by highly evacuated activated sugar charcoal," *Journal of the American Chemical Society*, **52**, 2668 (1930).

14. McBain, J.W. and A.M. Bakr, "A new sorption balance," *Journal of the American Chemical Society*, **48**, 690 (1926).

15. Jacques, C.H.M. and H.B. Hopfenberg, "Vapor and liquid equilibriums in glassy polyblends of polystyrene and poly(2,6-dimethyl-1,4-phenylene oxide)," *Polymer Engineering and Science*, **14**(6), 441 (1974).

16. O'Brien, K.C., et al., "A new technique for the measurement of multicomponent gas transport through polymeric films," *Journal of Membrane Science*, **29**(3), 229 (1986).

17. Pye, D.G., H.H. Hoehn, and M. Panar, "Measurement of gas permeability of polymers. I. Permeabilities in constant volume/variable pressure apparatus," *Journal of Applied Polymer Science*, **20**(7), 1921 (1976).

18. Moore, T.T., et al., "Characterization of low permeability gas separation membranes and barrier materials; design and operation considerations," *Journal of Membrane Science*, **245**(1-2), 227 (2004).

19. Kesting, R.E. and A.K. Fritzsche, *Polymeric Gas Separation Membranes*. 1993, New York: John Wiley & Sons, Inc.

20. *HP 3396 Integrator Operating Manual*. 2nd ed. 1997: Hewlett-Packard Company.

CHAPTER 4

AGE-DEPENDENT SORPTION AND TRANSPORT OF CARBON DIOXIDE IN ASYMMETRIC HOLLOW FIBER MEMBRANES

This chapter presents efforts made to replicate previous observations of highly age-dependent sorption of carbon dioxide into Matrimid® asymmetric hollow fiber membranes. Furthermore, this chapter presents first time observation of an age-dependent carbon dioxide plasticization pressure in Matrimid® asymmetric hollow fiber membranes.

4.1 Age Dependent Sorption

Previous investigators observed highly age-dependent sorption of carbon dioxide in Matrimid® asymmetric hollow fiber membranes as shown in Figure 4.1 [1, 2]. The age-dependence is characterized by a pronounced inflection in the sorption isotherm at a carbon dioxide pressure of approximately 450 psia. As the age of the fibers increases, the degree of the inflection at 450 psia diminishes, until the sorption of carbon dioxide in the fiber sample is approximately equivalent to that in the film sample. Each isotherm shown in Figure 4.1 was measured using previously untested fiber samples formed at the same time using the same set of spinning parameters. During the aging period, the fiber samples are simply stored in a sealed plastic bag in ambient laboratory conditions. A subsequent batch of fibers, labeled Sample B in Figure 4.1, was tested by a separate investigator, Mohammed Al-Juaied, and showed similar anomalous sorption behavior.

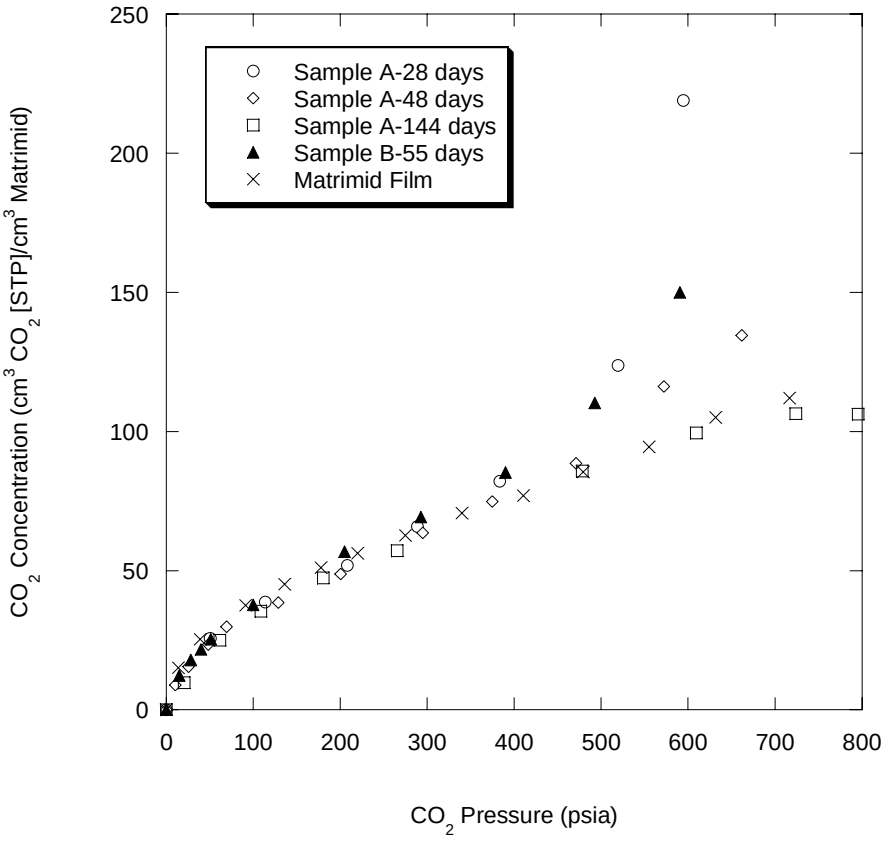

Figure 4.1: Enhanced, age dependent sorption of CO_2 in Matrimid® asymmetric hollow fibers (Samples A and B) compared to sorption in a thick, dense Matrimid® film at 35 ^{o}C [2].

Observations of inflections in sorption isotherms have been made previously in highly sorbing and highly plasticized penetrant/polymer systems [3-6]. In these cases, the plasticization caused by penetrant sorption is known to greatly lower the glass transition temperature of the material. In this case, the inflection point in the sorption isotherm marks the penetrant pressure at which the glass transition temperature of the material has been reduced to the temperature of observation, indicating the occurrence of a glass-to-rubber transition during collection of the

isotherm. However, it is hard to explain how this type of extreme plasticization would diminish over time, as required to explain the behavior shown in Figure 4.1.

4.1.1 Attempts to Replicate Anomalous Behavior

Unfortunately, efforts to controllably replicate the behavior observed in Figure 4.1 were unsuccessful. Despite the fact that the behavior in Figure 4.1 has proven hard to controllable replicate, it is not simply believed to be an artifact or result of poor experimental procedure; since the anomalous sorption behavior was observed by two independent researchers using two separate batches of fibers, Samples A and B. Two series of experiments were conducted in an effort to replicate the behavior in Figure 4.1 and are described below. Even though the results of these experiments did not successfully replicate the anomalous sorption behavior, they may be used as guide for future efforts.

4.1.1.1 Alteration of THF concentration

The Matrimid® fibers produced in our laboratory are unique because they are characterized by a thin, defect-free skin layer, which achieves a selectivity of at least 95% of the observed selectivity in a thick, dense Matrimid® film. As described in Chapter 3, these defect-free fibers are spun from a quaternary solution which contains a volatile solvent, tetrahydrofuran (THF), to facilitate skin formation. Increasing the concentration of THF in the spin dope has two effects on fiber formation [7]. Firstly, the increased concentration of THF allows for greater solvent evaporation as the nascent fiber passes through the air gap. This greater loss of solvent in the air gap

leads to a thicker selective skin. The second effect is a direct result of the first. The thicker skin slows the transport of water from the quench bath into the bulk of the fiber. This slower transport of water into the bulk of the fiber results in slowing the phase separation process which produces the porous substructure of the fiber.

It was believed that the highly age-dependent carbon dioxide sorption behavior shown in Figure 4.1 was the result of quenching the fiber into a highly non-equilibrium initial state. This highly non-equilibrium initial state contained packets of unrelaxed free volume large enough to allow for capillary-like condensation of carbon dioxide resulting in the observed inflection in carbon dioxide sorption. As the fibers underwent the processes of physical aging described in Chapter 3, the initial large packets of unrelaxed free volume were recovered and the overall polymer matrix densified, resulting in the diminished inflection in carbon dioxide sorption with time.

As described earlier, by varying the composition of THF in the spin dope, one is able to affect the initial non-equilibrium state of the fiber substructure. A fiber spun from a dope containing a relatively high concentration of THF will have a thicker skin and thus a more slowly phase separated or (less non-equilibrium) substructure. A fiber spun from a dope containing a relatively low concentration of THF will have a thinner skin and thus a more quickly phase separated or more non-equilibrium substructure. With this understanding fibers were spun from spin dopes containing 0%, 5.9% and 20% THF and carbon dioxide sorption isotherms were collected for each set of fibers. The exact composition of the spin dope solutions are given in Table 4.1. The sorption isotherms shown in Figure 4.1 were collected for

fibers spun from a spin dope containing 5.9% THF, nominally the same concentrations as shown for Sample D in Table 4.1.

Table 4.1: Concentration of Matrimid® spin dopes in wt. %

	Matrimid®	NMP	Methanol	THF
Sample C	26.2	58.8	15.0	-
Sample D	26.2	52.9	15.0	5.9
Sample E	26.2	42.0	11.7	20.1

Surprisingly, as shown in Figure 4.2, varying the THF concentration of the spin dope resulted in only small differences in the carbon dioxide sorption isotherms. There is no discernable trend in carbon dioxide sorption with THF dope concentration. For reference Figure 4.2 includes the sorption isotherm for carbon dioxide in a dense, thick, solvent-cast Matrimid® film. Unlike the sorption behavior shown in Figure 4.1, for all fiber samples tested in Figure 4.2 the sorption of carbon dioxide is in close agreement with that observed in a film sample. It is important to note that all samples shown in Figure 4.2 are of a relatively "young" age, well within the 144 day aging period shown in Figure 4.1.

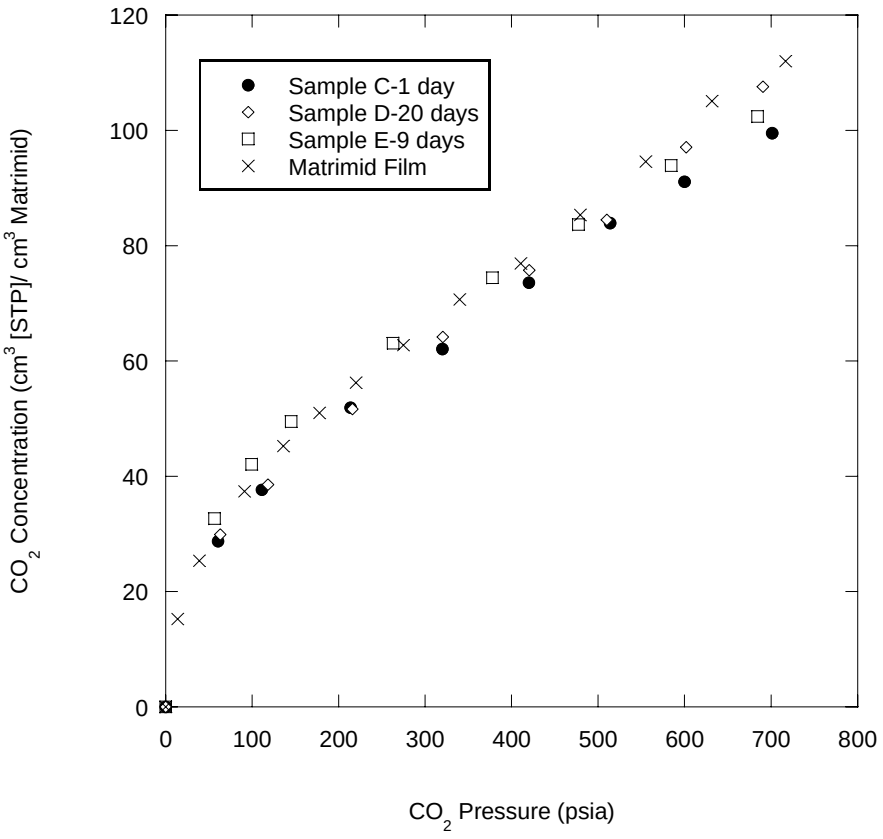

Figure 4.2: Effect of THF spin dope concentration on carbon dioxide sorption at 35 ^{o}C in Matrimid® asymmetric hollow fiber membranes

4.1.1.2 Alteration of solvent exchange/drying procedures

The dry-jet/wet-quench spinning technique used in our laboratory and described in Chapter 3 produces a water saturated fiber. These water saturated fibers are solvent exchanged and dried under vacuum prior to sorption testing. The standard solvent exchange process used in our laboratory involves three 20-minute washes in methanol, followed by three 20-minute washes in hexanes, a 30-minute air dry, and final drying at 120^{o}C under vacuum for one hour. This solvent exchange process preserves the delicate asymmetric morphology and removes any residual chemicals

left in the fibers from the spinning solution (i.e. THF, ethanol, N-methylpyrrolidinone).

The possibility of residual solvent or water left in the fibers, due to a poor solvent exchange or inadequate drying, leading to the behavior shown in Figure 4.1 was investigated. Three sets of fiber were spun and underwent varying solvent exchange processes. One set of fibers was solvent exchanged using the normal procedure as described above and is labeled as "Sample F-21" days in Figure 4.3. A separate set of fibers was not solvent exchanged with methanol and hexanes but was dried at 120 ^{o}C for one hour under vacuum and is labeled as "Sample G-7" days in Figure 4.3. The final set of fibers was simply air dried after spinning and is labeled as "Sample H-7" days in Figure 4.3. Table 4.2 summarizes the various solvent exchange/drying histories of all fibers shown in Figure 4.3. These fibers were also tested by thermo-gravimetric analysis and had a mass loss of 1.1%, 1.4%, 5.9%, respectively, after heating to 400 ^{o}C at a rate of 10 ^{o}C/min. Even though the poorly solvent exchanged fibers showed a greater mass loss, their carbon dioxide sorption isotherms do not reflect the behavior shown in Figure 4.1.

Table 4.2: Summary of solvent exchange and drying procedures used for fiber samples tested in Figure 4.3

	Solvent Exchanged	Air Dried	Vacuum Dried
Sample F	Yes	Yes	Yes
Sample G	No	Yes	Yes
Sample H	No	Yes	No

As shown in Figure 4.3, the carbon dioxide sorption isotherms of the poorly solvent exchanged fibers actually lie below the sorption isotherm of the properly solvent exchanged fibers and that of the thick, dense Matrimid® film. This behavior is believed to occur because residual solvent or water is occupying sorption sites in the poorly solvent exchanged fibers and thereby lowering the overall carbon dioxide sorption.

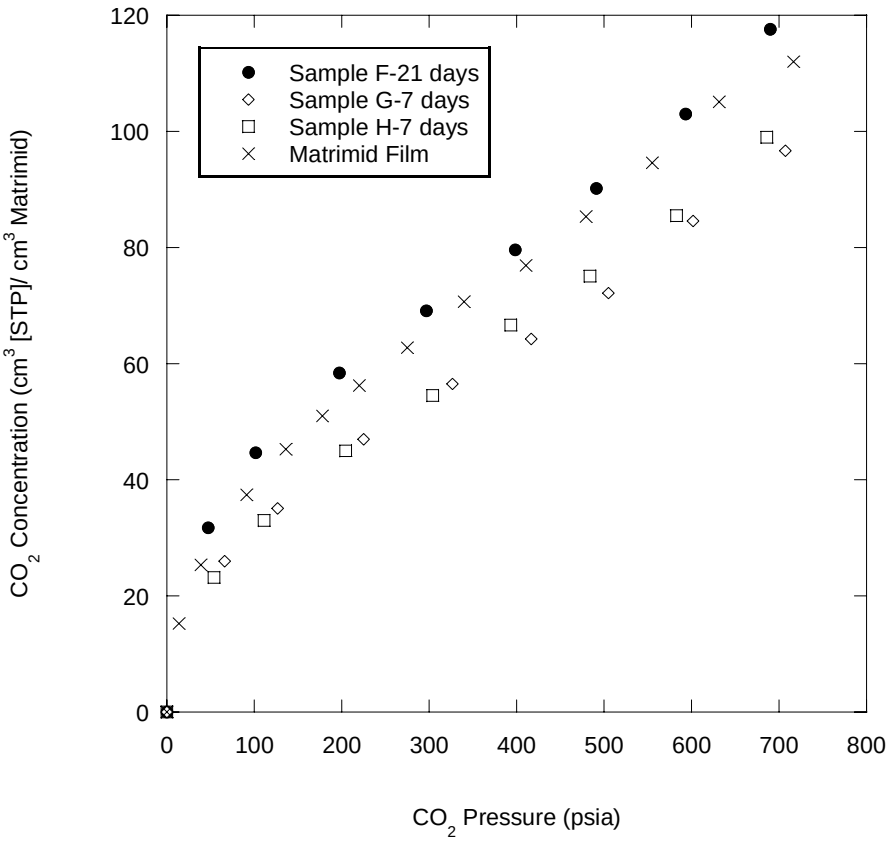

Figure 4.3: Effect of solvent exchange/drying procedures on carbon dioxide sorption at 35 °C in Matrimid® asymmetric hollow fiber membranes [2]

4.1.2 Current Understanding

Although efforts to consistently replicate the behavior shown in Figure 4.1 were unsuccessful, this behavior is not believed to be a result of poor experimental procedure or some other such artifact. Furthermore, a series of experiments, described in the previous section, rules out the possibility of improper solvent exchange or drying inducing the sorption behavior shown in Figure 4.1.

The highly age-dependent carbon dioxide sorption behavior shown in Figure 4.1 is most likely the result of quenching the fiber into an initially highly non-equilibrium state. This highly non-equilibrium state relaxes through the mechanisms of physical aging, described in Chapter 3, manifesting the observed age-dependency of carbon dioxide sorption. From examination of Figure 3.4, it is apparent that the characteristic dimension of the porous substructure is of the same order of magnitude as the skin thickness, ~120 nanometers. Dramatic effects on gas permeation due to physical aging in thin films and asymmetric membranes with selective skin thicknesses of this order of magnitude have been previously observed [8-10]. It is quite possible that relaxation of the bulk fiber, with a comparable characteristic dimension, from a highly non-equilibrium state could be observed via sorption measurements.

To test this hypothesis the initial non-equilibrium state of the fibers was altered by varying the THF concentration of the spin dope; however, as previously described, this set of experiments was unsuccessful in replicating the sorption behavior shown in Figure 4.1. This set of experiments was most likely unsuccessful because the hollow fiber spinning process is so dynamic that quenching the fiber

along precisely the same pathway to achieve the same initial glassy state is very hard to replicate. Admittedly, the effects of differences between similar non-equilibrium quenching trajectories are usually not so extreme. However, it may be that a vary narrow set of parameters (spinneret temperature, quench bath temperature, draw ratio, etc.) lead to the highly non-equilibrium initial state, while a much wider window of these variables leads to an initial state much more akin to that seen in the dense film. Unfortunately, at the present time, a parameter set is not known to reliably capture these variables in a reproducible manner.

4.2 Carbon Dioxide Permeation

This section discusses the permeation of carbon dioxide through Matrimid® asymmetric hollow fiber membranes. The fibers tested in this section do not undergo the dramatic changes in carbon dioxide sorption observed in Figure 4.1. The fibers tested here experience more traditional physical aging with only small changes observed in the carbon dioxide sorption isotherm over time [11]. To the author's knowledge, the work presented here is the first study of the effect physical aging on the permeation of a plasticizing gas through asymmetric membranes.

4.2.1 Age Dependent Carbon Dioxide Permeation

Pure gas carbon dioxide permeation isotherms were collected on a set of Matrimid® asymmetric hollow fiber membranes over a 278 day aging period and are shown in Figure 4.4. During the aging period, the hollow fiber membranes were stored in a sealed plastic bag under ambient laboratory conditions. Each permeation

isotherm presented in Figure 4.4 was collected from a single fiber module with no previous gas exposure history. Carbon dioxide permeances were measured up to an upstream pressure of approximately 600 psia. The membrane was allowed to equilibrate for 1 hour at each upstream pressure prior to measurement. Below the plasticization pressure, the minima in permeance versus feed pressure, the 1 hour equilibration is much greater than the time required to reach steady state flux through the membrane. Above the plasticization pressure, a steady-state permeance is not reached due to slow relaxations of the plasticized membrane [12]. These slow relaxations result in a prolonged upward creep in permeance at a given feed pressure.

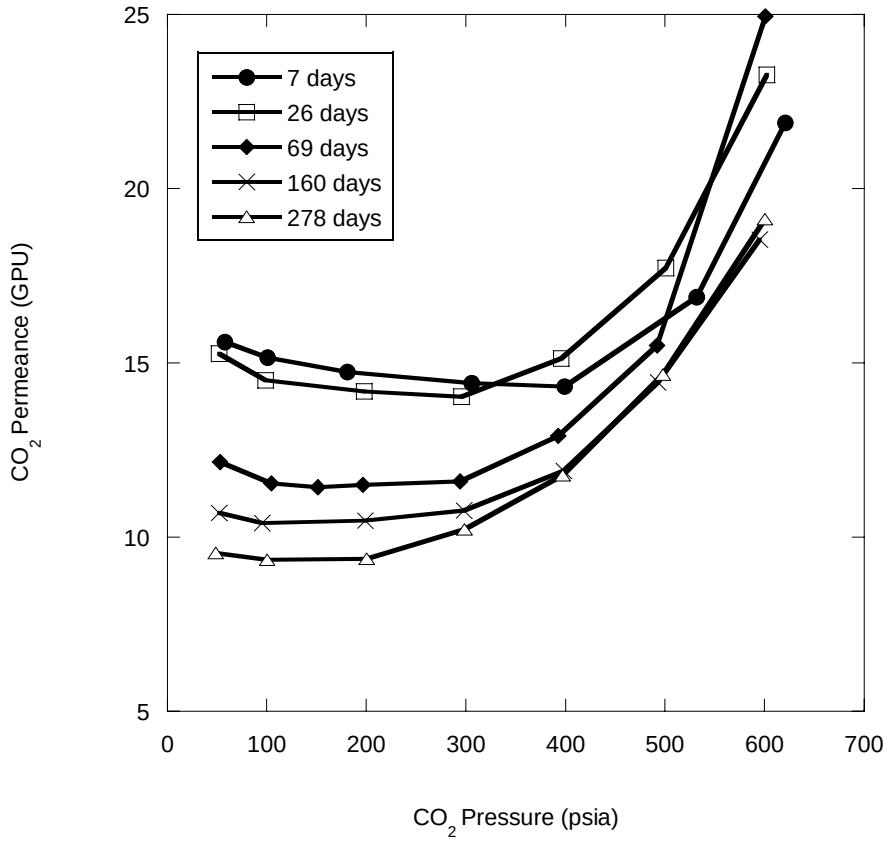

Figure 4.4: Effect of physical aging on carbon dioxide permeation through Matrimid® asymmetric hollow fiber membranes at 35 °C

All of the permeation isotherms in Figure 4.4 show an initial decrease in carbon dioxide permeance with feed pressure. This effect is the result of Langmuir site saturation described by the dual mode transport model detailed in Chapter 2. Furthermore, all of the permeation isotherms in Figure 4.4 clearly show a plasticization pressure, a critical upstream pressure above which the carbon dioxide permeance increases. More importantly, from examination of Figure 4.4, two trends are observed with respect to fiber "age": the loss of permeance at low feed pressures and the reduction of the plasticization pressure as the fiber sample "ages".

Over the 278 day aging period, the carbon dioxide permeance at a feed pressure of 50 psia is reduced by approximately a third. The asymptotic behavior of the reduction in carbon dioxide permeance at 50 psia is best illustrated in Figure 4.5, where the carbon dioxide permance at 50 psia is plotted versus fiber "age". This type of asymptotic loss of permeance is well described by the models of physical aging discussed in Chapter 3, and is similar to accelerated physical aging behavior previously observed for non-plasticizing gases in thin films and asymmetric membranes [8-10].

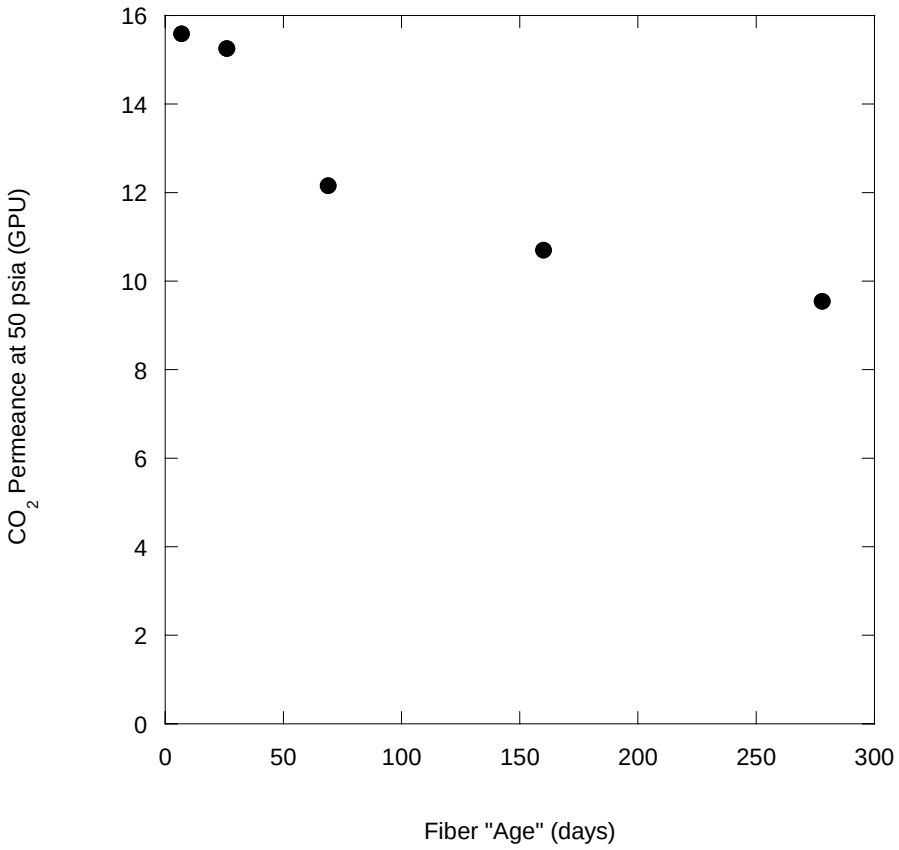

Figure 4.5: Asymptotic reduction in carbon dioxide permeance at 50 psia and 35 ^{o}C due to physical aging

The second trend observed in Figure 4.4 was the reduction in the carbon dioxide plasticization pressure over time. For the "youngest" fiber tested at 7 days, the plasticization pressure was approximately 400 psia. After 278 days, the plasticization pressure was decreased to less than 200 psia. The proposed reason for this reduction in plasticization pressure is explained schematically in Figure 4.6.

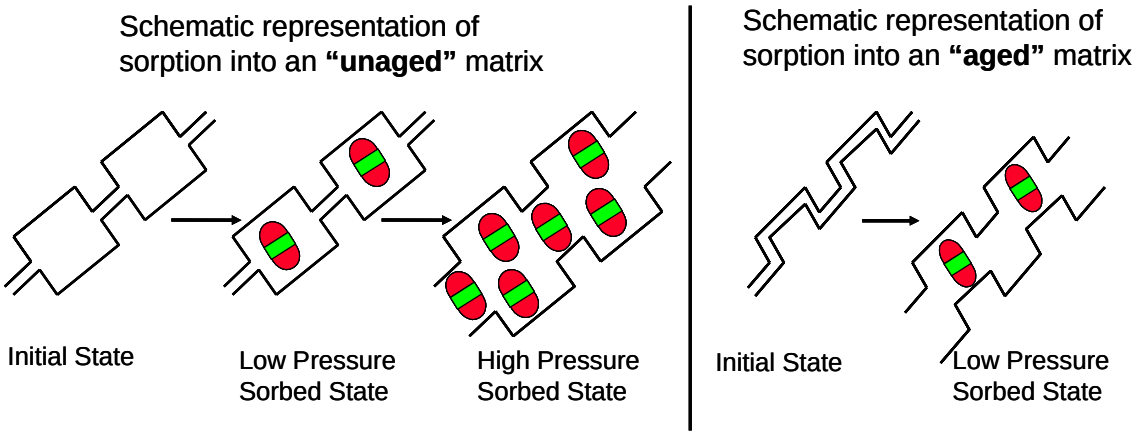

Figure 4.6: Schematic explanation of the reduction carbon dioxide plasticization pressure due to physical aging

In Figure 4.6, the glassy polymer matrix of the membrane is idealized as being composed of polymers chains restricted to simple "crankshaft conformations". In the unaged or "young" fiber samples, these crankshafts are arranged in an initial state containing relatively large amounts of unrelaxed free volume. When fibers of this non-equilibrium state are contacted with carbon dioxide, sorption of carbon dioxide occurs initially into these areas of unrelaxed free volume. In this case only minimal rearrangement of the glassy matrix is required to allow for sorption of carbon dioxide. As the upstream pressure of carbon dioxide is increased, more carbon dioxide is sorbed into the glassy polymer matrix. At a critical upstream pressure, namely the plasticization pressure, the glassy polymer matrix of the membrane must dilate or swell to accommodate the higher concentration of sorbed carbon dioxide. Above the plasticization pressure, the swollen, more open glassy matrix is less resistant to gas transport resulting in an increased carbon dioxide permeance.

In contrast to the "unaged" fiber sample, in the "aged" fiber samples relatively large amounts of unrelaxed free volume are not initially present. These packets of

unrelaxed free volume are not present in the "aged" fiber samples since these samples have been subjected to the processes of physical aging. The one third drop in carbon dioxide permeance at 50 psia over the 278 day aging period as shown in Figure 4.5 is an indication of the substantially denser morphology of the "aged" fiber samples. When carbon dioxide is contacted with this much denser, "aged" glassy polymer matrix, no packets of unrelaxed free volume are available for sorption of carbon dioxide. For the "unaged" sample, even at low concentrations of sorbed carbon dioxide the dense, "aged" glassy polymer matrix must swell to accommodate the sorbed carbon dioxide. This swelling at low upstream pressures of carbon dioxide is reflected by a reduction of the carbon dioxide plasticization pressure in the "aged" fiber samples.

It is important to note that previous investigators have described accelerated plasticization, or plasticization at a lower than expected pressure, in dense, thin films and asymmetric materials [13, 14]. With regards to the current work, the results detailed here indicate that these previous investigations were most likely conducted on "aged" samples. Unfortunately, comparing the "age" of samples from different investigations is very difficult, since the rate of physical aging is highly dependent on the polymer, and its inherent mobility in the glassy state, as well as the characteristic dimension of the sample.

4.2.2. Age Dependent Carbon Dioxide Permeation in Annealed Fibers

In industrial usage, membranes are often heat treated to increase plasticization resistance. The specifics of the heat treatment processes used industrially are closely-

guarded intellectual property; however, several studies on the effects of annealing Matrimid® membranes are available in the academic literature [15-17]. The work of Bos et al. indicated that plasticization resistance in the carbon dioxide/methane system was significantly increased for dense, thick Matrimid® films annealed at a temperature of 220 ^{0}C [15]. Krol et al. using similar annealing treatments observed increased plasticization resistance for Matrimid® membranes to propylene [16]. Zhou observed improved performance for annealed Matrimid® asymmetric hollow fiber membranes used in the pervaporation of acetic acid and water [17].

In this work, the impact of annealing on the carbon dioxide induced plasticization of Matrimid® asymmetric hollow fiber membranes was studied. The fibers were annealed overnight, under vacuum, and at a temperature of 220 ^{0}C, following the work of Bos and Zhou. The actual annealing time for all fiber samples tested ranged between 12 and 16 hours.

The impact of this annealing treatment on permeation isotherms for pure carbon dioxide is shown in Figure 4.7. The annealed fibers used in these tests were obtained from the same batch of fibers shown in Figure 4.4. The annealed fibers were heat treated after an aging period of 303 and 389 days, respectively. The fibers were permeation tested 24-hours after completion of the annealing treatment. In Figure 4.7, the carbon dioxide permeation isotherms for 7-day and 278-day "old" non-annealed fibers from Figure 4.4 are shown for reference.

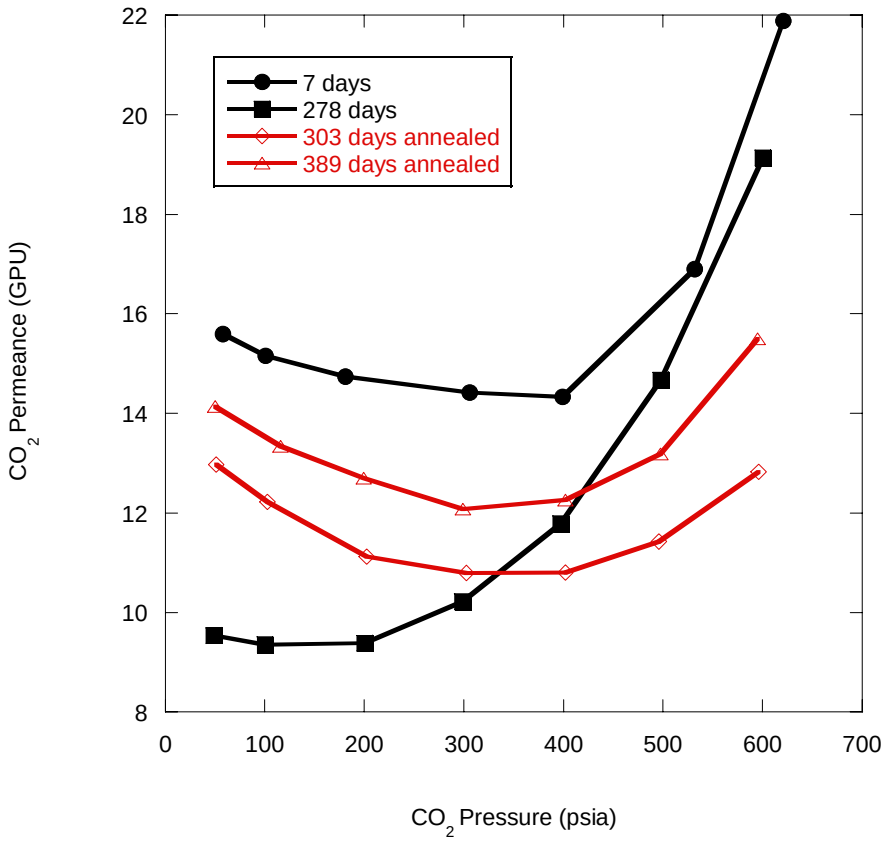

Figure 4.7: Effect of annealing on carbon dioxide permeation through Matrimid® asymmetric hollow fiber membranes at 35 ^{o}C

From examination of Figure 4.7, it is evident that the annealing treatment increases the carbon dioxide plasticization pressure. For non-annealed fibers of a similar "age", the plasticization pressure is less than 200 psia. In the annealed fibers, the plasticization pressure increases to approximately 350 psia. A plasticization pressure of approximately 350 psia was also observed for 7 day "old" non-annealed fibers. Annealing at 220 ^{0}C effectively restores the plasticization resistance lost as a result of physical aging. Furthermore, the degree of upswing in the carbon dioxide permeance above the plasticization pressure is less in the annealed fibers indicating an added stability relative to the 7-day "old" non-annealed fiber sample.

Molecularly, the increases in plasticization resistance brought about by annealing have been described as a result of the formation of charge transfer complexes [15, 18, 19]. Specifically, in recent work, Zhou obtained results from fluorescence spectroscopy supporting the formation of charge transfer complexes in Matrimid® hollow fiber membranes annealed at 220 ^{o}C [17]. The formation of charge transfer complexes is a well-known phenomenon in polyimides, resulting from the interaction of areas of high and low electron densities along the polymer backbone [20-24]. The regions of high electron density are the six-member aromatic rings, and the regions of low electron density are the five-member rings [16]. These regions are clearly shown for Matrimid® in Figure 3.1. When these regions approach each other π-electron interaction occurs, forming a complex which restricts chain mobility. During the annealing process, even at temperatures below the glass transition temperature, it is believed that enough additional segmental motion is available to allow these areas of opposing electron density to align. The resulting Coulombic interactions, both inter and intra chain, hold the polymer matrix more tightly together, making it harder for sorbed carbon dioxide to swell; thus leading to an increase in the plasticization pressure.

The more surprising effect of annealing shown in Figure 4.7 is the increase in carbon dioxide permeance, relative to non-annealed fibers of a similar age, prior to plasticization. At this time, the molecular underpinnings of this effect are only speculative. It may be that the formation of charge transfer complexes during the annealing process produces a similar effect to the formation of crosslinks in other

systems. Wind et al. studied the crosslinking of the 6FDA-DAM:DABA system shown in Figure 4.8 [25, 26].

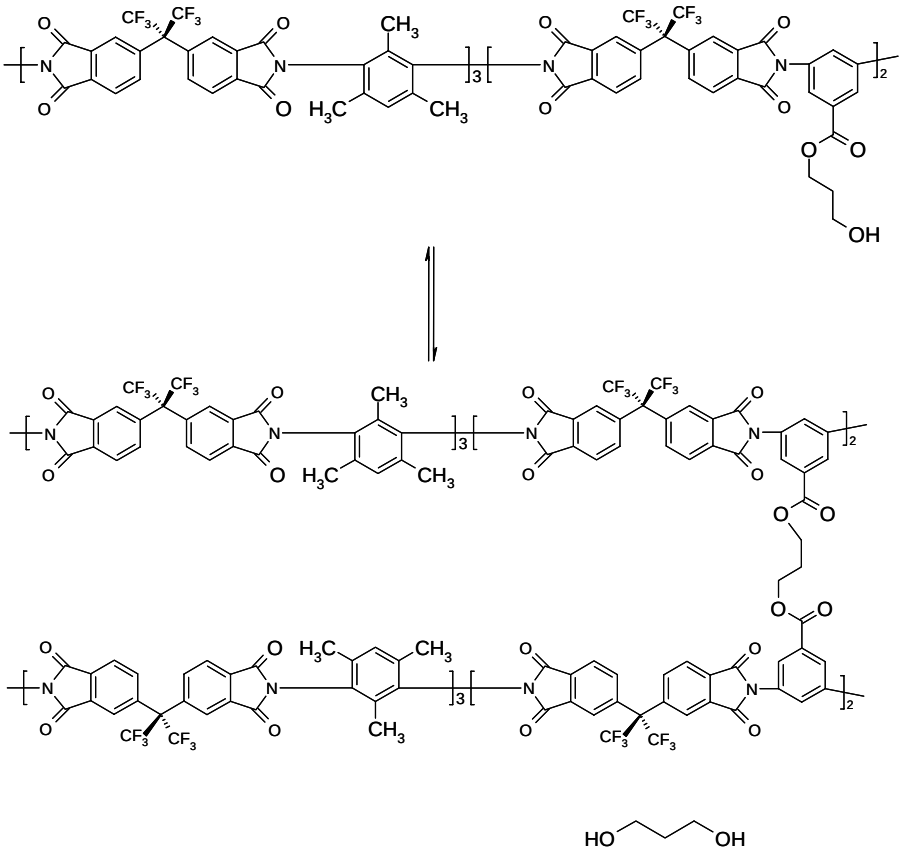

Figure 4.8: 6FDA-DAM:DABA system crosslinked with propylene glycol [27]

In this system, various crosslinking agents were used to covalently bond the polymer chains together. The role of the crosslinking agent size on the carbon dioxide permeance was studied. It was found that for small crosslinking agents, such as ethylene glycol, the carbon dioxide permeance was greater in the crosslinked polymer than in the non-crosslinked polymer as shown in Figure 4.9.

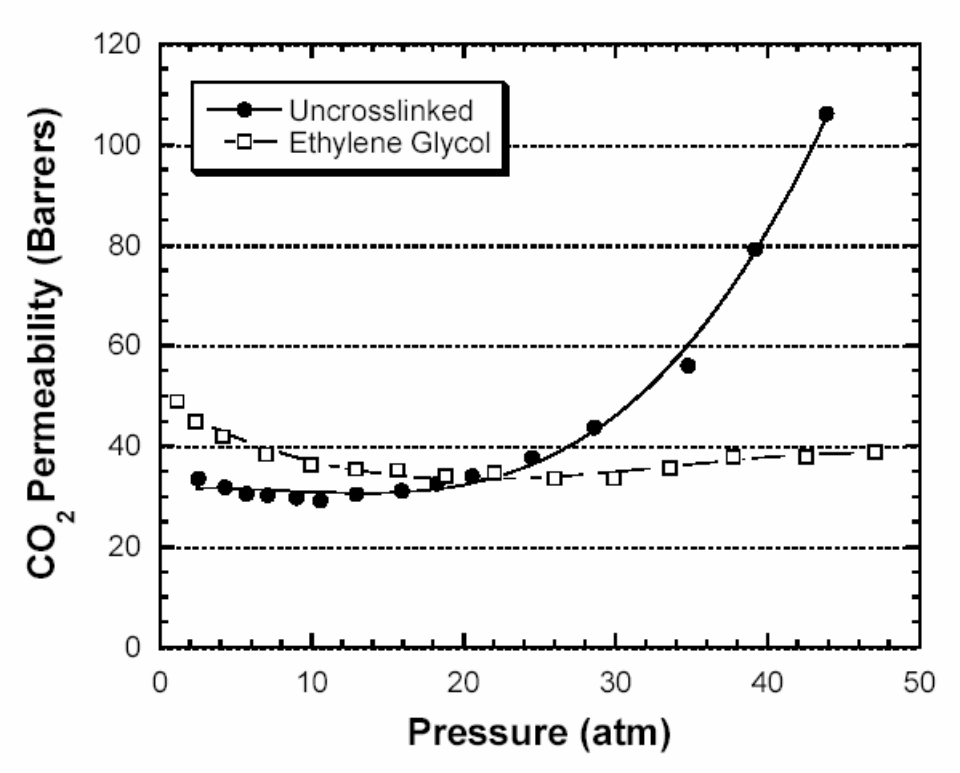

Figure 4.9: Effect of crosslinking on carbon dioxide permeance in 6FDA-DAM:DABA [26]

This effect was explained by considering that the small crosslinking agent acted as a non-flexible linker, which propped the matrix open and increased the carbon dioxide permeance. As the size of the crosslinking agent increases, the crosslinking agent gains more flexibility and no longer acts as a stiff linker between polymer chains. In the case where butylenes glycol was used as a crosslinking agent, the carbon dioxide permeance in the crosslinked polymer was less than the carbon dioxide permeance in the uncrosslinked polymer. Due to the similarity in the behaviors shown in Figures 4.7 and 4.9, charge transfer complexes in annealed samples of Matrimid® may be

acting as stiff, non-flexible linkers between the chains; however, at this time, this interpretation is completely speculative.

4.3 Summary

Previous researchers observed significant age-dependent sorption of carbon dioxide in Matrimid® asymmetric hollow fiber membranes [1, 2]. Attempts to consistently replicate this behavior by altering the spin dope composition and solvent exchange/drying procedures were unsuccessful. The age-dependent carbon dioxide sorption behavior is most likely the result of quenching the bulk of the fiber into an initially highly non-equilibrium state which rapidly ages away due to the small characteristic dimension of the fiber substructure and skin. It is believed that only a small window of dope composition and spinning parameters will lead to this initially highly non-equilibrium state.

In the vast majority of fibers produced in our laboratory, only subtle effects on carbon dioxide sorption are observed as the fibers "age". In these traditional fibers, even though only small effects are seen in the carbon dioxide sorption, significant effects are observed in the carbon dioxide permeance as the fibers "age". The carbon dioxide permeance prior to plasticization experiences a substantial decline over time, which is an effect of physical aging previously seen with non-plasticizing gases. More interesting is the first time observation of an age-dependent plasticization pressure. The carbon dioxide plasticization pressure was observed to decrease by approximately 150 psia over a 278 day period. The effect of annealing on the carbon dioxide permeance was also studied. In fibers annealed overnight at 220 ^{0}C, the

carbon dioxide permeance prior to plasticization and the plasticization pressure increased relative to non-annealed fibers of a similar age.

In the future, work studying the effect of physical aging on carbon dioxide plasticization using mixed gas feed streams of carbon dioxide and methane would be of great interest. There is recent evidence that the effect of carbon dioxide plasticization is diminished in the mixed gas case compared to the pure gas case [28]. Understanding how physical aging affects both the carbon dioxide permeance and carbon dioxide/methane selectivity in the mixed gas case would be of significant interest industrially. Furthermore, a better understanding of the molecular-scale impact of annealing on the glassy polymer matrix is required. This fundamental work would best be conducted in dense, thin films of Matrimid® where the initial non-equilibrium state is better controlled.

4.4 References

1. Punsalan, D.T., *A sorption and dilation investigation of amorphous glassy polymers and physical aging*, in *Chemical Engineering*. 2001, The University of Texas: Austin, TX.

2. Madden, W.C., D. Punsalan, and W.J. Koros, "Age dependent CO2 sorption in Matrimid asymmetric hollow fiber membranes," *Polymer*, **46**(15), 5433 (2005).

3. Wissinger, R.G. and M.E. Paulaitis, "Glass transitions in polymer/carbon dioxide mixtures at elevated pressures," *Journal of Polymer Science, Part B: Polymer Physics*, **29**(5), 631 (1991).

4. Alessi, P., et al., "Plasticization of polymers with supercritical carbon dioxide: Experimental determination of glass-transition temperatures," *Journal of Applied Polymer Science*, **88**(9), 2189 (2003).

5. Chiou, J.S. and D.R. Paul, "Gas sorption and permeation in poly(ethyl methacrylate)," *Journal of Membrane Science*, **45**(1-2), 167 (1989).

6. Chiou, J.S., Y. Maeda, and D.R. Paul, "Gas and vapor sorption in polymers just below Tg," *Journal of Applied Polymer Science*, **30**(10), 4019 (1985).

7. Carruthers, S.B., G.L. Ramos, and W.J. Koros, "Morphology of integral-skin layers in hollow-fiber gas-separation membranes," *Journal of Applied Polymer Science*, **90**(2), 399 (2003).

8. Pfromm, P.H. and W.J. Koros, "Accelerated physical aging of thin glassy polymer films: evidence from gas transport measurements," *Polymer*, **36**(12), 2379 (1995).

9. Rezac, M.E., et al., "Aging of thin polyimide-ceramic and polycarbonate-ceramic composite membranes," *Industrial & Engineering Chemistry Research*, **32**(9), 1921 (1993).

10. Chung, T.S. and S.K. Teoh, "The ageing phenomenon of polyethersulphone hollow fibre membranes for gas separation and their characteristics," *Journal of Membrane Science*, **152**(2), 175 (1999).

11. Punsalan, D. and W.J. Koros, "Thickness-dependent sorption and effects of physical aging in a polyimide sample," *Journal of Applied Polymer Science*, **96**(4), 1115 (2005).

12. Wessling, M., et al., "Plasticization of gas separation membranes," *Gas Separation & Purification*, **5**(4), 222 (1991).

13. Kapantaidakis, G.C., et al., "CO2 plasticization of polyethersulfone/polyimide gas-separation membranes," *AIChE Journal*, **49**(7), 1702 (2003).

14. Wessling, M., M.L. Lopez, and H. Strathmann, "Accelerated plasticization of thin-film composite membranes used in gas separation," *Separation and Purification Technology*, **24**(1-2), 223 (2001).

15. Bos, A., et al., "Plasticization-resistant glassy polyimide membranes for CO2/CH4 separations," *Separation and Purification Technology*, **14**(1-3), 27 (1998).

16. Krol, J.J., M. Boerrigter, and G.H. Koops, "Polyimide hollow fiber gas separation membranes: preparation and the suppression of plasticization in propane/propylene environments," *Journal of Membrane Science*, **184**(2), 275 (2001).

17. Zhou, F., *Novel Pervaporation for Separating Acetic Acid and Water Mixtures Using Hollow Fiber Membranes*, in *Chemical and Biomolecular Engineering*. 2005, Georgia Institute of Technology: Atlanta, GA.

18. Mikawa, M., S. Nagaoka, and H. Kawakami, "Gas transport properties and molecular motions of 6FDA copolyimides," *Journal of Membrane Science*, **163**(2), 167 (1999).

19. Kawakami, H., M. Mikawa, and S. Nagaoka, "Gas transport properties in thermally cured aromatic polyimide membranes," *Journal of Membrane Science*, **118**(2), 223 (1996).

20. Hasegawa, M., et al., "Molecular aggregation and fluorescence spectra of aromatic polyimides," *European Polymer Journal*, **25**(4), 349 (1989).

21. Ishida, H., et al., "Spectroscopic studies of poly[N,N'-bis(phenoxyphenyl)pyromellitimide]. 1. Structures of the polyimide and three model compounds," *Macromolecules*, **13**(4), 826 (1980).

22. Dine-Hart, R.A. and W.W. Wright, "Properties of aromatic imides," *Makromolekulare Chemie*, **143**, 189 (1971).

23. Huang, H.W., K. Horie, and R. Yokota, "Differences in thermo-mechanical properties and intermolecular charge-transfer characteristics of the aromatic polyimide PI(BPDA/PDA) from various precursors," *Macromolecular Chemistry and Physics*, **200**(4), 791 (1999).

24. Dinan, F.J., et al., "Solid-state carbon-13 NMR spectral evidence for charge transfer complex formation in aromatic diimides and dianhydrides," *Journal of Polymer Science, Part A: Polymer Chemistry*, **30**(1), 111 (1992).

25. Wind, J.D., et al., "Solid-State Covalent Cross-Linking of Polyimide Membranes for Carbon Dioxide Plasticization Reduction," *Macromolecules*, **36**(6), 1882 (2003).

26. Wind, J.D., *Improving Polyimide Membrane Resistance to Carbon Dioxide Plasticization in Natural Gas Separations*, in *Chemical Engineering*. 2002, The University of Texas at Austin: Austin, TX.

27. Wallace, D.W., *Crosslinked Hollow Fiber Membranes for Natural Gas Purification and Their Manufacture from Novel Polymers*, in *Chemical Engineering*. 2004, The University of Texas: Austin, TX.

28. Visser, T., G.H. Koops, and M. Wessling, "On the subtle balance between competitive sorption and plasticization effects in asymmetric hollow fiber gas separation membranes," *Journal of Membrane Science*, **252**(1-2), 265 (2005).

CHAPTER 5

SORPTION OF CARBON DIOXIDE, METHANE, TOLUENE, AND n-HEPTANE IN MATRIMID®

In this chapter, the equilibrium sorption isotherms of carbon dioxide, methane, toluene, and n-heptane in Matrimid® asymmetric hollow fiber membranes at 35 ^{o}C will be described. Equilibrium sorption isotherms for these penetrants were collected for both annealed and non-annealed samples. The equilibrium sorption isotherms will be characterized using the dual mode model of sorption in glassy polymers. Furthermore, the transient sorption kinetics were collected for toluene and n-heptane. The kinetic sorption data are analyzed in terms of the Berens-Hopfenberg model, which accounts for both diffusion and relaxation-controlled mass uptake of penetrant into the polymer [1].

5.1 Equilibrium Sorption in Matrimid® Asymmetric Hollow Fiber Membranes

Equilibrium sorption isotherms were collected for carbon dioxide and methane using the pressure-decay technique described in Chapter 3. Equilibrium sorption isotherms for toluene and n-heptane were collected gravimetrically using a McBain quartz spring as described in Chapter 3. All isotherms described in this chapter were collected from fibers at least one year after spinning to minimize the effects of physical aging described in Chapter 4. Furthermore, fibers marked as

annealed underwent the same annealing procedure as previously described in Chapter 4 (i.e. 12-16 hour annealing at 220 ^{o}C under vacuum).

5.1.1 Equilibrium Sorption of Carbon Dioxide

The equilibrium sorption isotherms for carbon dioxide in both non-annealed and annealed samples of Matrimid® asymmetric hollow fiber membranes are given in Figure 5.1. The sorption capacity of the annealed fiber sample is substantially lower than that of the non-annealed sample.

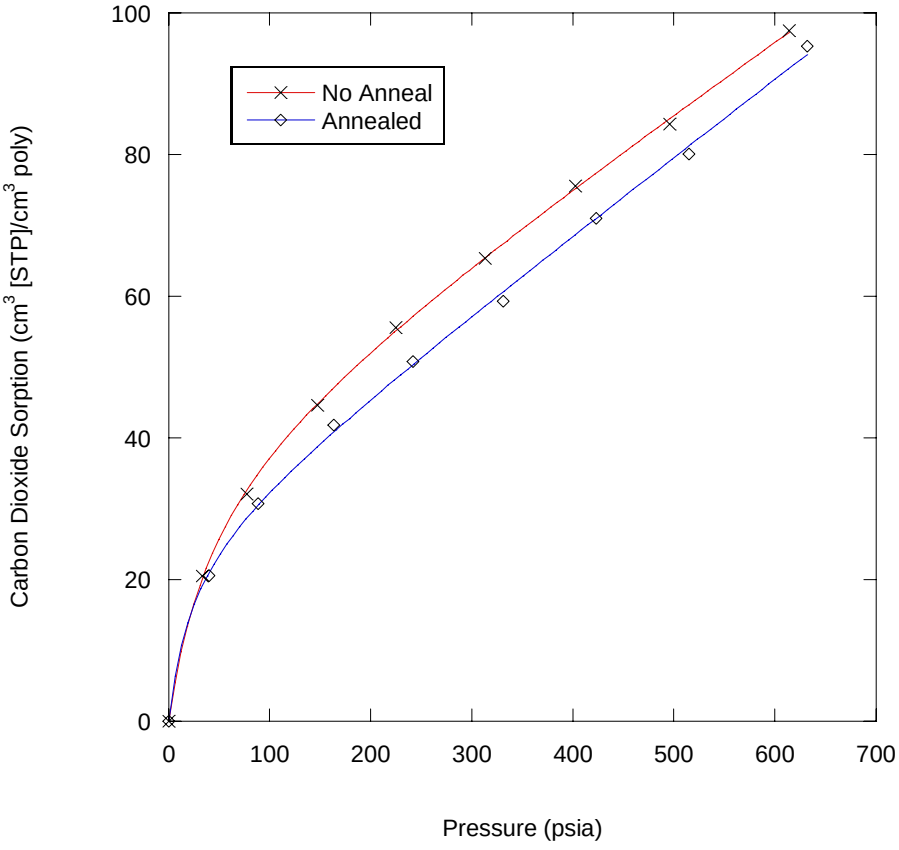

Figure 5.1: Carbon dioxide sorption in Matrimid® asymmetric hollow fibers at 35 ^{o}C. Solid lines are fit to dual mode model.

Both isotherms in Figure 5.1 are well described by the dual mode model of sorption in glassy polymers. The dual mode parameters for carbon dioxide are given in Table 5.1. Annealing of the fiber sample results in a slight increase in the Henry's law constant, k_D, a substantial reduction in the Langmuir capacity constant, C_H', and an increase in the Langmuir affinity constant, *b*.

Table 5.1: Dual mode model parameters for carbon dioxide sorption in Matrimid® asymmetric hollow fibers at 35 °C

Fiber Sample	$k_D \left(\frac{\text{cm}^3\,[\text{STP}]}{\text{cm}^3\ \text{poly} \cdot \text{psia}} \right)$	$C_H' \left(\frac{\text{cm}^3\,[\text{STP}]}{\text{cm}^3\ \text{poly}} \right)$	$b \left(\frac{1}{\text{psia}} \right)$
Non-Annealed	0.098	39	0.022
Annealed	0.110	26	0.043

5.1.2 Equilibrium Sorption of Methane

The equilibrium sorption isotherms for methane in both non-annealed and annealed samples of Matrimid® asymmetric hollow fiber membranes are given in Figure 5.2. The sorption capacity of the annealed fiber sample is substantially lower than that of the non-annealed sample.

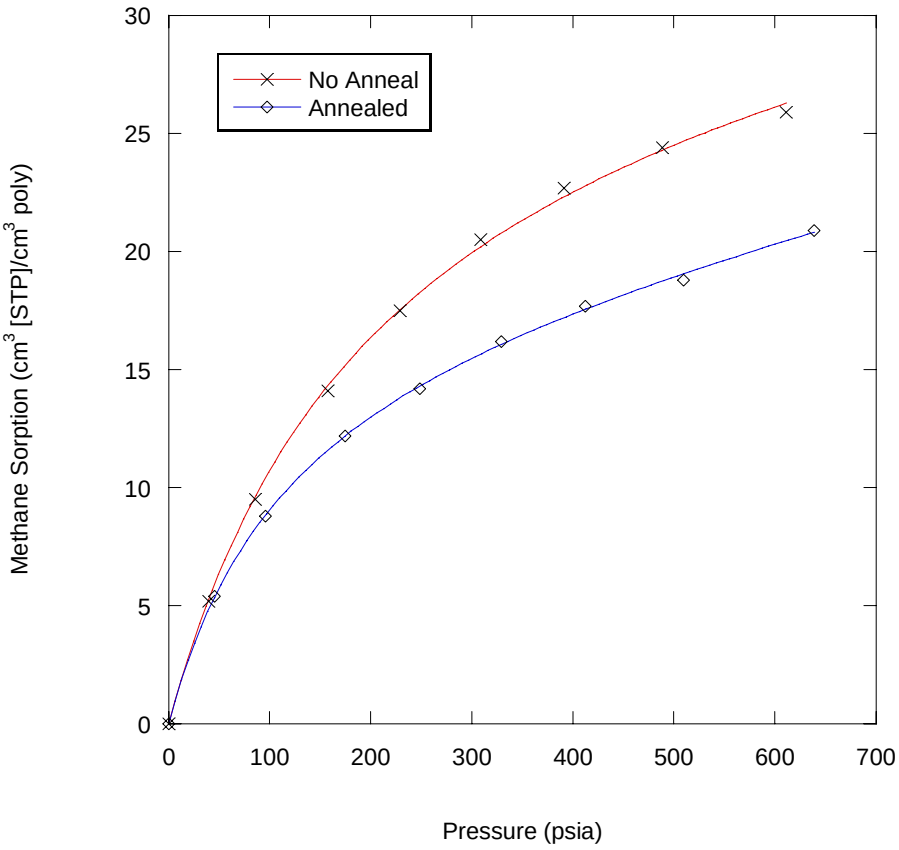

Figure 5.2: Methane sorption in Matrimid® asymmetric hollow fibers at 35 °C. Solid lines are fit to dual mode model.

Both isotherms in Figure 5.2 are well described by the dual mode model of sorption in glassy polymers. The dual mode parameters for methane are given in Table 5.2. As with carbon dioxide, annealing of the fiber sample results in an increase in the Henry's law constant, k_D, a substantial reduction in the Langmuir capacity constant, C_H', and an increase in the Langmuir affinity constant, b.

Table 5.2: Dual mode model parameters for methane sorption in Matrimid® asymmetric hollow fibers at 35 °C

Fiber Sample	$k_D \left(\frac{\text{cm}^3\,[\text{STP}]}{\text{cm}^3\,\text{poly} \cdot \text{psia}} \right)$	$C_H' \left(\frac{\text{cm}^3\,[\text{STP}]}{\text{cm}^3\,\text{poly}} \right)$	$b \left(\frac{1}{\text{psia}} \right)$
Non-Annealed	0.0053	31	0.0050
Annealed	0.0092	18	0.0086

5.1.3 Equilibrium Sorption of Toluene

The equilibrium sorption isotherms for toluene in both non-annealed and annealed samples of Matrimid® asymmetric hollow fiber membranes are given in Figure 5.3. It is important to notice the difference in scale along the pressure axis between Figure 5.3 and Figures 5.1 and 5.2. The pressure in Figure 5.3 is much lower than that in Figures 5.1 and 5.2 due to the finite vapor pressure of toluene; however, even at these low pressures the sorption of toluene is quite substantial. In fact, due to the much higher affinity for toluene, the sorption of toluene at a pressure of only 0.7 psia is approximately the same as the sorption of carbon dioxide at a pressure of 600 psia in non-annealed fibers. As observed previously for carbon dioxide and methane, the toluene sorption capacity of the annealed fiber sample is substantially lower than that of the non-annealed sample.

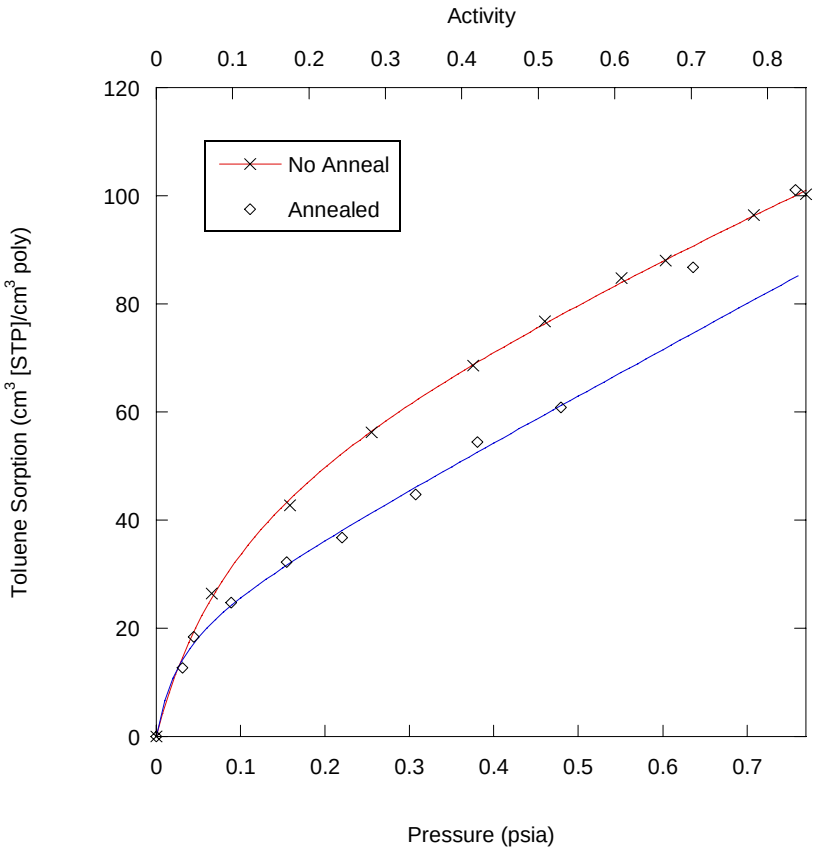

Figure 5.3: Toluene sorption in Matrimid® asymmetric hollow fibers at 35 °C. Solid lines are fit to dual mode model.

The toluene sorption isotherm for non-annealed fibers is well described by the dual mode model at all pressures. The toluene sorption isotherm for annealed fibers is well described by the dual mode model below a pressure of 0.5 psia; however, above 0.5 psia the isotherm shows an upward infliction that the dual mode model is not capable of capturing. At these relatively high pressures, the sorption of toluene in annealed fibers approaches that of non-annealed fibers. Zhou saw a similar behavior for the sorption of acetic acid at high activity in Matrimid® asymmetric hollow fiber membranes [2]. Apparently, the effect of annealing is lost in the presence of high activities of highly sorbing penetrants. The dual mode parameters for toluene are

given in Table 5.3. As with carbon dioxide and methane, annealing of the fiber sample results in an increase in the Henry's law constant, k_D, a substantial reduction in the Langmuir capacity constant, C_H', and an increase in the Langmuir affinity constant, *b*.

Table 5.3: Dual mode model parameters for toluene sorption in Matrimid® asymmetric hollow fibers at 35 °C. Annealed fiber parameters regressed from data below 0.5 psia.

Fiber Sample	$k_D \left(\frac{\text{cm}^3\,[\text{STP}]}{\text{cm}^3\ \text{poly}\cdot\text{psia}}\right)$	$C_H' \left(\frac{\text{cm}^3\,[\text{STP}]}{\text{cm}^3\ \text{poly}}\right)$	$b \left(\frac{1}{\text{psia}}\right)$
Non-Annealed	68	56	9.3
Annealed	84	22	34

5.1.4 Equilibrium Sorption of n-Heptane

The equilibrium sorption isotherms for n-heptane in both non-annealed and annealed samples of Matrimid® asymmetric hollow fiber membranes are given in Figure 5.4. As was seen in the preceding section for toluene, the sorption of n-heptane at a given pressure is also much higher than the sorption of carbon dioxide and methane. As with the previous gases tested, the n-heptane sorption capacity in the annealed fiber samples is substantially lower than that in non-annealed fibers.

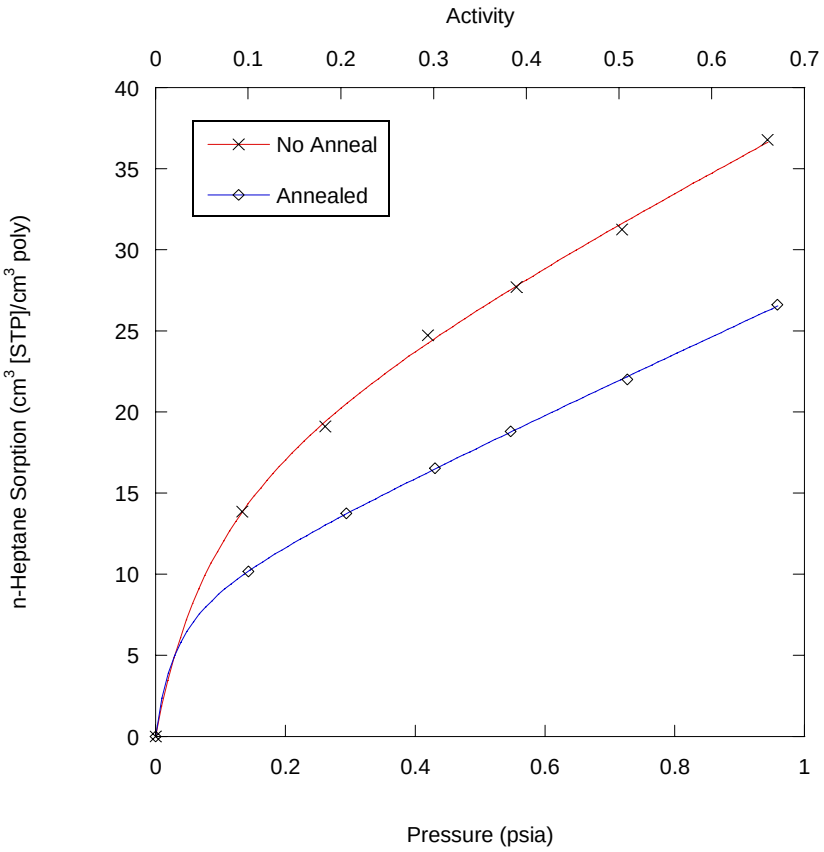

Figure 5.4: n-Heptane sorption in Matrimid® asymmetric hollow fibers at 35 °C. Solid lines are fit to dual mode model.

Both isotherms in Figure 5.4 are well described by the dual mode model of sorption in glassy polymers. The dual mode parameters for n-heptane are given in Table 5.2. Unlike the previous penetrants, annealing of the fiber sample slightly lowers the Henry's law constant, k_D, for n-heptane. However, a substantial reduction in the Langmuir capacity constant, C_H', and an increase in the Langmuir affinity constant, *b*, are observed.

Table 5.4: Dual mode model parameters for n-heptane sorption in Matrimid® asymmetric hollow fibers at 35 °C

Fiber Sample	$k_D \left(\frac{\text{cm}^3\,[\text{STP}]}{\text{cm}^3\,\text{poly} \cdot \text{psia}} \right)$	$C_H' \left(\frac{\text{cm}^3\,[\text{STP}]}{\text{cm}^3\,\text{poly}} \right)$	$b \left(\frac{1}{\text{psia}} \right)$
Non-Annealed	20	20	9.7
Annealed	18	9.2	32

5.1.5 Effect of Annealing on Dual Mode Model Parameters

From examination of Tables 5.1-5.4, it is apparent that the effect of annealing on the dual mode model parameters is quite consistent across the range of penetrants studied in this work. For all penetrants, the value of the Langmuir capacity constant, C_H', decreases and the value of the Langmuir affinity constant, *b*, increases due to annealing. Except for n-heptane, where k_D remains approximately constant, the value of the Henry's Law constant, k_D, increases due to annealing. The fact that annealing results in an increase in k_D and *b* for most cases studied in this work is surprising. In past studies of annealing and physical aging, the effects of these phenomena on the dual mode model parameters were limited to a decrease in C_H' [3-5]. The values of k_D and *b* remained relatively unaffected. In this work, the observed increases in k_D and *b* due to annealing are most likely the result of charge transfer complex formation as discussed in Chapter 4. The formation of these charge transfer complexes essentially forms a new material with the same chemical structure but vastly different inter and intra-chain interactions, which ultimately affect the values of k_D and *b*.

The reduction in C_H' due to annealing, however, exceeds the increases observed in k_D and *b* resulting in the lower equilibrium uptake of penetrant in the annealed samples. The value of C_H' is often correlated with the excess fractional free volume of polymer as [6-9]:

$$C_H' = \left(\frac{V_g - V_\ell}{V_g} \right) \rho^*, \tag{5.1}$$

where, V_g is the specific volume of the polymer in the glassy state, V_ℓ is the specific volume of the polymer in a hypothetical liquid state, and ρ^* is the liquid-like molar density of the penetrant in the Langmuir region. The significant reductions in C_H' for all penetrants due to annealing therefore represent a significant reduction in the free volume of the fibers.

The combination of the work presented in this chapter for equilibrium sorption and the work presented in Chapter 4 for permeation of carbon dioxide in Matrimid® asymmetric hollow fiber membranes *indicate the differences between physical aging and thermal annealing.* In previous studies [10-12], sub-T_g thermal annealing was thought to simply accelerate the rate of physical aging, or the rate of volume reduction. If this assumption holds, only reductions in C_H' would be observed from annealing; however, annealing of Matrimid® asymmetric hollow fibers also results in increased values of k_D and *b*. Furthermore, a simple reduction of C_H' due to annealing would not result in the increase in carbon dioxide permeance prior to plasticization and the increase in carbon dioxide plasticization pressure shown in Chapter 4. This work shows that more than just a reduction in C_H' occurs for thermal

annealing of Matrimid® due to the formation of charge transfer complexes. Furthermore, physical aging, or simply the loss of free volume over time, does not result in the formation of charge transfer complexes. The added mobility at high temperature from thermal annealing is a necessary condition for the formation of charge transfer complexes.

5.2 Transient Vapor Sorption in Matrimid® Asymmetric Hollow Fiber Membranes

Transient sorption isotherms were collected for toluene and n-heptane in non-annealed and annealed Matrimid® asymmetric hollow fiber membranes. Four types of isotherms were observed. Purely Fickian uptake was seen only for toluene sorption in annealed fibers for a change in activity from 0 to 0.05 and is shown in Figure 5.5.

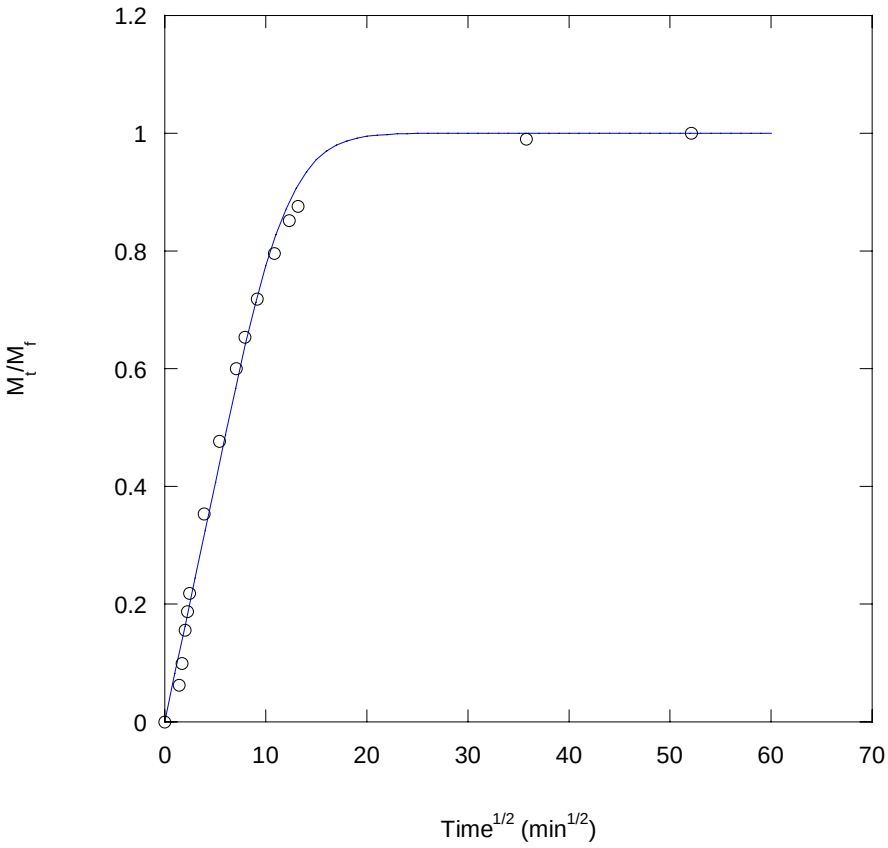

Figure 5.5: Example of diffusion-controlled Fickian uptake for toluene sorption in annealed Matrimid® asymmetric hollow fiber membranes from an activity change of 0.0 to 0.05 at 35 °C. Solid line is Berens-Hopfenberg model fit with $\alpha_R = 0$, $D_A / L^2 = 1.3\times10^{-3}$ cm^2/sec, and $\tau_R = 0$ min.

.

At the other end of the spectrum, purely relaxation-controlled uptake was observed for n-heptane sorption in non-annealed fibers for a change in activity from 0 to 0.09. This behavior is shown in Figure 5.6.

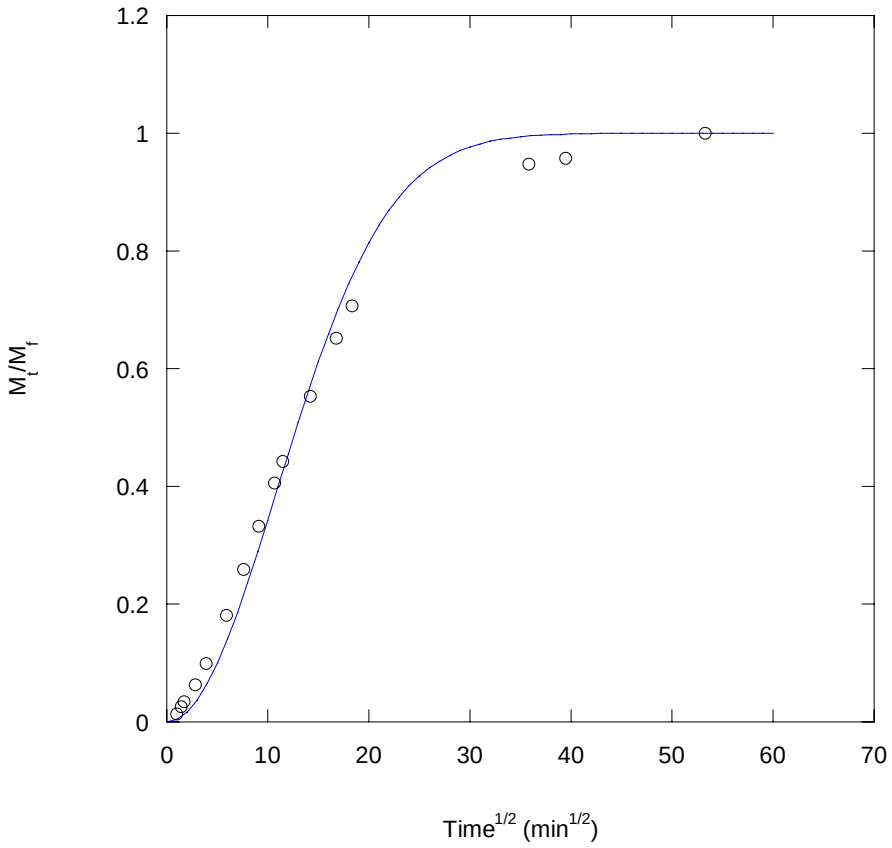

Figure 5.6: Example of relaxation-controlled uptake for n-heptane sorption in Matrimid® asymmetric hollow fiber membranes from an activity change of 0.0 to 0.09 at 35 °C. Solid line is Berens-Hopfenberg model fit with $\alpha_R = 1$, $D_A / L^2 = 0$ cm^2/sec, and $\tau_R =$ 238 min.

However, the majority of the transient sorption isotherms showed some amount of simultaneous diffusion controlled (i.e. Fickian) uptake and relaxation controlled uptake. Transient isotherms which showed uptake by both mechanisms were of two distinct types. The first type was a smooth, concave-down curve gradually approaching the final equilibrium uptake. Figure 5.7 shows this behavior for n-heptane sorption in non-annealed fibers from a 0.09 to 0.18 step in activity.

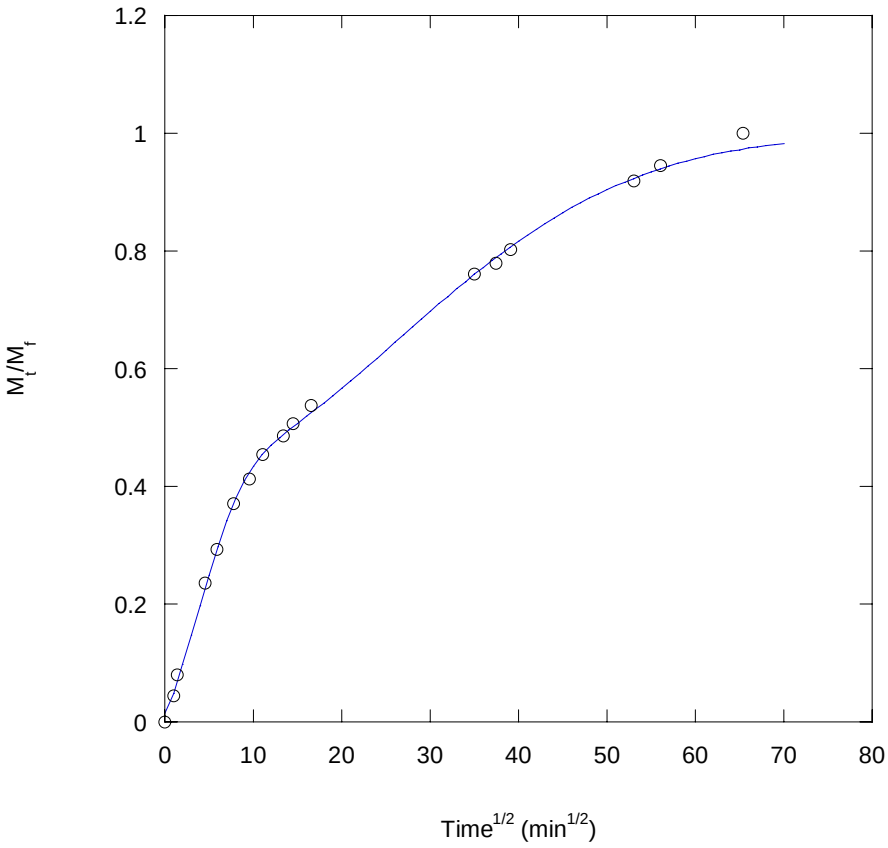

Figure 5.7: Example of simultaneous diffusion and relaxation-controlled uptake for n-heptane sorption in Matrimid® asymmetric hollow fiber membranes from an activity change of 0.09 to 0.18 at 35 °C. Solid line is Berens-Hopfenberg model fit with $\alpha_R = 0.58$, $D_A / L^2 = 2.5\times10^{-3}$ cm^2/sec, and $\tau_R = 1391$ min.

.

The second type of transient isotherm more clearly showed vapor uptake by both diffusion and relaxation-controlled processes. In these so-called "two-stage" transient sorption isotherms, an initial quick diffusion-controlled, Fickian uptake is followed by a longer relaxation-controlled uptake [13, 14]. This behavior is show in Figure 5.8 for toluene sorption in non-annealed fibers from a 0.51 to 0.61 activity step.

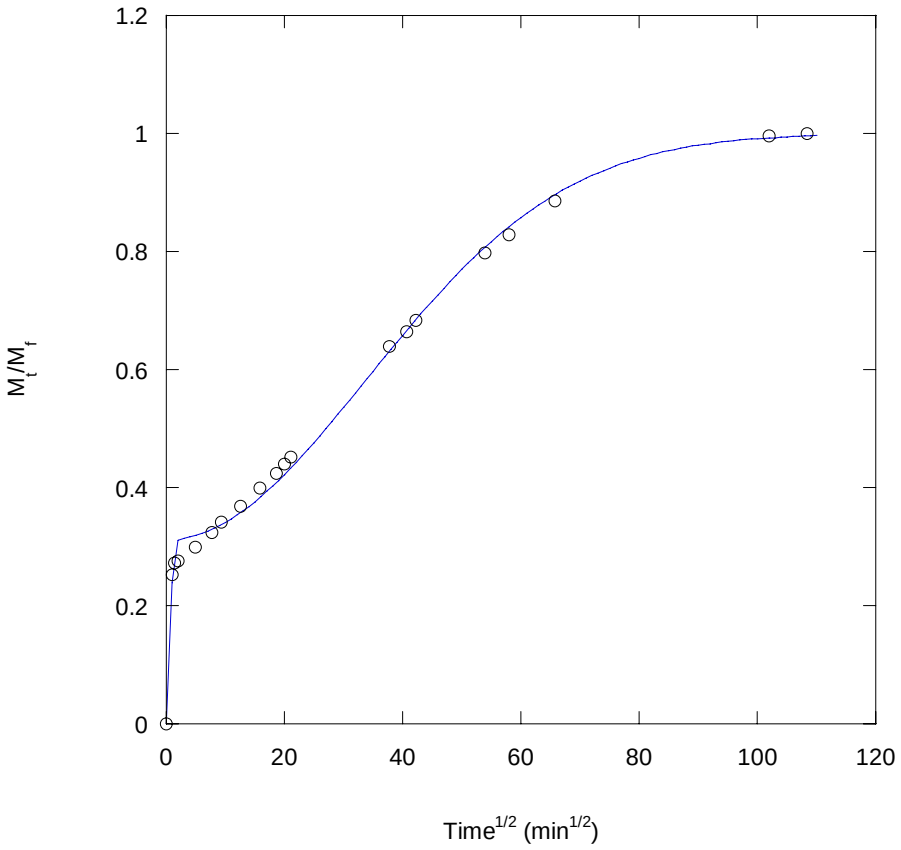

Figure 5.8: Example of "two-stage" uptake for toluene sorption in Matrimid® asymmetric hollow fiber membranes from an activity change of 0.51 to 0.61 at 35 °C. Solid line is Berens-Hopfenberg model fit with $\alpha_R = 0.69$, $D_A / L^2 = 1.3\times10^{-1}$ cm^2/sec, and $\tau_R = 2285$ min.

5.2.1 Application of the Berens-Hopfenberg Model

The Berens-Hopfenberg model successfully captures all of the various transient sorption behaviors observed for toluene and n-heptane in Matrimid®. As described in Chapter 2, the Berens-Hopfenberg model accounts for sorption occurring through simultaneous diffusion and relaxation-controlled uptake and is given analytically as [1]:

$$\left(\frac{M_t}{M_\infty}\right)_A = \left[(1-\alpha_R)\left\{1-\sum_{n=0}^{\infty}\frac{8}{\pi^2(2n+1)^2}\exp\left(\frac{-D_A(2n+1)^2\pi^2 t}{L^2}\right)\right\}\right] + \left[\alpha_R\left\{1-\exp\left(\frac{-t}{\tau_R}\right)\right\}\right], \quad (2.15)$$

where D_A is the diffusion coefficient of penetant 'A', L is the characteristic thickness, α_R is the fraction of mass uptake occurring via a relaxation-controlled process, $(1-\alpha_R)$ is the fraction of mass uptake occurring via a diffusion-controlled process, and τ_R is the time constant of the relaxation process. For the case of asymmetric hollow fiber membranes, the characteristic thickness, L, is not precisely known. For this reason, when the Berens-Hopfenberg model is applied to transient sorption in asymmetric hollow fiber membranes, the term D_A / L^2 is treated as a single parameter.

The Berens-Hopfenberg model reduces to purely Fickian uptake when α_R is equal to zero. In this case, the Berens-Hopfenberg model is able to capture the behavior shown in Figure 5.5. On the other hand, when α_R is equal to one, the Berens-Hopfenberg model captures relaxation-controlled uptake as shown in Figure 5.6. In cases where both diffusion and relaxation-controlled uptake occur, such as those shown in Figures 5.7 and 5.8, α_R is equal to a value between 0 and 1. The smooth gradual uptake illustrated in Figure 5.7 occurs when the value of D_A / L^2 is relatively small and the value of τ_R is small to intermediate. The more pronounced "two-stage" sorption, shown in Figure 4.8, occurs when the value of D_A / L^2 is relatively large and the value of τ_R is large.

5.2.2 Description of Berens-Hopfenberg Model Parameters

The Berens-Hopfenberg model parameters are given for toluene and n-heptane sorption in annealed and non-annealed Matrimid® asymmetric hollow fiber membranes for all activities tested in this work in Tables 5.6-5.9, and the raw transient sorption data are available in Appendix C. The Berens-Hopfenberg model fit all of the data remarkably well; however, interpretation of the model parameters is extremely complex. In this section the effect of penetrant activity and thermal history on the Berens-Hopfenberg parameters will be described, and in the following section an interpretation of these results will be offered. Although all of the transient sorption isotherms collected as part of this work are not shown here for the sake of space, the ability of the Berens-Hopfenberg model to fit the diverse range of behaviors observed in this work may be judged from examination of Figures 5.5 to 5.8.

The Berens-Hopfenberg parameters for toluene sorption in non-annealed Matrimid® asymmetric hollow fiber membranes are given in Table 5.6. The sorption of toluene into non-annealed Matrimid® fibers is characterized by a significant relaxation-controlled contribution to the overall mass uptake at all activities. The value of α_R is relatively constant between 0.68 and 0.75 up to an activity of 0.61. At higher activities the value of α_R experiences a decrease to a value of 0.27 at an activity of 0.85. The value of D_A / L^2 continually increases up to an activity of 0.67. At the two activities tested above 0.67, the value of D_A / L^2 is decreased. The value

of the relaxation constant, τ_R, increases continually up to an activity of 0.61. Above this activity τ_R experiences a general decrease.

Table 5.6: Berens-Hopfenberg model parameters for toluene sorption in Matrimid® asymmetric hollow fiber membranes at 35 °C

Activity Change	D_A/L^2 (min^{-1})	α_R	τ_R (min)
0 to 0.07	3.6×10^{-3}	0.75	278
0.07 to 0.18	1.6×10^{-3}	0.68	554
0.18 to 0.28	3.5×10^{-3}	0.76	914
0.28 to 0.41	9.6×10^{-3}	0.74	1141
0.41 to 0.51	5.5×10^{-2}	0.73	1781
0.51 to 0.61	1.3×10^{-1}	0.69	2285
0.61 to 0.67	2.0×10^{-1}	0.40	1352
0.67 to 0.78	7.3×10^{-2}	0.49	1621
0.78 to 0.85	6.0×10^{-2}	0.27	1065

The Berens-Hopfenberg parameters for toluene sorption in annealed Matrimid® asymmetric hollow fiber membranes are given in Table 5.7. Except for the lowest activity data point, all transient sorption isotherms for toluene in annealed Matrimid® fibers show a significant relaxation-controlled contribution to the overall mass uptake. The value of α_R remains fairly constant between values of 0.53 and 0.58 for activities up to 0.34. At higher activities, the value of α_R varies greatly between 0.35 and 0.92. The value of D_A / L^2 continually increases from a value of 1.3×10^{-3} min^{-1} to a value of 3.8×10^{-1} min^{-1} over the tested activity range. The trend in the relaxation constant, τ_R, with activity is less clear. In general, τ_R seems to increase in value up to intermediate activities, and at higher activities τ_R experiences a general decrease in value.

Table 5.7: Berens-Hopfenberg model parameters for toluene sorption in annealed Matrimid® asymmetric hollow fiber membranes at 35 °C

Activity Change	D_A/L^2 (min^{-1})	α_R	τ_R (min)
0 to 0.05	1.3×10^{-3}	0	-
0.05 to 0.10	8.3×10^{-3}	0.53	900
0.10 to 0.17	9.8×10^{-3}	0.58	1381
0.17 to 0.24	1.4×10^{-2}	0.55	2413
0.24 to 0.34	2.2×10^{-2}	0.58	1125
0.34 to 0.39	3.0×10^{-2}	0.72	1709
0.39 to 0.53	9.3×10^{-2}	0.35	857
0.53 to 0.70	5.5×10^{-2}	0.92	695
0.70 to 0.84	3.8×10^{-1}	0.68	743

The Berens-Hopfenberg parameters for n-heptane sorption in non-annealed Matrimid® asymmetric hollow fiber membranes are given in Table 5.8. All transient sorption isotherms for n-heptane in Matrimid® fibers show a significant relaxation-controlled contribution to the overall mass uptake. In fact, the uptake at an activity of 0.09 is completely relaxation controlled (see Figure 5.6). Above this initial activity, the value of α_R remains fairly stable between a value of 0.51 and 0.68 except for at the highest measured activity. At an activity of 0.83, the value of α_R is reduced to 0.18 with the majority of the mass uptake contributed through a diffusion-controlled process. The value of D_A / L^2 increases with activity at low activities. At activities above 0.29, the value of D_A / L^2 is relatively constant between a value of 1.3×10^{-2} min^{-1} and 1.7×10^{-2} min^{-1}. The value of the relaxation constant, τ_R, increases from 238 minutes to 4182 minutes over an activity range of 0.09 to 0.66. At the highest measure activity, 0.83, the value of τ_R decreases to 1900 minutes.

Table 5.8: Berens-Hopfenberg model parameters for n-heptane sorption in Matrimid® asymmetric hollow fiber membranes at 35 °C

Activity Change	D_A/L^2 (min^{-1})	α_R	τ_R (min)
0 to 0.09	-	1	238
0.09 to 0.18	2.5×10^{-3}	0.58	1391
0.18 to 0.29	6.1×10^{-3}	0.68	3324
0.29 to 0.39	1.3×10^{-2}	0.56	2934
0.39 to 0.50	1.7×10^{-2}	0.51	3250
0.50 to 0.66	1.4×10^{-2}	0.52	4182
0.66 to 0.83	1.5×10^{-2}	0.18	1900

The Berens-Hopfenberg parameters for n-heptane sorption in annealed Matrimid® asymmetric hollow fiber membranes are given in Table 5.9. All transient sorption isotherms for n-heptane in annealed Matrimid® fibers show a significant relaxation-controlled contribution to the overall mass uptake. For intermediate activities, the value of α_R is relatively stable between 0.44 and 0.50. At the lowest and highest activity measured, the value of α_R is decreased to a value of 0.13 and 0.36, respectively. The value of D_A / L^2 continually increases with activity. The value of τ_R generally increases with activity.

Table 5.9: Berens-Hopfenberg model parameters for n-heptane sorption in annealed Matrimid® asymmetric hollow fiber membranes at 35 °C

Activity Change	D_A/L^2 (min^{-1})	α_R	τ_R (min)
0 to 0.10	2.4×10^{-3}	0.13	1300
0.10 to 0.21	2.2×10^{-2}	0.44	1340
0.21 to 0.30	3.6×10^{-2}	0.51	2225
0.30 to 0.38	4.8×10^{-2}	0.50	3413
0.38 to 0.51	5.1×10^{-2}	0.50	4355
0.51 to 0.67	5.7×10^{-2}	0.36	3608

5.2.3 Analysis of Berens-Hopfenberg Model Parameters

As shown in Figure 5.5, uptake of toluene in annealed fibers at an activity of 0.05 precedes via a purely diffusion-controlled process. In this case, a Fickian diffusion coefficient of 1.1×10^{-11} cm^2/sec may be calculated by assuming a characteristic thickness of 120 nm for the asymmetric hollow fiber membranes, as shown in Figure 3.4. This value of the diffusion coefficient is reasonable based on previous investigations of solvent transport in other polymers [15-17]. However, it is important not to regard this calculation of the diffusion coefficient as highly accurate, since the characteristic thickness of 120 nm was simply estimated. Although the value of 120 nm is an estimate, the observation of Fickian uptake in Matrimid® asymmetric hollow fibers indicates that a single characteristic thickness exists for this morphology. Zimmerman et al. showed that in morphologies where a distribution exists in the characteristic dimension, apparent Fickian uptake, such as that shown in Figure 5.5, will not be observed [18]. The fact that such a well-behaved Fickian response is observed strongly suggests that a well-defined characteristic dimension does exist within this complex asymmetric hollow fiber morphology.

While each transient sorption isotherm collected in this work is well described by the Berens-Hopfenberg model, interpretation of the model parameters across all of the isotherms is not clear cut. This complexity is due to a number of simultaneous, interacting effects which occur during sorption of highly-sorbing penetrants in glassy polymers. A list of these effects is provided below.

1. As described in Chapter 2, antiplasticization of the polymer is known to result from sorption of all penetrants at low concentration. In the antiplasticization regime, sorbed penetrant hinders polymer segmental motion and thereby decreases the diffusion coefficient and possibly the chain relaxation rate responsible for relaxation-controlled uptake. Evidence of antiplasticization exists from examination of Table 5.6, where D_A / L^2 in non-annealed fibers for toluene decreases from a value of 3.6×10^{-3} min^{-1} at an activity of 0.07 to a value of 1.6×10^{-3} min^{-1} at an activity of 0.18. The fact that no evidence for antiplasticization (i.e., a decrease in D_A / L^2 at low activity) was observed in the other systems studied in this work (Tables 5.7-5.9) may be the result of antiplasticization occurring in these systems at an activity lower than the initial measured activity. Antiplasticization simply has not been studied adequately to define the key parameters responsible for promoting or suppressing it.
2. At intermediate to high penetrant activity, plasticization of the polymer occurs. In the plasticization regime, sorbed penetrant facilitates polymer segmental motion and thereby increases the diffusion coefficient of the sorbed penetrant. At intermediate to high activity, the value of D_A / L^2 increases

with activity for all of the systems studied in this work (see Tables 5.6-5.9) indicating plasticization.

3. As shown earlier in this chapter, from interpretation of the equilibrium sorption measurements it is apparent that sub-T_g annealing reduces the non-equilibrium excess fractional free volume.

While the above list does not attempt to account for all of the observed trends in the transient sorption behavior, a complete, fundamental understanding of the transient sorption behavior is not required to achieve the research objectives of this work as described in Chapter 1.

5.3 Summary

The equilibrium sorption of carbon dioxide, methane, toluene, and n-heptane in Matrimid® asymmetric hollow fiber membranes was shown to exhibit classical dual mode model behavior. In all cases, the effective equilibrium uptake of penetrant in annealed fibers was significantly less than in non-annealed fibers at a given pressure. From examination of the dual mode parameters, the loss of sorption capacity in the annealed fibers was attributed to a significant reduction in the value of $C_H^{'}$, which exceeded increases in the values of k_D and b. The significant reductions in $C_H^{'}$ were correlated to a loss of excess free volume. The increases in k_D and b were unexpected in the annealed samples and are possibly due to the formation of charge transfer complexes unique to Matrimid®. The combination of the equilibrium sorption data presented in this chapter and the carbon dioxide permeation data presented in Chapter 4 indicate the difference in physical aging at ambient

temperature and sub-T_g annealing at 220 ^oC. While physical aging at ambient temperature only allows for reduction of excess free volume, sub-T_g annealing also induces the formation of charge transfer complexes.

The transient sorption kinetics of toluene and n-heptane in Matrimid® asymmetric hollow fiber membranes were well described by the empirical Berens-Hopfenberg model. The fraction of relaxation-controlled uptake, α_R, was a significant portion of the total uptake for most activities tested in this work. The combination of large values of τ_R and α_R led to a slow approach to equilibrium uptake for sorption of toluene and n-heptane, which would be greatly underestimated by a purely Fickian analysis. The use of the Berens-Hopfenberg which accounts for diffusion and relaxation controlled uptake is required for an accurate estimate of the sorption kinetics for the organic penetrants studied in this work. Furthermore, the use of the Berens-Hopfenberg model reveals the complex effect of annealing and penetrant activity on the kinetic parameters (D_A / L^2, α_R, and τ_R), which is not apparent from analysis of only the equilibrium sorption isotherm. Unfortunately, an adequate fundamental framework does not exist to understand the complex trends observed in the Berens-Hopfenberg model; however, significant trends in the parameters were observed. Since membranes are operated under steady state conditions, the complex time dependent sorption kinetic responses observed, while interesting, are not as important as the equilibrium thermodynamic trends describable in terms of the dual mode sorption model.

5.4 References

1. Berens, A.R. and H.B. Hopfenberg, "Diffusion and relaxation in glassy polymer powders. 2. Separation of diffusion and relaxation parameters," *Polymer*, **19**(5), 489 (1978).

2. Zhou, F., *Novel Pervaporation for Separating Acetic Acid and Water Mixtures Using Hollow Fiber Membranes*, in *Chemical and Biomolecular Engineering*. 2005, Georgia Institute of Technology: Atlanta, GA.

3. Stewart, M.E., H.B. Hopfenberg, and W.J. Koros, "Characterization of physical aging of poly(methyl methacrylate) powders by a novel high pressure sorption technique," *Journal of Applied Polymer Science*, **38**(6), 1111 (1989).

4. Hachisuka, H., et al., "Gas transport properties of annealed polyimide films," *Journal of Polymer Science, Part B: Polymer Physics*, **29**(1), 11 (1991).

5. Mohamed, H.F.M., A.M.A. El-Sayed, and E.E. Abdel-Hady, "Study of sorption in poly(vinyl alcohol) using the positron annihilation technique," *Journal of Physics: Condensed Matter*, **11**(22), 4461 (1999).

6. Wonders, A.G. and D.R. Paul, "Effect of carbon dioxide exposure history on sorption and transport in polycarbonate," *Journal of Membrane Science*, **5**(1), 63 (1979).

7. Koros, W.J. and D.R. Paul, "Carbon dioxide sorption in poly(ethylene terephthalate) above and below the glass transition," *Journal of Polymer Science, Polymer Physics Edition*, **16**(11), 1947 (1978).

8. Koros, W.J. and D.R. Paul, "Transient and steady-state permeation in poly(ethylene terephthlate) above and below the glass transition," *Journal of Polymer Science, Polymer Physics Edition*, **16**(12), 2171 (1978).

9. Kanehashi, S. and K. Nagai, "Analysis of dual-mode model parameters for gas sorption in glassy polymers," *Journal of Membrane Science*, **253**(1-2), 117 (2005).

10. Fuhrman, C., et al., "Effect of thermal hysteresis on the gas permeation properties of 6FDA-based polyimides," *Journal of Applied Polymer Science*, **91**(2), 1174 (2004).

11. Ho, C.H. and T. Vu-Khanh, "Effects of time and temperature on physical aging of polycarbonate," *Theoretical and Applied Fracture Mechanics*, **39**(2), 107 (2003).

12. Wang, Y., D. Shen, and R. Qian, "Subglass-transition-temperature annealing of poly(ethylene terephthalate) studied by FTIR," *Journal of Polymer Science, Part B: Polymer Physics*, **36**(5), 783 (1998).

13. Bagley, E.B. and F.A. Long, "Two-stage sorption and desorption of organic vapors in cellulose acetate," *Journal of the American Chemical Society*, **77**, 2172 (1955).

14. McDowell, C.C., B.D. Freeman, and G.W. McNeely, "Acetone sorption and uptake kinetics in poly(ethylene terephthalate)," *Polymer*, **40**(12), 3487 (1999).

15. Tihminlioglu, F., et al., "Solvent diffusion in amorphous polymers: polyvinyl acetate-toluene system," *Journal of Polymer Science, Part B: Polymer Physics*, **38**(18), 2429 (2000).

16. Wang, B.-G., T. Yamaguchi, and S.-I. Nakao, "Solvent diffusion in amorphous glassy polymers," *Journal of Polymer Science, Part B: Polymer Physics*, **38**(6), 846 (2000).

17. Lutzow, N., et al., "Diffusion of toluene and n-heptane in polyethylenes of different crystallinity," *Polymer*, **40**(10), 2797 (1999).

18. Zimmerman, C.M., A. Singh, and W.J. Koros, "Diffusion in gas separation membrane materials: a comparison and analysis of experimental characterization techniques," *Journal of Polymer Science, Part B: Polymer Physics*, **36**(10), 1747 (1998).

19. Rogers, C.E., V. Stannett, and M. Szwarc, "The sorption of organic vapors by polyethylene," *Journal of Physical Chemistry*, **63**, 1406 (1959).

20. Fleming, G.K. and W.J. Koros, "Dilation of substituted polycarbonates caused by high-pressure carbon dioxide sorption," *Journal of Polymer Science, Part B: Polymer Physics*, **28**(7), 1137 (1990).

CHAPTER 6

PERMEATION OF AGGRESSIVE FEED STREAMS

In this chapter the permeation of mixed gas feed streams containing trace amounts of toluene and n-heptane through Matrimid® asymmetric hollow fiber membranes will be investigated. Toluene and n-heptane are common contaminants found in natural gas feed streams [1]. Trace levels of such highly sorbing feed stream components are known to cause significant degradation of membrane performance during industrial operation. Only a few studies of membrane performance in such situations are available in the literature [2-5]. The work presented in this chapter quantifies membrane performance during contaminant exposure and the sustained effects on membrane performance after removal of the contaminant from the feed stream. This work was performed in both non-annealed and annealed Matrimid® asymmetric hollow fiber membranes, to investigate the potential of annealing to stabilize membrane performance in aggressive feed streams. The annealing treatment studied here is the same used in the preceding chapters.

6.1 Permeation Protocol

The permeation protocol used in this chapter is a slightly modified version of the protocol used previously by Al-Juaied [2]. Each of the steps in the protocol is described below.

1. Nitrogen, oxygen, and helium permeation experiments are performed at a feed pressure of 50 psia and a temperature of 35 ^{o}C. The oxygen/nitrogen

and helium/nitrogen selectivities determined in this step ensure that the membrane module is defect-free (i.e. the measured fiber selectivity is >90% of the bulk selectivity given in Table 3.1).

2. The membrane module is pressurized with a 10/90 CO_2/CH_4 feed gas (Gas Mixture 1 in Table 3.2). Permeation experiments are performed at pressures of 50, 100, 200, 300, and 400 psia at a temperature of 35 ^oC. The membrane is operated at each pressure for at least one hour prior to permeation testing to ensure the steady-state flux is measured. As is discussed later, only very slight (~4%) long term non-Fickian "creep" occurs even up to 5 days of exposure at 400 psia.
3. A trace amount of either toluene or n-heptane is introduced into the 10/90 CO_2/CH_4 feed gas at 400 psia. This process is achieved by switching the feed gas to Gas Mixtures 2-4 in Table 3.2 or by introducing a wet gas feed stream from the bubbler system described in Appendix A. During this process, the upstream pressure on the membrane is maintained continuously at 400 psia.
4. Permeation measurements are made daily over a 5-day conditioning period. During the conditioning period, the contaminant concentration established in Step 3 is maintained and the upstream pressure is maintained at 400 psia.
5. After the 5-day conditioning period, the contaminant, toluene or n-heptane, is removed from the feed stream by switching to Gas Mixture 1 or by shutting off the wet gas feed stream from the bubbler system. During this process, the upstream feed pressure is maintained at 400 psia.

6. The membrane is operated with an uncontaminated 10/90 CO_2/CH_4 feed gas at 400 psia for a period of 2 days to allow for complete desorption of contaminant from the membrane. The upstream side of the membrane is sampled via gas chromatography to ensure no residual contaminant remains sorbed in the membrane.
7. The contaminant-free membrane is depressurized with 10/90 CO_2/CH_4 feed gas. Permeation experiments are performed at pressures of 400, 300, 200, 100, and 50 psia at a temperature of 35 ^{o}C. The membrane is operated at each pressure for at least one hour prior to permeation testing to ensure the steady-state flux is measured.

This permeation protocol allows for the analysis of membrane performance during contaminant exposure (Step 4). On the other hand, comparison of permeation isotherms before and after contaminant exposure (Steps 3 and 7) allows for analysis of the long-lived conditioning effect on membrane performance after removal of the contaminant from the feed stream.

The conditioning pressure of 400 psia used throughout this work was set by practical considerations. The cylinder pressure of the 10/90 CO_2/CH_4, toluene, and n-heptane containing gas (Cylinder 4 in Table 3.2) was 525 psia. A conditioning pressure of 400 psia allowed for multiple experiments to be conducted prior to the cylinder pressure being reduced to 400 psia. The development of the bubbler system detailed in Appendix A allows for conditioning at pressures up to 1000 psia in future work.

6.2 Gas Permeation with Low Sorbing Feeds

Nitrogen, oxygen, and helium permeances were determined before each membrane was exposed to conditioning agent. Measurement of the permeance for each of these inert gases was primarily made to ensure that the membrane module was initially defect-free (i.e. an oxygen/nitrogen selectivity >90% of the value for bulk Matrimid® given in Table 3.1). However, tracking of the gas permeances of these probes, prior to conditioning agent exposure, over the course of this experimental work also allows for observation of the effects of physical aging.

As discussed in Chapter 2, previous researchers observed substantial reductions in the permeation of inert gases over time due to the process of physical aging in thin film and asymmetric glassy polymer membranes [6-8]. Recent work has shown that the reduction in permeance may continue over an extremely long period of time before reaching an asymptote [9]. The fibers used in this chapter were tested at least 250 days after spinning to limit the impact of physical aging. However, from examination of Figure 6.1, it is apparent that a significant decay in nitrogen permeance due to physical aging occurs over the course of the experimental work presented in this chapter.

Surprisingly, Figure 6.1 shows that annealing of the fibers does not have a noticeable impact on the loss of nitrogen permeance associated with physical aging. This is a surprising result since as shown in Chapter 4 annealing increased the permeance of carbon dioxide; however, the batch of fibers tested in Chapter 4 is different than the fibers tested here. It may be that fibers with different degrees of physical aging are affected differently by the thermal annealing procedure used in this

work. As shown in Figure 4.7, the substantial loss of carbon dioxide permeance at ~50 psia in non-annealed fibers over the 278 day aging period indicates a significant loss of excess free volume due to physical aging. Annealing of fibers in this highly aged, denser state resulted in actually increasing the carbon dioxide permeance. In Chapter 4, this counterintuitive effect was explained by analogy to similar effects observed in cross-linked systems. However, in a relatively "young" fiber, where more free volume exists relative to the fibers tested in Chapter 4, an increase in permeance may not be observed upon annealing. Future work should investigate this point more closely.

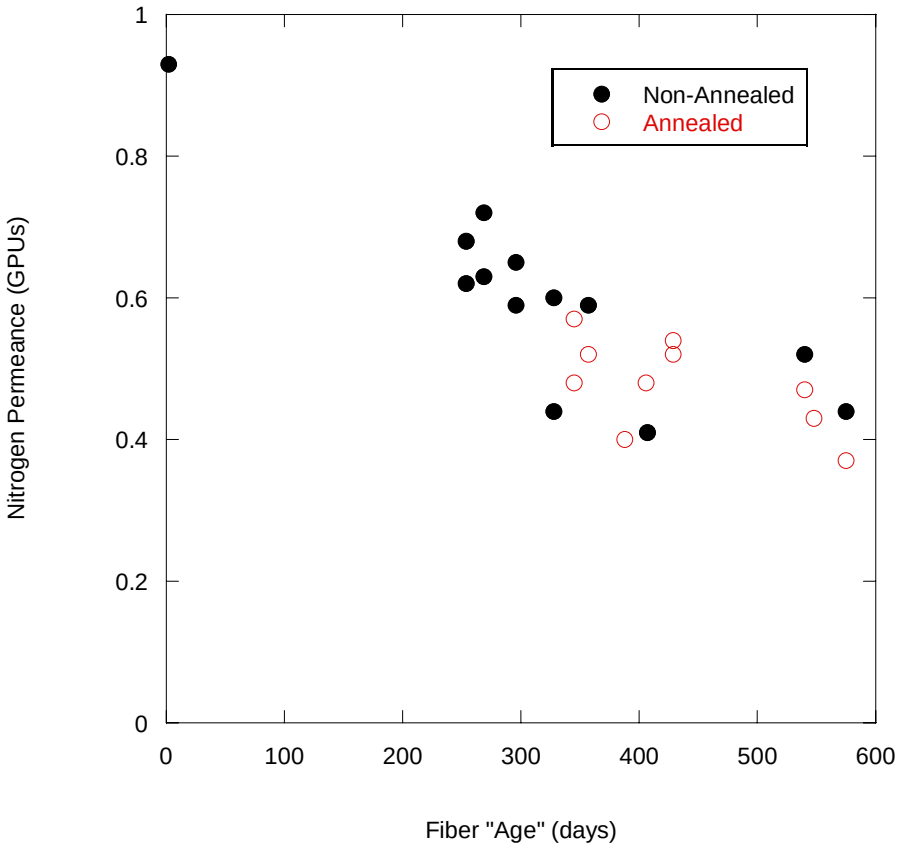

Figure 6.1: Nitrogen permeance decay due to physical aging in Matrimid® asymmetric hollow fiber membranes at 50 psia and 35 °C

6.3 Membrane Pressurization

As described in the previous section, before contaminant exposure, each membrane module is pressurized to 400 psia incrementally with a 10/90 CO_2/CH_4 feed gas. The carbon dioxide permeation isotherms in Figure 6.2 show the average response from 12 separate membrane pressurizations with associated error bars for the 95% confidence interval. Since the fibers tested in this chapter were all spun at the same time, with the same spinning parameters, have no previous gas exposure history, and were stored in the same laboratory conditions, the permeation responses shown in Figure 6.2 should be nominally equivalent for fibers of the same thermal history. The error bars therefore account for experimental uncertainty and module-to-module variation.

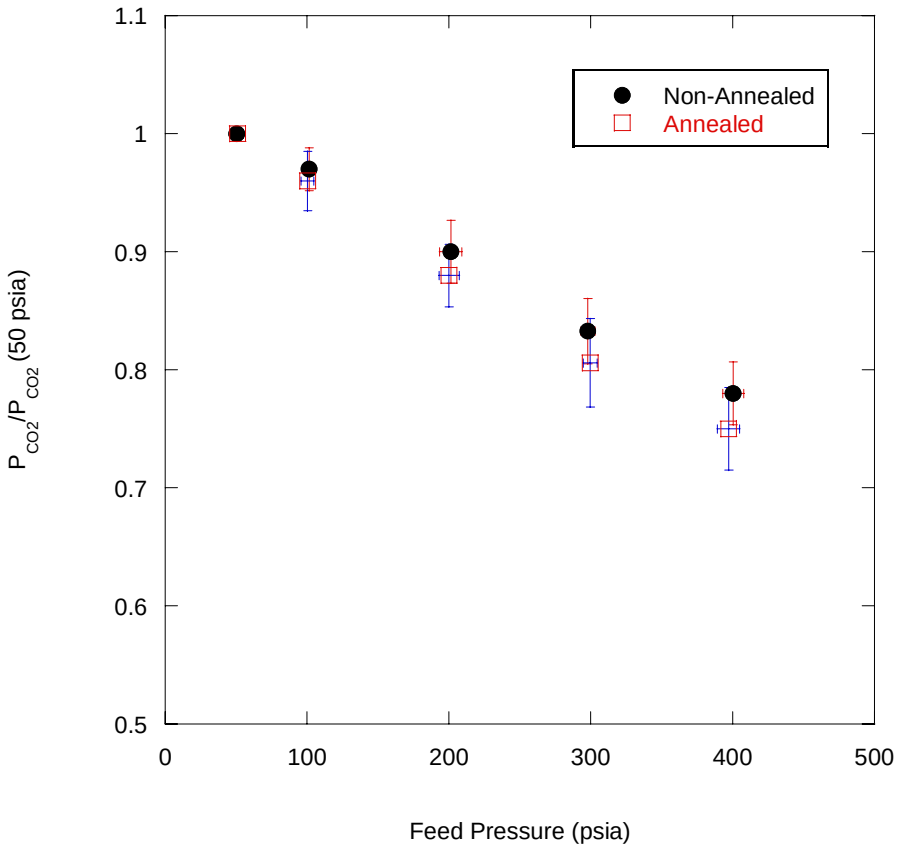

Figure 6.2: Carbon dioxide permeation isotherm for 10/90 CO_2/CH_4 in Matrimid® asymmetric hollow fiber membranes at 35 °C

In Figure 6.2, the carbon dioxide permeance measured at each pressure is normalized by the permeance at 50 psia. This normalization procedure reduces the scatter in permeance values between membrane modules due to the significant physical aging which occurs over the course of this experimental work as discussed in the previous section. From examination of Figure 6.2, it is apparent that the normalized carbon dioxide permeance decreases with increasing feed pressure. This reduction in carbon dioxide permeance is the expected result of Langmuir site saturation as described by the dual mode transport model in Chapter 2. It is important to notice the magnitude of the reduction in carbon dioxide permeance. In non-

annealed membranes, the carbon dioxide permeance at a feed pressure of 400 psia is ~25% lower than the carbon dioxide permeance at a feed pressure of 50 psia. Statistically, there is very little difference in the reduction in carbon dioxide permeance with pressure between non-annealed and annealed fibers. The error bars are slightly greater in annealed fibers relative to non-annealed fibers. The slightly greater variability in annealed fibers is most likely the result of slight differences in the annealing treatment.

In Figure 6.3, the normalized carbon dioxide/methane selectivity is plotted versus pressure for annealed and non-annealed fibers. As with permeance, a reduction in selectivity with increasing feed pressure is observed; however, the effect on selectivity is not as large as that observed on the carbon dioxide permeance. In non-annealed fibers, the selectivity is ~10% lower at a feed pressure of 400 psia compared to a feed pressure of 50 psia. Again, statistically there is very little difference in the pressure dependence of selectivity between non-annealed and annealed fibers.

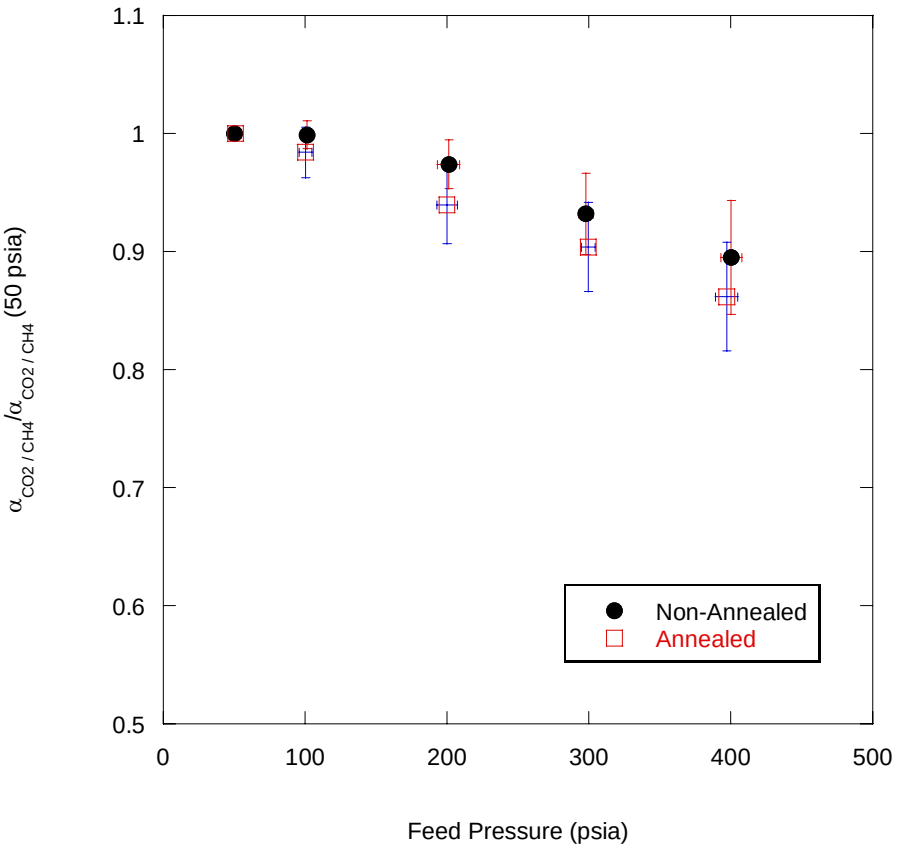

Figure 6.3: Selectivity isotherm for 10/90 CO_2/CH_4 in Matrimid® asymmetric hollow fiber membranes at 35 °C

6.4 Membrane Conditioning

After pressurization to 400 psia with a 10/90 CO_2/CH_4 feed gas, the membrane is exposed to a conditioning agent. The conditioning agent is introduced to the feed stream while maintaining the upstream pressure at 400 psia. The membrane is operated in the presence of the conditioning agent for a period of 5 days. This process experimentally simulates a feed stream upset during industrial operation. Toluene and n-heptane are used as conditioning agents in this work, since both are common contaminants in natural gas feed streams.

The conditioning experiments were conducted in both annealed and non-annealed Matrimid® asymmetric hollow fiber membranes. Replicates of the experiment were conducted at each conditioning agent concentration. Unfortunately triplicates could not be performed at each concentration due to lack of feed gas, membranes, and time; however, the difference between replicates was less than 5% in all cases.

6.4.1 Control Case: Conditioning with 10/90 CO_2/CH_4 Feed Gas

Since carbon dioxide, a known plasticizer, is a component of the feed stream it was important to conduct a control experimental to assess membrane performance in the presence of 10/90 CO_2/CH_4 over a 5 day period. During this control experiment, the membrane was never exposed to toluene or n-heptane.

The normalized carbon dioxide permeance at a feed pressure of 400 psia over a 5 day conditioning period is shown in Figure 6.4 for annealed and non-annealed Matrimid® asymmetric hollow fiber membranes. In Figure 6.4, the carbon dioxide permeance is normalized by the "pre-exposure" carbon dioxide permeance at 400 psia. The "pre-exposure" carbon dioxide permeance is the value of the carbon dioxide permeance shown in Figure 6.2 at a feed pressure of 400 psia. This normalization procedure allows for examination of the effect on the carbon dioxide permeance from the introduction of the conditioning agent decoupled from the previous reduction in carbon dioxide permeance due to pressurization.

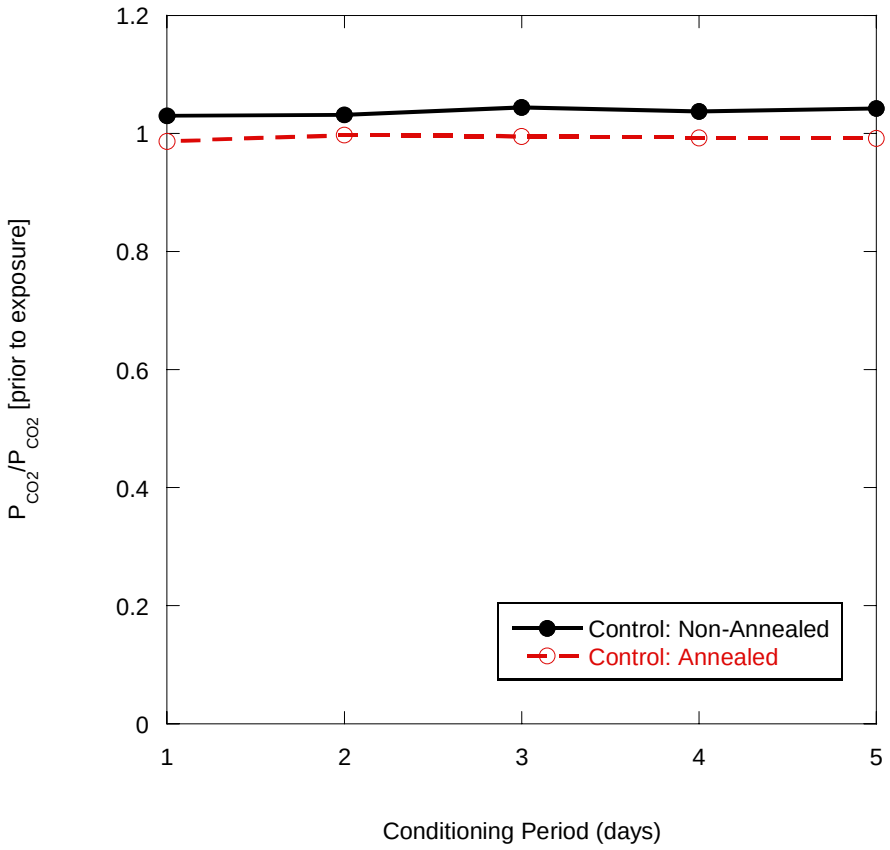

Figure 6.4: Carbon dioxide permeance in Matrimid® asymmetric hollow fiber membranes during 5 days of operation at 400 psia and 35 °C with a 10/90 CO_2/CH_4 feed gas

In Figure 6.4, the normalized carbon dioxide permeance is slightly greater than 1 over the entire 5 day period of operation in non-annealed fibers. The slight, approximately 4%, increase from Day 0 (the day of contaminant introduction to the feed stream) to Day 1 is mostly likely the result of plasticization by carbon dioxide. This slight increase in carbon dioxide permeance is not seen in annealed fibers, which as shown in Chapter 4 are more resistant to carbon dioxide induced plasticization.

The normalized carbon dioxide/methane selectivity at a feed pressure of 400 psia over a 5 day period of operation is shown in Figure 6.5 for annealed and non-

annealed Matrimid® asymmetric hollow fiber membranes. In Figure 6.5, the carbon dioxide/methane selectivity is normalized by the "pre-exposure" carbon dioxide/methane selectivty at 400 psia. The "pre-exposure" carbon dioxide/methane selectivity is the value of the carbon dioxide/methane selectivity shown in Figure 6.3 at a feed pressure of 400 psia. The normalized carbon dioxide/methane selectivity is decreased by ~3% over the 5 day period of operation. There is no discernible difference in the selectivity response for annealed and non-annealed fibers during this period of operation.

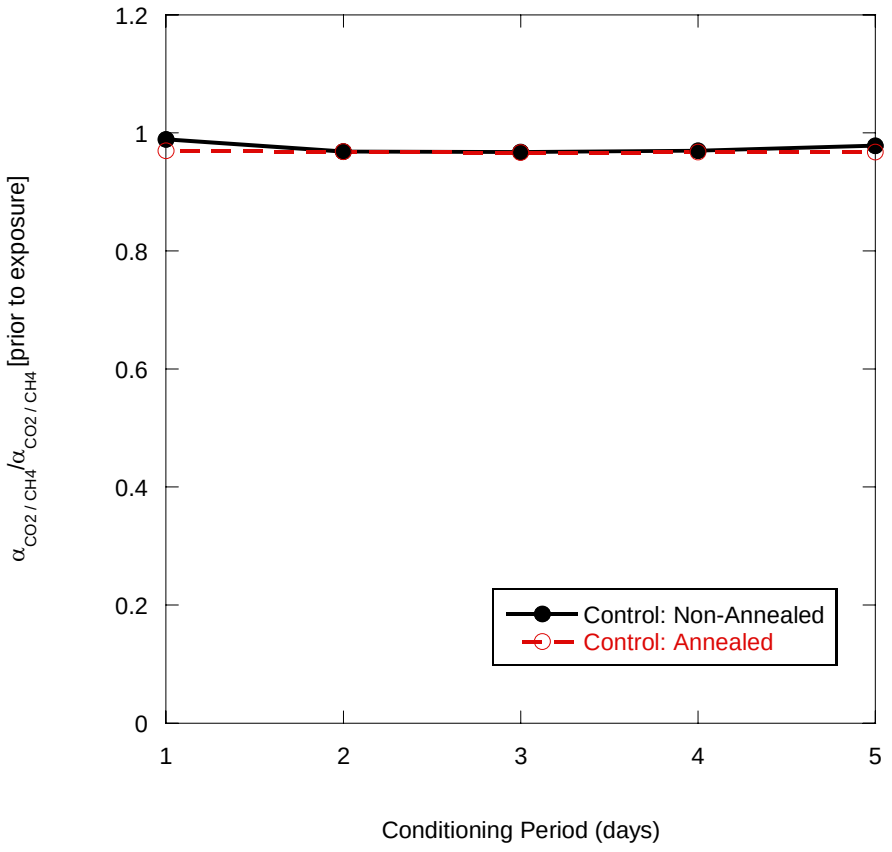

Figure 6.5: Carbon dioxide/methane selectivity in Matrimid® asymmetric hollow fiber membranes during 5 days of operation at 400 psia and 35 ^{o}C with a 10/90 CO_2/CH_4 feed gas

6.4.2 Conditioning with Toluene

Matrimid® asymmetric hollow fiber membranes were exposed to toluene concentrations of 293 and 544 ppm. The normalized carbon dioxide permeance in non-annealed and annealed fibers during the 5 day toluene exposure period is given in Figure 6.6. In the presence of 293 ppm toluene, for non-annealed fiber samples the carbon dioxide permeance is reduced to approximately 55% of the pre-exposure value over the 5 day exposure period. In the presence of 544 ppm toluene, in non-annealed fibers the carbon dioxide permeance gradually increases over the first three days of exposure to 66% of the pre-exposure permeance. These effects are clearly very large compared to the small time dependent changes noted earlier for binary feeds.

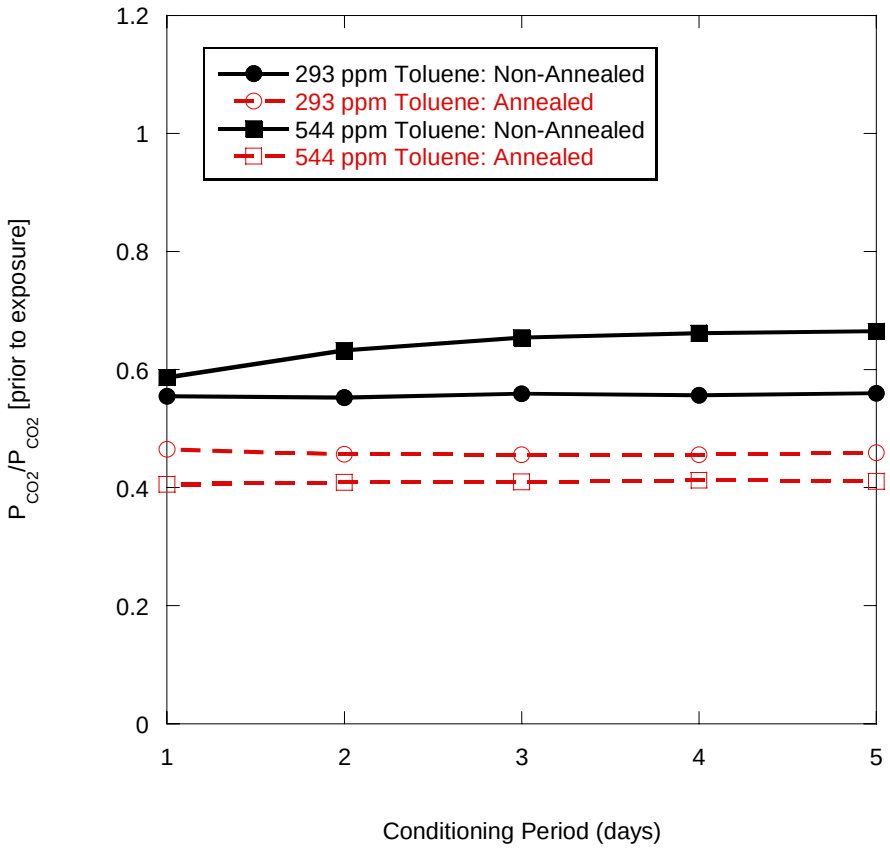

Figure 6.6: Carbon dioxide permeance in Matrimid® asymmetric hollow fiber membranes during 5 days of conditioning at 400 psia and 35 °C with a 10/90 CO_2/CH_4 + toluene feed gas

At both toluene concentrations, annealing increases the reduction in carbon dioxide permeance during exposure relative to non-annealed fiber samples. In the presence of 293 ppm toluene, for annealed fiber samples the carbon dioxide permeance is reduced to 46% of the pre-exposure permeance over the 5 day exposure period. In the presence of 544 ppm toluene, for annealed fiber samples the carbon dioxide permeance is reduced to 41% of the pre-exposure permeance over the 5 day exposure period. These are both large and practically very serious decrements in productivity that would require roughly 2.5 times as much membrane area to achieve carbon dioxide/methane separation as for the binary case.

In Figure 6.7, the normalized carbon dioxide/methane selectivity is given during the 5 day toluene exposure period. The reduction in the selectivity due to toluene exposure is not as large as the reduction in the carbon dioxide permeance. In the presence of 293 ppm toluene, for non-annealed fibers the carbon dioxide/methane selectivity is reduced to 83% of the pre-exposure selectivity over the 5 day exposure period. In the presence of 544 ppm toluene, for non-annealed fibers the selectivity decreases over the first two days of toluene exposure to 75% of the pre-exposure selectivity.

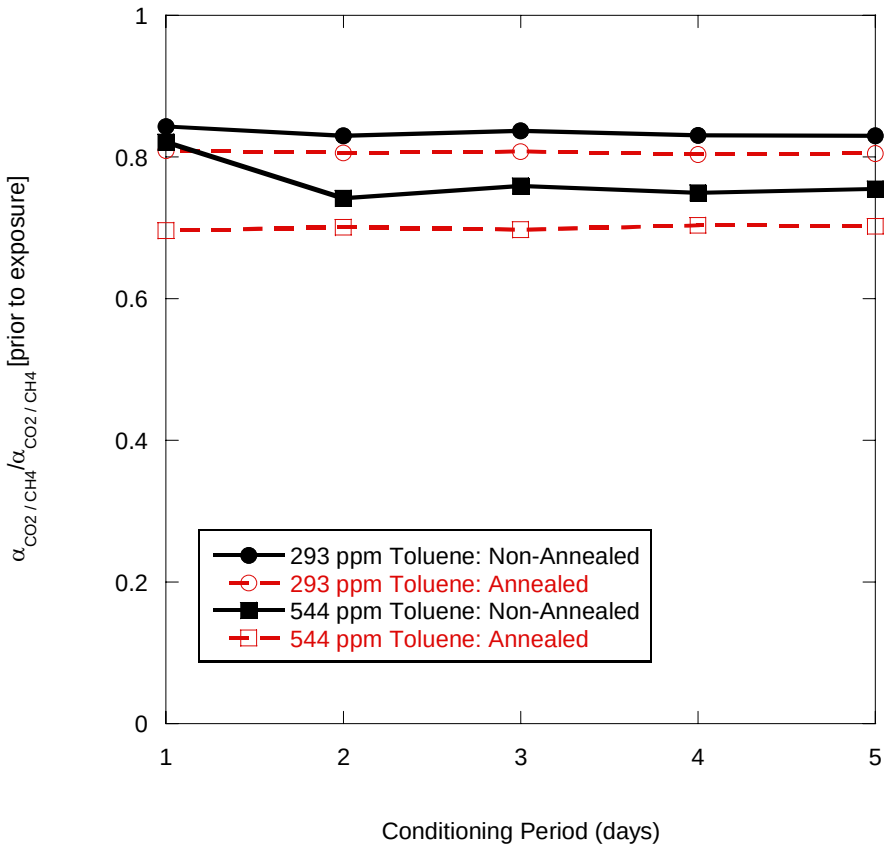

Figure 6.7: Carbon dioxide/methane selectivity in Matrimid® asymmetric hollow fiber membranes during 5 days of conditioning at 400 psia and 35 °C with a 10/90 CO_2/CH_4 + toluene feed gas

At both toluene concentrations, annealing increases the reduction in carbon dioxide/methane selectivity during exposure relative to non-annealed fiber samples. In the presence of 293 ppm toluene, for annealed fiber samples the carbon dioxide/methane selectivity is reduced to 81% of the pre-exposure selectivity over the 5 day exposure period. In the presence of 544 ppm toluene, for annealed fiber samples the carbon dioxide permeance is reduced to 70% of the pre-exposure permeance over the 5 day exposure period. These effects of toluene impurities are also very serious, as they would require a larger "stage cut" of non-saleable gas to reduce carbon dioxide levels to equivalent levels to that achievable in the absence of toluene impurity.

6.4.3 Conditioning with n-Heptane

Matrimid® asymmetric hollow fiber membranes were exposed to n-heptane concentrations of 505 and 2003 ppm. The normalized carbon dioxide permeance in non-annealed and annealed fibers during the 5 day n-heptane exposure period is given in Figure 6.8. In the presence of 505 ppm n-heptane, for non-annealed fiber samples the carbon dioxide permeance is reduced to approximately 85% of the pre-exposure value over the 5 day exposure period. In the presence of 2003 ppm n-heptane, in non-annealed fibers the carbon dioxide permeance gradually increases over the entire 5 days of exposure to 80% of the pre-exposure permeance.

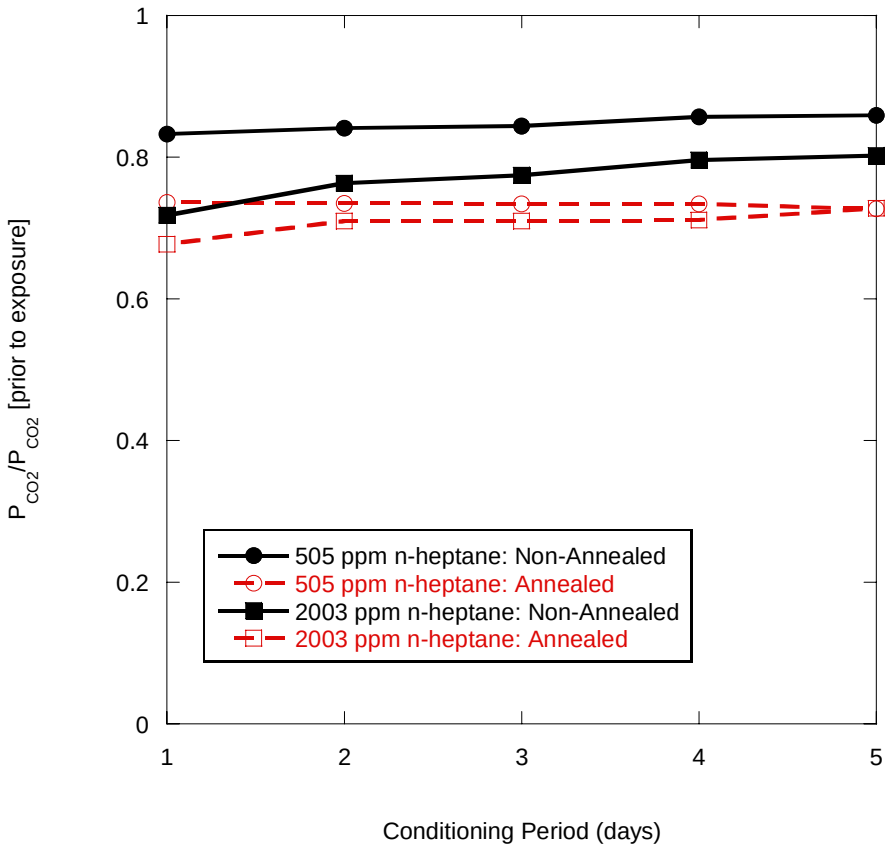

Figure 6.8: Carbon dioxide permeance in Matrimid® asymmetric hollow fiber membranes during 5 days of conditioning at 400 psia and 35 °C with a 10/90 CO_2/CH_4 + n-heptane feed gas

At both n-heptane concentrations, annealing increases the reduction in carbon dioxide permeance during exposure relative to non-annealed fiber samples. In the presence of 505 ppm n-heptane, for annealed fiber samples the carbon dioxide permeance is reduced to 73% of the pre-exposure permeance over the 5 day exposure period. The reduction in carbon dioxide in annealed fibers during exposure to 2003 ppm n-heptane is remarkably close to the permeance reduction in the presence of 505 ppm n-heptane. In the presence of 2003 ppm n-heptane, the reduction in carbon

dioxide permeance increases from 68% of the pre-exposure permeance on the first day of exposure to 73% of the pre-exposure permeance on the fifth day of exposure.

In Figure 6.9, the normalized carbon dioxide/methane selectivity is given during the 5 day n-heptane exposure period. The reduction in the selectivity due to n-heptane exposure is not as large as the reduction in the carbon dioxide permeance. In the presence of 505 ppm n-heptane, for non-annealed fibers the carbon dioxide/methane selectivity is reduced to 96% of the pre-exposure selectivity over the 5 day exposure period. The presence of 505 ppm n-heptane essentially has no impact on the selectivity, since the 4% loss in selectivity is equivalent to the loss in selectivity for the control case shown in Figure 6.5. In the presence of 2003 ppm n-heptane a significant impact on the selectivity is observed. For non-annealed fibers, the selectivity decreases during exposure to 88% of the pre-exposure selectivity. At both n-heptane concentrations, annealing maintains the carbon dioxide/methane selectivity at 96% of the pre-exposure selectivity over the 5 day exposure period.

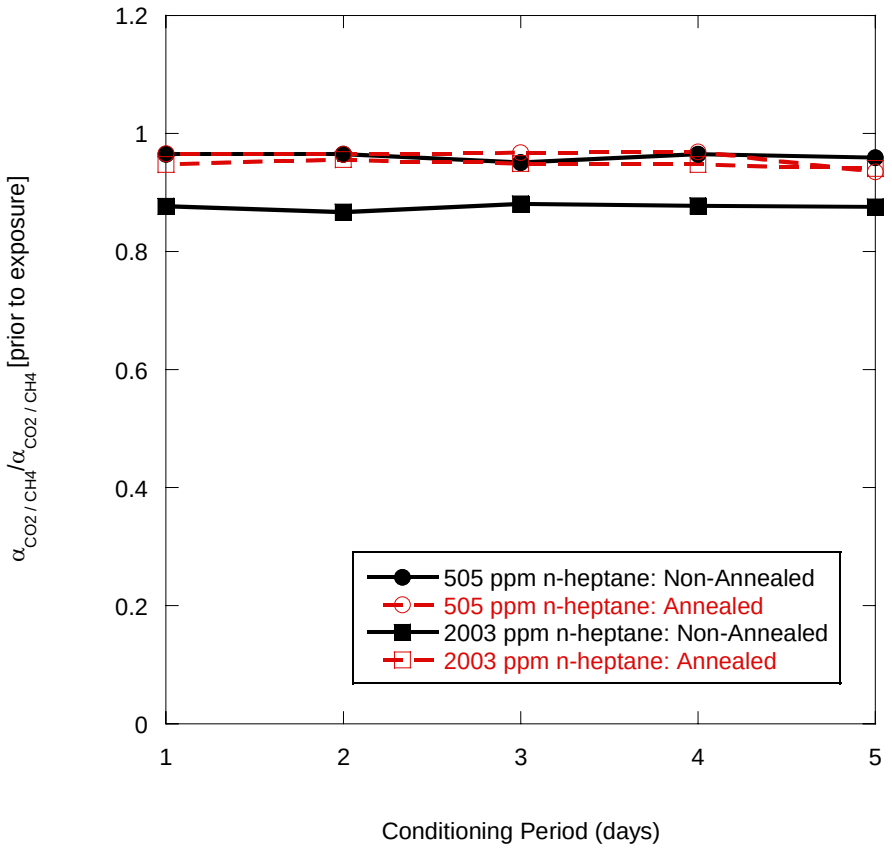

Figure 6.9: Carbon dioxide/methane selectivity in Matrimid® asymmetric hollow fiber membranes during 5 days of conditioning at 400 psia and 35 °C with a 10/90 CO_2/CH_4 + n-heptane feed gas

6.4.4 Conditioning with Toluene and n-Heptane

Matrimid® asymmetric hollow fiber membranes were exposed to concentrations of 284 ppm toluene and 504 ppm n-heptane simultaneously. The normalized carbon dioxide permeance in non-annealed and annealed fibers during the 5 day toluene and n-heptane exposure period is given in Figure 6.10. In the presence of 284 ppm toluene and 504 ppm n-heptane, for non-annealed fiber samples the carbon dioxide permeance is reduced to approximately 42% of the pre-exposure value over the 5 day exposure period. In annealed fibers during simultaneous exposure to

284 ppm toluene and 504 ppm n-heptane, the carbon dioxide permeance is reduced to 36% of the pre-exposure permeance.

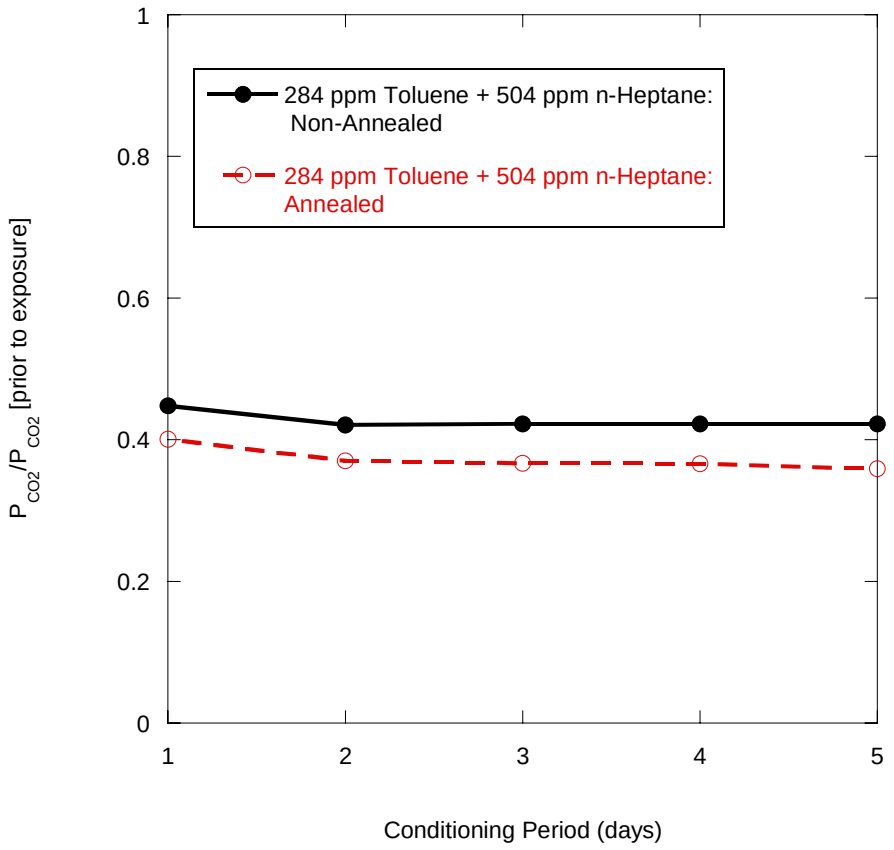

Figure 6.10: Carbon dioxide permeance in Matrimid® asymmetric hollow fiber membranes during 5 days of conditioning at 400 psia and 35 °C with a 10/90 CO_2/CH_4 + toluene + n-heptane feed gas

In Figure 6.11, the carbon dioxide/methane selectivity during simultaneous exposure to 283 ppm toluene and 504 ppm n-heptane is given. In non-annealed fibers the simultaneous exposure of toluene and n-heptane reduces the carbon dioxide/methane selectivity to 70% of the pre-exposure selectivity. For annealed fibers, the simultaneous exposure of toluene and n-heptanes reduces the carbon dioxide/methane selectivity to 75% of the pre-exposure selectivity.

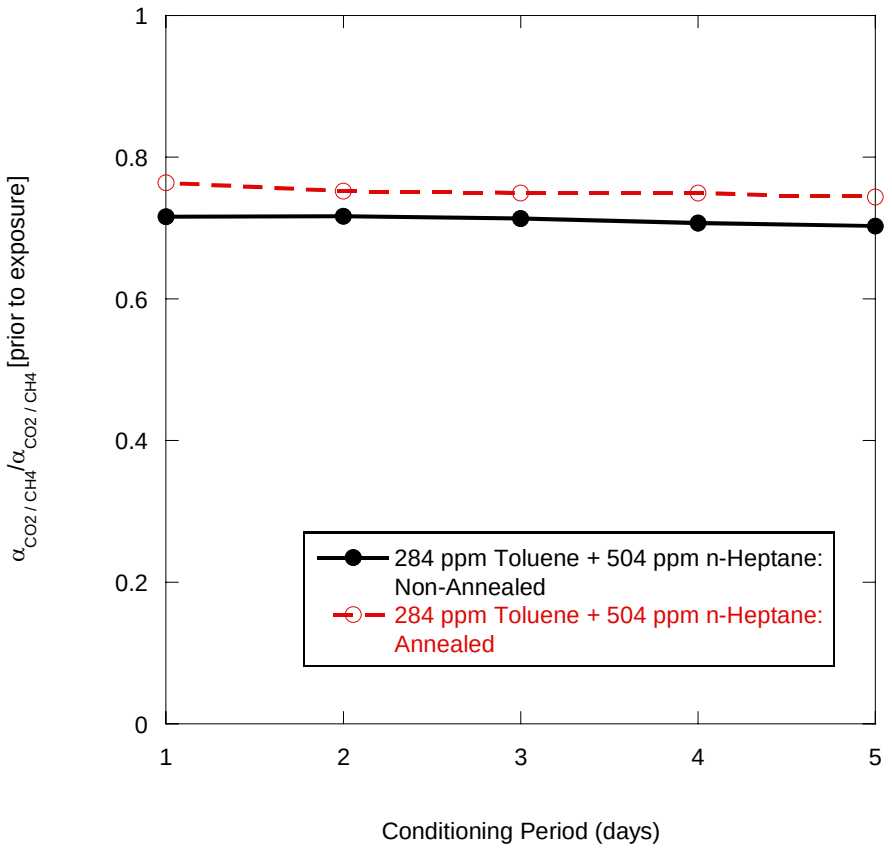

Figure 6.11: Carbon dioxide/methane selectivity in Matrimid® asymmetric hollow fiber membranes during 5 days of conditioning at 400 psia and 35 °C with a 10/90 CO_2/CH_4 + toluene + n-heptane feed gas

From examination of Figures 6.10 and 6.11, it is apparent that the simultaneous exposure of toluene and n-heptane results in a greater reduction of membrane performance than exposure to toluene or n-heptane individually. Moreover, the degradation in membrane performance during simultaneous contaminant exposure does not equal the sum of the contributions measured individually for toluene and n-heptane. This is, of course, fortunate since the sum of the two individual contaminants would have led to only ~29% residual permeance in annealed fibers. This point will be discussed in Chapter 7.

6.5 Membrane Depressurization

After removal of the conditioning agent from the feed stream and complete degassing of the conditioning agent from the membrane, the pressure of the 10/90 CO_2/CH_4 feed gas is decreased. This depressurization reveals a hysteresis in the carbon dioxide permeance and carbon dioxide/methane selectivity due to the conditioning process as described in Chapter 2.

6.5.1 Control Case: Depressurization after Exposure to 10/90 CO_2/CH_4 Feed Gas

Since carbon dioxide is a known plasticizer of Matrimid®, a control experiment was performed to quantify the conditioning effect which results after operation for a 5 day period with a 10/90 CO_2/CH_4 feed gas at 400 psia and 35 ^oC. In this experiment, the membrane was never exposed to toluene or n-heptane. In Figure 6.12, the normalized carbon dioxide permeance upon depressurization from 400 psia is given for non-annealed and annealed Matrimid® asymmetric hollow fiber membranes. It is important to notice that in Figure 6.12 the carbon dioxide permeance is normalized by the initial carbon dioxide permeance at 50 psia given in Figure 6.2. The pressurization isotherms from Figure 6.2 are given in Figure 6.12 for reference.

From Examination of Figure 6.12, it is apparent upon depressurization a significant hysteresis exists in the carbon dioxide permeance in non-annealed fibers. Upon depressurization to 50 psia, the carbon dioxide permeance is 15% greater than the initial carbon dioxide permeance prior to the 5 day exposure period at 400 psia. This behavior is the well known result of carbon dioxide induced conditioning studied

by previous researchers [10-12] and discussed in Chapter 2. In annealed fibers upon depressurization from 400 psia, a hysteresis in the carbon dioxide permeance is not observed. This lack of hysteresis is indicative of the increased carbon dioxide plasticization resistance of Matrimid® after annealing as studied by previous investigators [13-15].

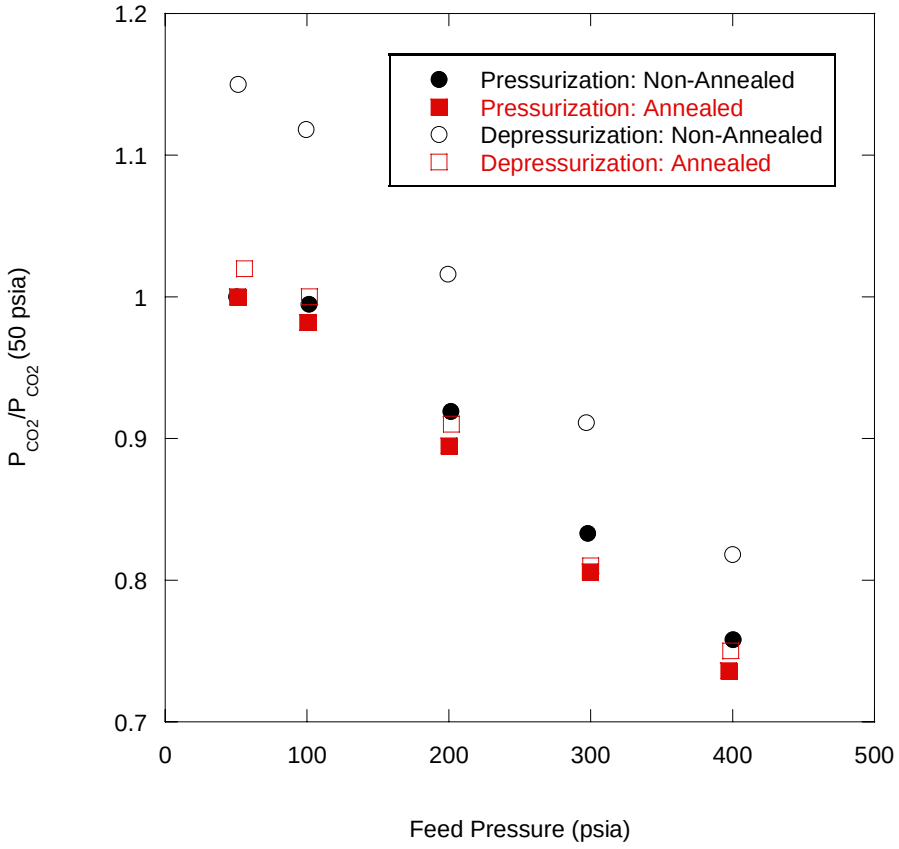

Figure 6.12: Conditioning effect on carbon dioxide permeance after 5 day exposure to 10/90 CO_2/CH_4 feed gas at 400 psia and 35 ^oC

In Figure 6.13, the normalized carbon dioxide/methane selectivity is given upon depressurization from 400 psia for non-annealed and annealed Matrimid® asymmetric hollow fiber membranes. It is important to notice that in Figure 6.13 the carbon dioxide/methane selectivity is normalized by the initial carbon

dioxide/methane selectivity at 50 psia given in Figure 6.3. The pressurization isotherms from Figure 6.3 are given in Figure 6.13 for reference. From examination of Figure 6.13, upon depressurization from 400 psia after the 5 day exposure period no hysteresis exists in the carbon dioxide/methane selectivity for either non-annealed or annealed fibers. In the non-annealed fibers, the carbon dioxide/methane selectivity is ~5% less than the initial selectivity prior to exposure; however, this slight reduction is within the experimental uncertainty as shown by the error bars in Figure 6.3.

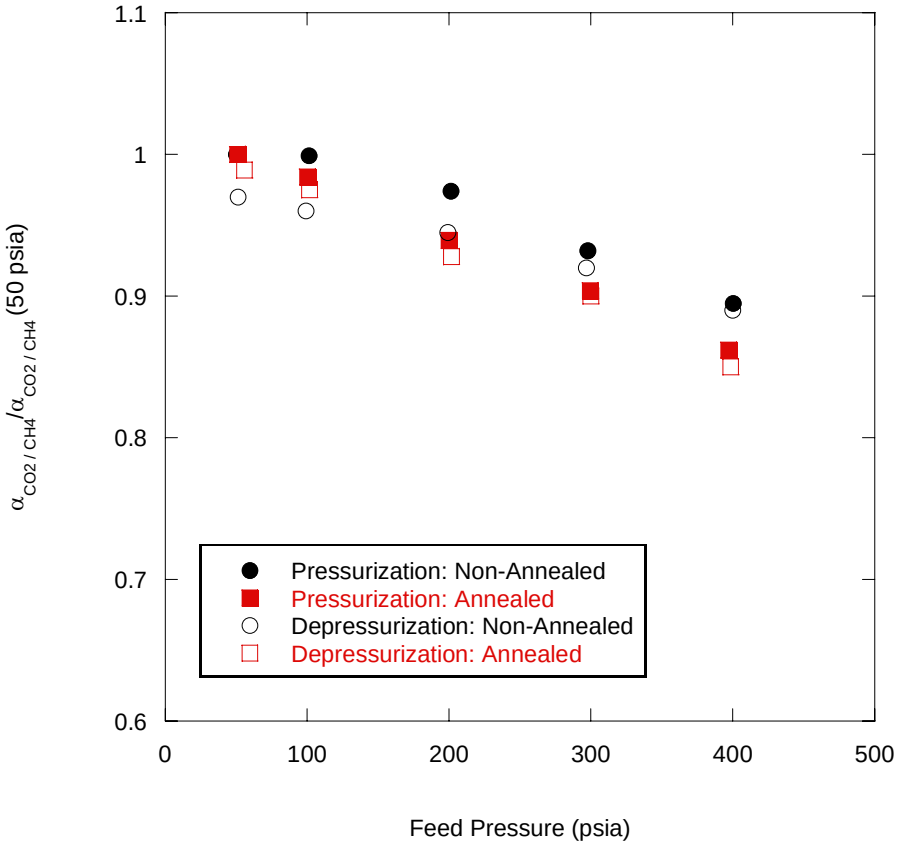

Figure 6.13: Conditioning effect on carbon dioxide/methane selectivity after 5 day exposure to 10/90 CO_2/CH_4 feed gas at 400 psia and 35 ^oC

6.5.2 Depressurization after Exposure to Toluene

The conditioning effect on carbon dioxide permeance after exposure to 293 ppm and 544 ppm toluene in the feed gas is shown in Figure 6.14 for non-annealed and annealed Matrimid® asymmetric hollow fiber membranes. The depressurization isotherms for the control case of no toluene exposure from Figure 6.12 are given in Figure 6.14 for reference. For non-annealed fibers it is apparent that toluene exposure greatly increases the observed hysteresis in carbon dioxide permeance. In non-annealed fibers, after exposure to 293 ppm toluene, the carbon dioxide permeance at 50 psia is 45% greater than the initial carbon dioxide permeance prior to the 5 day toluene exposure period. In non-annealed fibers, after exposure to 544 ppm toluene, the carbon dioxide permeance at 50 psia is 70% greater than the initial carbon dioxide permeance prior to the 5 day toluene exposure period. In the annealed fiber samples, the hysteresis in carbon dioxide permeance due to toluene exposure is greatly reduced.

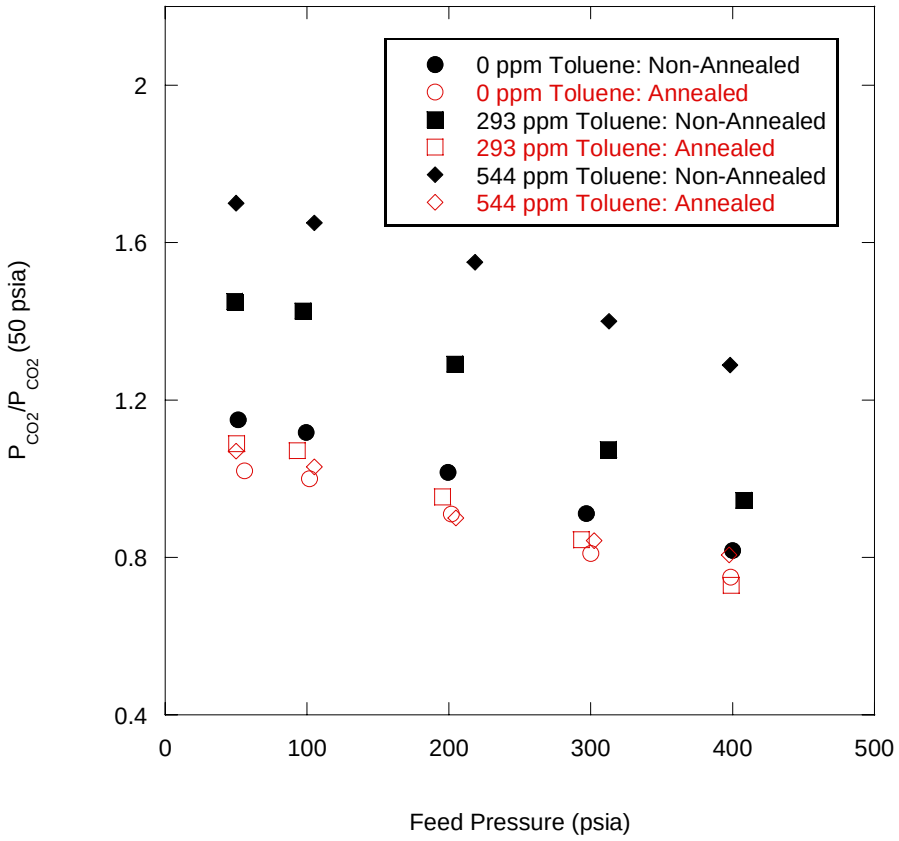

Figure 6.14: Conditioning effect on carbon dioxide permeance after 5 day exposure to 10/90 CO_2/CH_4 + toluene feed gas at 400 psia and 35 ^oC

In Figure 6.15 the conditioning effect on the carbon dioxide/methane selectivity is shown after exposure to 293 ppm and 544 ppm toluene in the feed gas stream. In non-annealed fibers, after exposure to 293 ppm toluene, the carbon dioxide/methane selectivity at 50 psia is reduced to only 93% of the carbon dioxide/methane selectivity prior to toluene exposure. In non-annealed fibers, after exposure to 544 ppm toluene in the feed gas, the carbon dioxide/methane selectivity at 50 psia is reduced to 82% of the selectivity prior to toluene exposure. In annealed

fiber samples, upon depressurization after toluene exposure no loss in carbon dioxide/methane selectivity is observed.

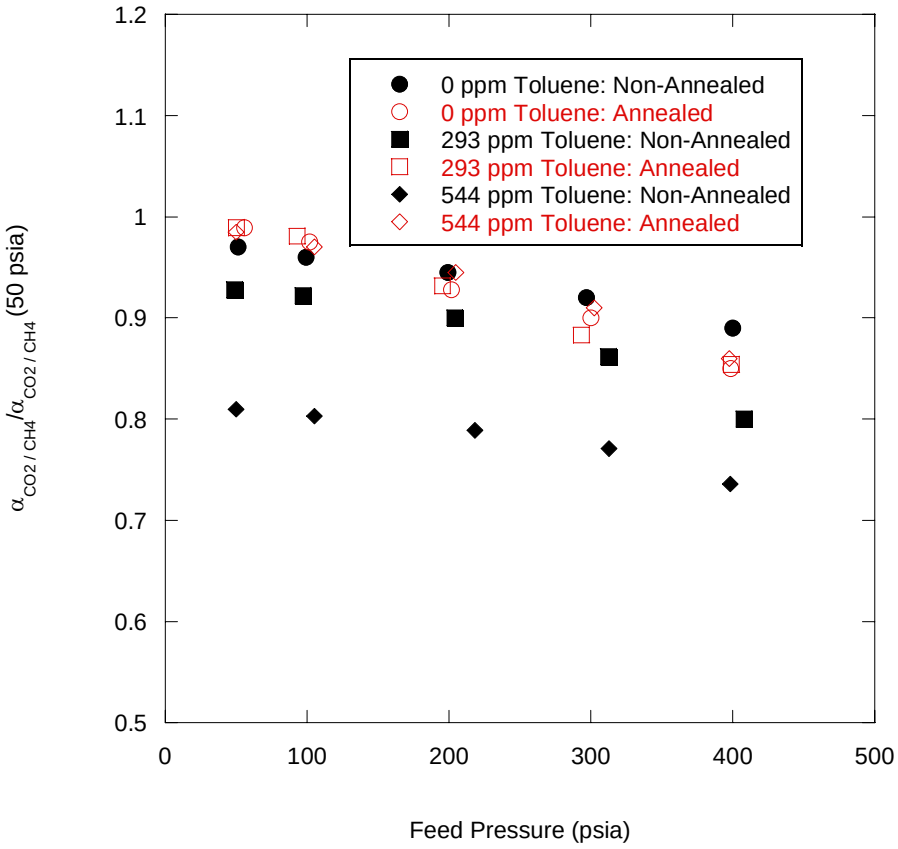

Figure 6.15: Conditioning effect on carbon dioxide/methane selectivity after 5 day exposure to 10/90 CO_2/CH_4 feed gas + toluene at 400 psia and 35 ^oC

6.5.3 Depressurization after Exposure to n-Heptane

The conditioning effect on carbon dioxide permeance after exposure to 505 ppm and 2003 ppm n-heptane in the feed gas is shown in Figure 6.16 for non-annealed and annealed Matrimid® asymmetric hollow fiber membranes. The depressurization isotherms for the control case of no n-heptane exposure from Figure

6.12 are given in Figure 6.16 for reference. For non-annealed fibers it is apparent that n-heptane exposure greatly increases the observed hysteresis in carbon dioxide permeance. In non-annealed fibers, after exposure to 505 ppm n-heptane, the carbon dioxide permeance at 50 psia is 28% greater than the initial carbon dioxide permeance prior to the 5 day n-heptane exposure period. In non-annealed fibers, after exposure to 2003 ppm n-heptane, the carbon dioxide permeance at 50 psia is 40% greater than the initial carbon dioxide permeance prior to the 5 day n-heptane exposure period.

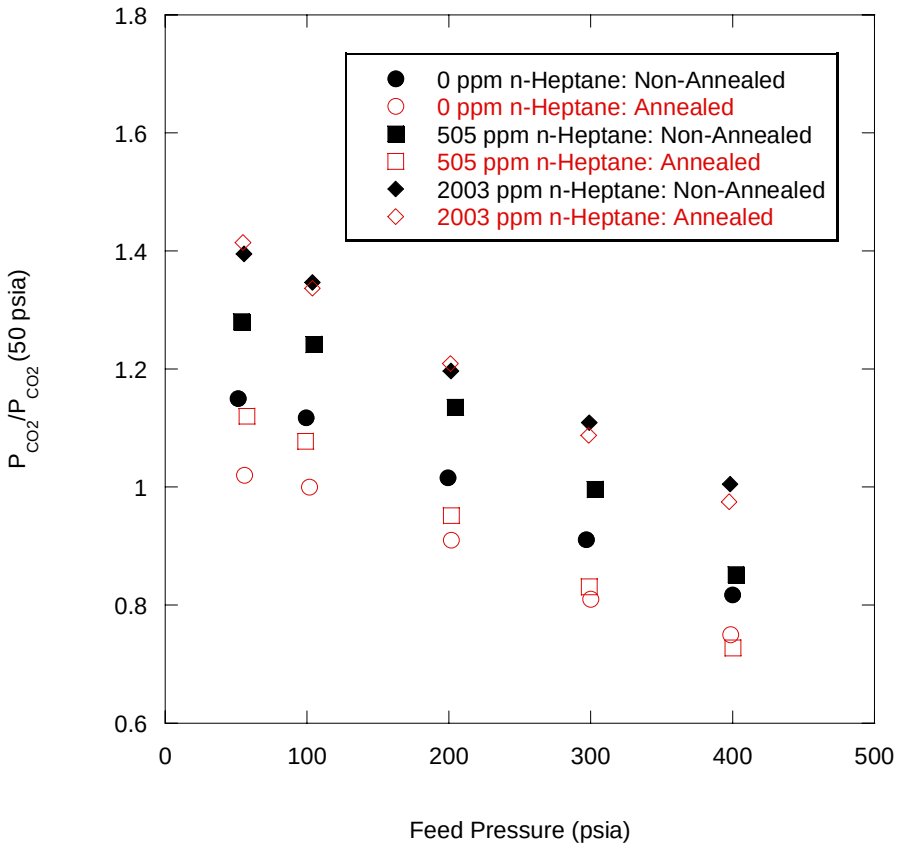

Figure 6.16: Conditioning effect on carbon dioxide permeance after 5 day exposure to 10/90 CO_2/CH_4 + n-heptane feed gas at 400 psia and 35 ^oC

In the annealed fiber samples, the hysteresis in carbon dioxide permeance due to n-heptane exposure is reduced at a concentration of 505 ppm relative to non-annealed fibers. However, in annealed fibers, after exposure to 2003 ppm n-heptane, a reduction in the carbon dioxide hysteresis is not observed. A similar effect was seen by Zhou for Matrimid® asymmetric hollow fiber membranes used for the pervaporation of acetic acid and water [14]. The performance of Matrimid® asymmetric hollow fiber membranes was only stabilized by thermal annealing up to a critical concentration of acetic acid, which acts as a plasticizer, in the feed stream.

In Figure 6.17 the conditioning effect on the carbon dioxide/methane selectivity is shown after exposure to 505 ppm and 2003 ppm n-heptane in the feed gas stream. In non-annealed fibers, after exposure to 505 ppm n-heptane, no loss in carbon dioxide/methane selectivity is observed after depressurization. In non-annealed fibers, after exposure to 2003 ppm n-heptane in the feed gas, the carbon dioxide/methane selectivity at 50 psia is reduced to 88% of the selectivity prior to n-hetpane exposure. In annealed fiber samples, upon depressurization after n-heptane exposure with in experimental uncertainty no loss in carbon dioxide/methane selectivity is observed.

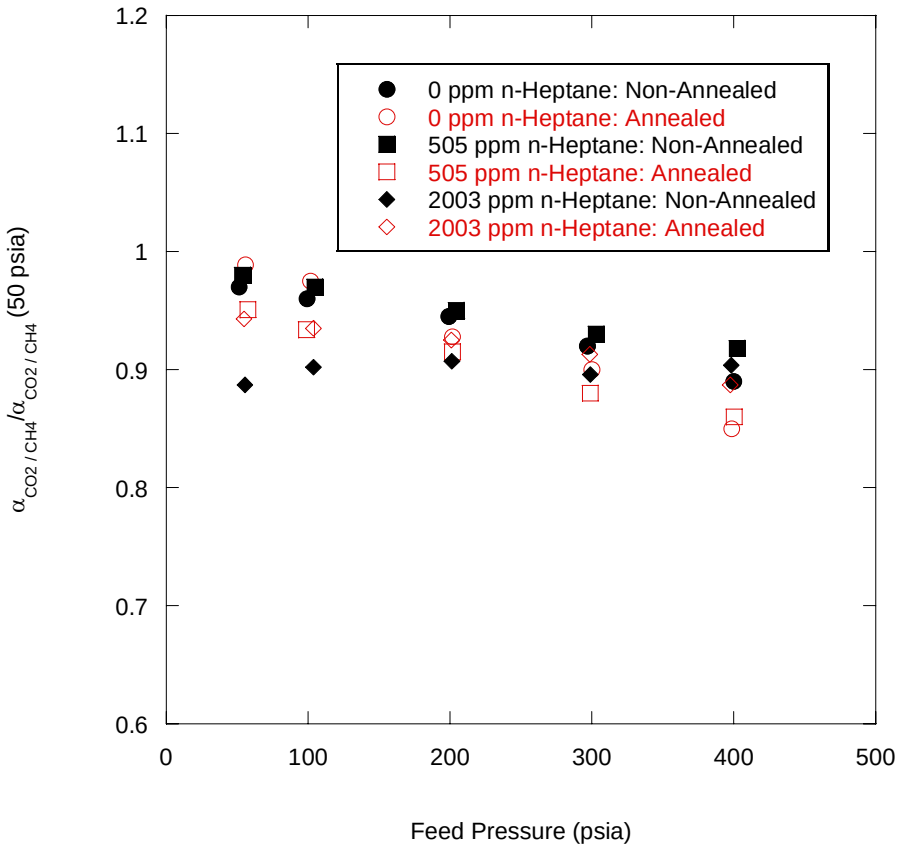

Figure 6.17: Conditioning effect on carbon dioxide/methane selectivity after 5 day exposure to 10/90 CO_2/CH_4 feed gas + n-heptane at 400 psia and 35 ^oC

6.5.4 Depressurization after Exposure to Toluene and n-Heptane

The conditioning effect on carbon dioxide permeance after simultaneous exposure to 284 ppm toluene and 504 ppm n-heptane in the feed gas is shown in Figure 6.18 for non-annealed and annealed Matrimid® asymmetric hollow fiber membranes. The depressurization isotherms for the control case of no n-heptane or toluene exposure from Figure 6.12 are given in Figure 6.18 for reference. For non-annealed fibers it is apparent that simultaneous toluene and n-heptane exposure increases the observed hysteresis in carbon dioxide permeance. In non-annealed

fibers, after simultaneous exposure to 284 ppm toluene and 504 ppm n-heptane, the carbon dioxide permeance at 50 psia is 25% greater than the initial carbon dioxide permeance prior to the 5 day toluene and n-heptane exposure period. In annealed fibers, after simultaneous exposure to toluene and n-heptane, no hysteresis in carbon dioxide permeance is observed.

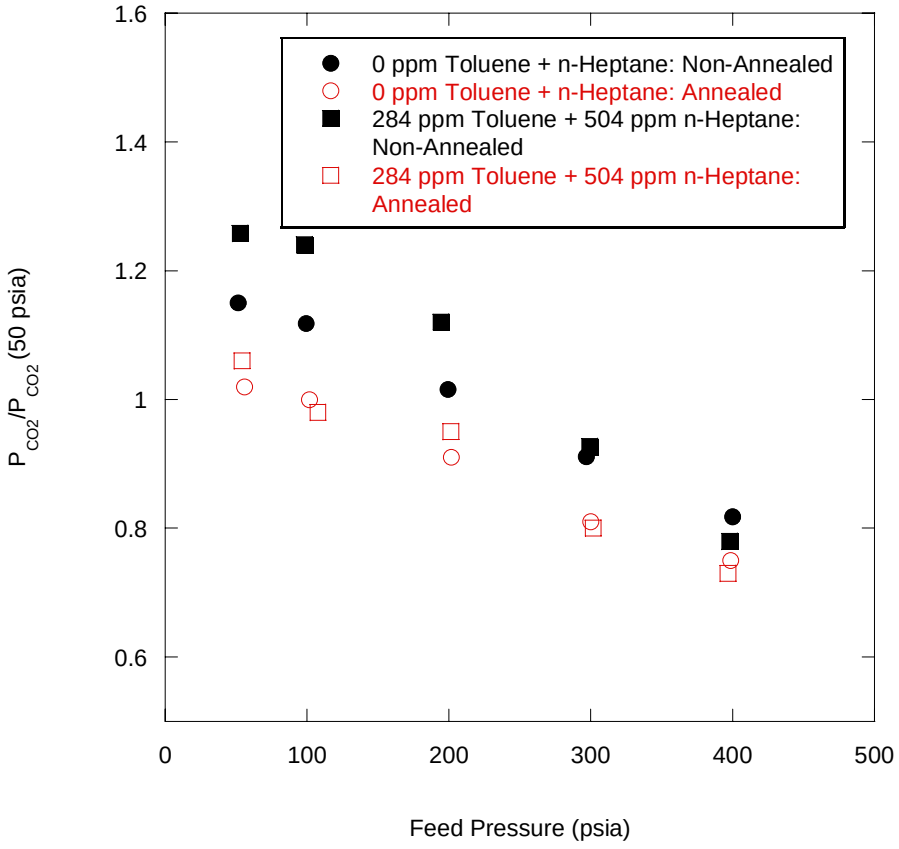

Figure 6.18: Conditioning effect on carbon dioxide permeance after 5 day exposure to 10/90 CO_2/CH_4 + toluene + n-heptane feed gas at 400 psia and 35 ^oC

It is quite surprising that the observed increase in carbon dioxide permeance after exposure to 284 ppm toluene and 504 ppm n-heptane is actually less than the increase in permeance observed after exposure to only 293 ppm toluene. In recent work, a decrease in the plasticization effect was observed in asymmetric hollow fiber membranes in multi-component feed gases [16]. The decrease in plasticization was attributed to competitive sorption between the feed gas components, which lessened the overall plasticizing ability of each component. A similar effect may be occurring in this work leading to a lessening of the conditioning effect when multiple conditioning agents are present in the feed gas.

In Figure 6.19 the conditioning effect on the carbon dioxide/methane selectivity is shown after simultaneous exposure to 284 ppm toluene and 504 ppm n-heptane in the feed gas stream. In non-annealed fibers, after simultaneous exposure to 284 ppm toluene and 504 ppm n-heptane, the carbon dioxide/methane selectivity is 6% less than the selectivity prior to the 5 day toluene and n-heptane exposure. This reduction in selectivity is very close to the experimental uncertainty in selectivity measurements given by the error bars in Figure 6.3. In annealed fibers, after simultaneous exposure to 284 ppm toluene and 504 ppm n-heptane, with in experimental uncertainty there is no change in the carbon dioxide/methane selectivity at 50 psia.

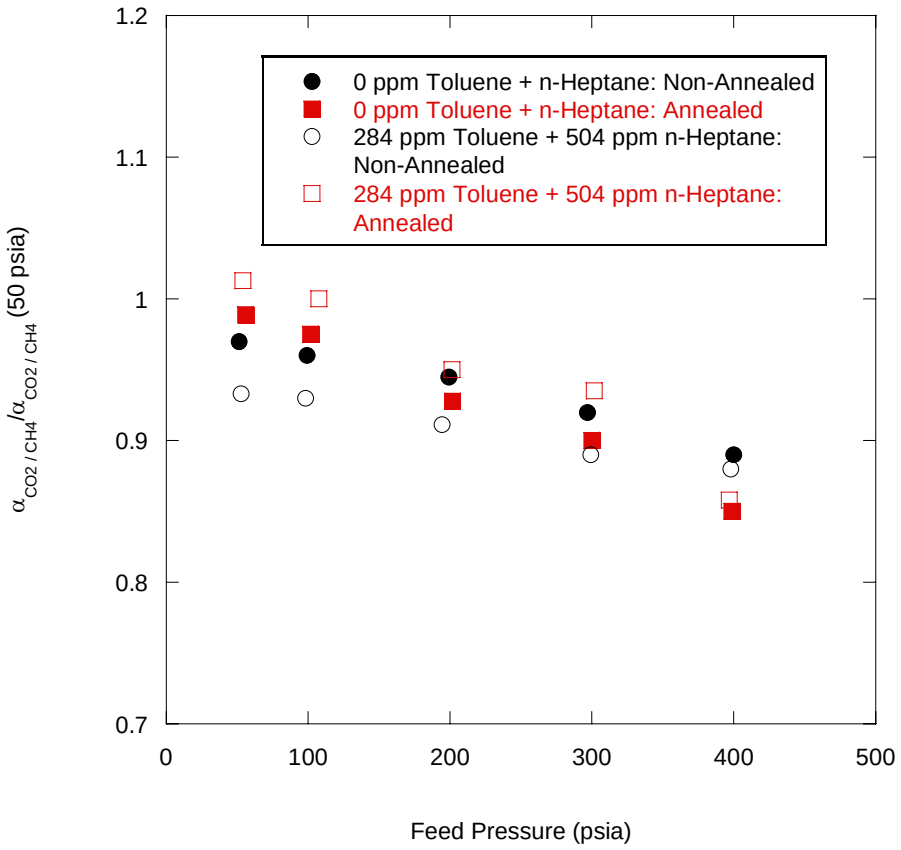

Figure 6.19: Conditioning effect on carbon dioxide/methane selectivity after 5 day exposure to 10/90 CO_2/CH_4 feed gas + toluene + n-heptane at 400 psia and 35 ^oC

6.6 Summary

In this chapter a standardized permeation protocol was used to investigate the effects of highly sorbing feed gas contaminants on membrane performance. The effect on membrane performance during exposure to feed gas contamination, as well as the sustained effect on membrane performance after contaminant removal was investigated in this work. Specifically, this work investigated the effect of two common feed stream contaminants in natural gas processing, toluene and n-heptane,

on membrane performance in non-annealed and annealed Matrimid® asymmetric hollow fiber membranes.

In non-annealed fibers, substantial reductions in the carbon dioxide permeance and the carbon dioxide/methane selectivity were observed during exposure to toluene. Exposure to n-heptane contamination of the feed stream resulted in smaller reductions in permeance and selectivity than those seen during exposure to much lower concentrations of toluene for non-annealed fibers. Simultaneous exposure to toluene and n-heptane resulted in a reduction of the carbon dioxide permeance and carbon dioxide/methane selectivity greater than during to toluene and n-heptane individually.

In non-annealed fibers, upon removal of the feed stream contaminant and depressurization, a hysteresis in the carbon dioxide permeance and carbon dioxide/methane selectivity was observed. The observed hysteresis in permeance and selectivity increased with contaminant exposure concentration for both toluene and n-heptane. The hysteresis in both permeance and selectivity was larger after toluene exposure compared to after n-heptane exposure. Interestingly, the hysteresis after simultaneous exposure to toluene and n-heptane was less than the hysteresis observed for either toluene or n-heptane individually.

Annealing of Matrimid® asymmetric hollow fiber membranes actually increased the reduction in carbon dioxide permeance during contaminant exposure relative to non-annealed fibers. The effect of annealing on the carbon dioxide/methane selectivity during contaminant exposure was more complex. During exposure to toluene, the carbon dioxide/methane selectivity experienced a greater

reduction relative to non-annealed fibers. However, during exposure to 2003 ppm n-heptane, annealing was able to eliminate the reduction in selectivity observed for non-annealed fibers. The more significant effect of annealing was seen upon contaminant removal and depressurization. Except for after exposure to 2003 ppm n-heptane, annealing significantly reduced the hysteresis observed in the carbon dioxide permeance and carbon dioxide/methane selectivity.

The results shown in this chapter allow for quantification of the significant effect of high sorbing feed stream contaminants on membrane performance. The hysteresis in membrane performance after contaminant exposure represents a significant challenge to plant control after feed stream upsets. Furthermore, since trace contamination is a reality in industrial operation, the degraded membrane performance that results from their presence must be accounted for in process calculations. The fundamental cause of the reduction in membrane performance during contaminant exposure will be investigated in Chapter 7.

6.7 References

1. Lee, A.L., et al., "Field tests of membrane modules for the separation of carbon dioxide from low-quality natural gas," *Gas Separation & Purification*, **9**(1), 35 (1995).

2. Al-Juaied, M., *Carbon Dioxide Removal from Natural Gas by Membranes in the Presence of Heavy Hydrocarbons and by Aqueous Diglycolamine/Morpholine*, in *Chemical Engineering*. 2004, The University of Texas: Austin, TX.

3. White, L.S., et al., "Properties of a polyimide gas separation membrane in natural gas streams," *Journal of Membrane Science*, **103**(1-2), 73 (1995).

4. Pereira, B. and W. Admassu, "Effects of chemical impurities on gas sorption in polymeric membranes. I. Polycarbonate and polysulfone," *Separation Science and Technology*, **36**(2), 177 (2001).

5. Pereira, B., W. Admassu, and J. Jensvold, "Effects of chemical impurities on gas sorption in polymeric membranes. II. PC-1 and PC-2," *Separation Science and Technology*, **36**(3), 417 (2001).

6. Pfromm, P.H. and W.J. Koros, "Accelerated physical aging of thin glassy polymer films: evidence from gas transport measurements," *Polymer*, **36**(12), 2379 (1995).

7. Rezac, M.E., et al., "Aging of thin polyimide-ceramic and polycarbonate-ceramic composite membranes," *Industrial & Engineering Chemistry Research*, **32**(9), 1921 (1993).

8. Chung, T.S. and S.K. Teoh, "The ageing phenomenon of polyethersulphone hollow fibre membranes for gas separation and their characteristics," *Journal of Membrane Science*, **152**(2), 175 (1999).

9. Huang, Y. and D.R. Paul, "Physical aging of thin glassy polymer films monitored by gas permeability," *Polymer*, **45**(25), 8377 (2004).

10. Jordan, S.M., M.A. Henson, and W.J. Koros, "The effects of carbon dioxide conditioning on the permeation behavior of hollow fiber asymmetric membranes," *Journal of Membrane Science*, **54**(1-2), 103 (1990).

11. Jordan, S.M., W.J. Koros, and J.K. Beasley, "Characterization of carbon dioxide-induced conditioning of polycarbonate films using penetrants with different solubilities," *Journal of Membrane Science*, **43**(1), 103 (1989).

12. Jordan, S.M., W.J. Koros, and G.K. Fleming, "The effects of carbon dioxide exposure on pure and mixed gas permeation behavior: comparison of glassy polycarbonate and silicone rubber," *Journal of Membrane Science*, **30**(2), 191 (1987).

13. Bos, A., et al., "Plasticization-resistant glassy polyimide membranes for CO2/CH4 separations," *Separation and Purification Technology*, **14**(1-3), 27 (1998).

14. Zhou, F., *Novel Pervaporation for Separating Acetic Acid and Water Mixtures Using Hollow Fiber Membranes*, in *Chemical and Biomolecular Engineering*. 2005, Georgia Institute of Technology: Atlanta, GA.

15. Krol, J.J., M. Boerrigter, and G.H. Koops, "Polyimide hollow fiber gas separation membranes: preparation and the suppression of plasticization in propane/propylene environments," *Journal of Membrane Science*, **184**(2), 275 (2001).

16. Visser, T., G.H. Koops, and M. Wessling, "On the subtle balance between competitive sorption and plasticization effects in asymmetric hollow fiber gas separation membranes," *Journal of Membrane Science*, **252**(1-2), 265 (2005).

CHAPTER 7

MODELING MEMBRANE PERFORMANCE DURING FEED STREAM CONTAMINATION

In this chapter, the underlying cause of the reduced membrane performance, described in Chapter 6, during the presence of highly-sorbing feed stream contaminants will be discussed. In past work, the degradation in membrane performance was attributed to competitive sorption effects, compaction of the asymmetric fiber structure, or antiplasticization; however, a quantitative analysis was not attempted [1]. In this work, it will be shown that while competitive sorption and fiber compaction do have deleterious effects on membrane performance, these mechanisms alone are not able to account for the magnitude of the loss in membrane performance described in Chapter 6. In this chapter, the effect of antiplasticization and plasticization on membrane performance during feed stream contamination will be investigated. It will be shown that the combined impact of competitive sorption and antiplasticization/plasticization are able to account for the loss in membrane performance observed during exposure to highly-sorbing feed stream contaminants.

7.1 Examination of Previous Hypotheses

In this section, the loss of membrane performance due to the effect of competitive sorption in the presence of highly-sorbing feed stream contaminants will be discussed. Furthermore, the possible loss of membrane performance due to compaction of the fiber substructure will be examined. It will be shown that neither

competitive sorption or fiber compaction is capable of predicting the experimentally observed loss of membrane performance, described in Chapter 6, upon introduction of highly-sorbing contaminants to the feed gas.

7.1.1 Dual Mode Transport Analysis

In the case of negligible pressure on the downstream side of the membrane, the dual mode transport model, described in Chapter 2, yields the following expression for the permeability of gas '*i*' in a multi-component feed stream [2]:

$$P_i = k_{D_i} D_{D_i} \left(1 + \frac{F_i K_i}{1 + \sum_{i=1}^{n} b_i p_{i_2}} \right), \tag{7.1}$$

where k_{D_i}, D_{D_i}, F_i, K_i, and b_i are the dual mode transport model parameters as described in Chapter 2. The parameter p_{i_2} is the upstream partial pressure of gas 'i' in a multi-component feed stream of *n* total components. Equation 7.1 is easily extended to express the permeance of gas '*i*' through asymmetric hollow fiber membranes as:

$$\frac{P_i}{L} = \frac{k_{D_i} D_{D_i}}{L} \left(1 + \frac{F_i K_i}{1 + \sum_{i=1}^{n} b_i p_{i_2}} \right), \tag{7.2}$$

where *L* is the selective skin thickness of the asymmetric membrane.

Using the dual mode sorption parameters given in Tables 5.1 and 5.2, which were obtained from the equilibrium sorption isotherms for carbon dioxide and methane, respectively, the dual mode transport model is able to describe the pressure

dependence of the carbon dioxide and methane permeances upon pressurization to 400 psia with a 10/90 CO_2/CH_4 feed gas. In Figures 7.1 and 7.2, the permeance through non-annealed and annealed Matrimid® asymmetric hollow fiber membranes is given along with the dual mode transport model fit for carbon dioxide and methane, respectively. The dual mode transport parameters used in Figures 7.1 and 7.2 are given in Table 7.1

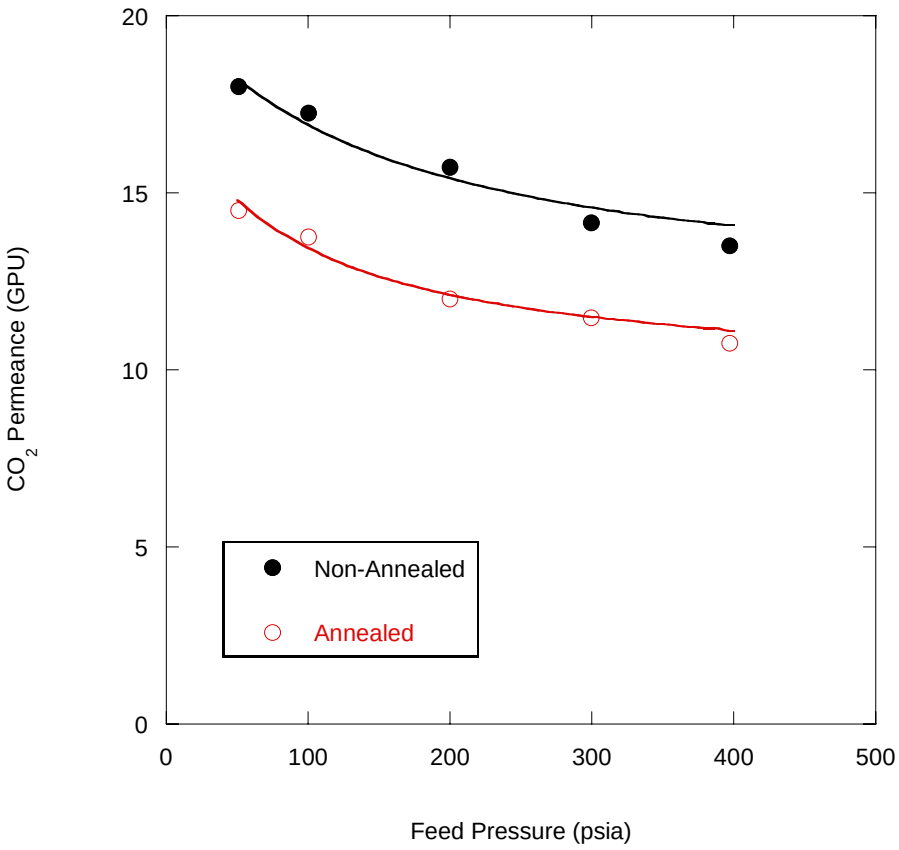

Figure 7.1: Carbon dioxide permeance in Matrimid® asymmetric hollow fiber membranes during pressurization with a 10/90 CO_2/CH_4 feed gas at 35 °C. Solid lines are dual mode transport model fits with parameters given in Table 7.1.

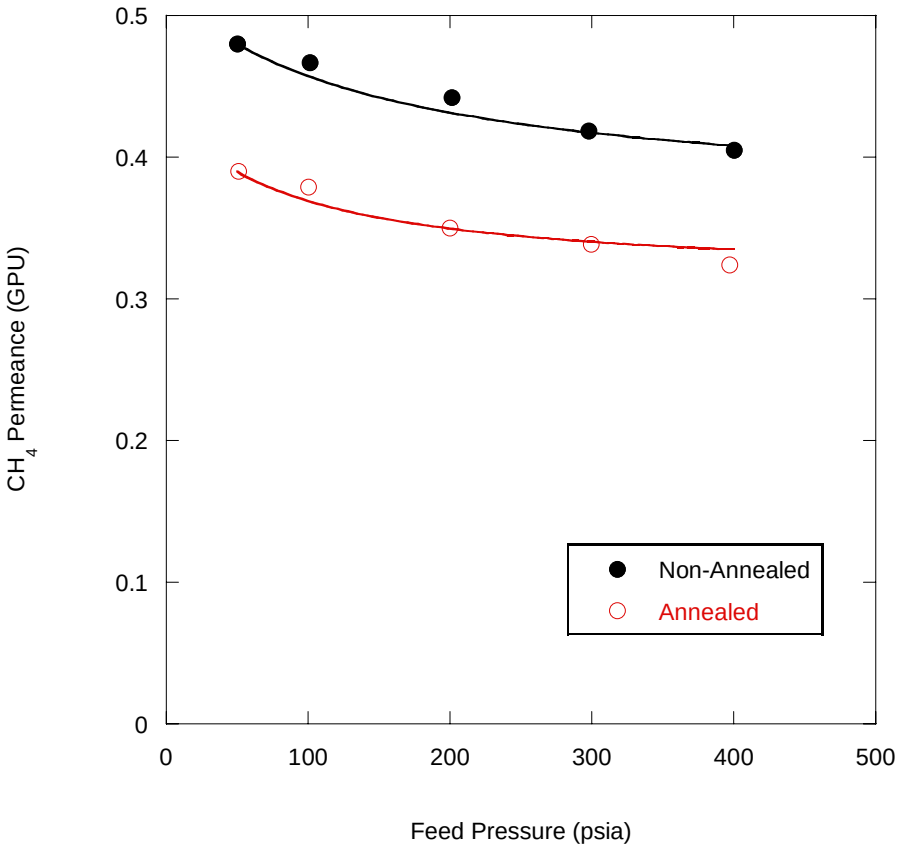

Figure 7.2: Methane permeance in Matrimid® asymmetric hollow fiber membranes during pressurization with a 10/90 CO_2/CH_4 feed gas at 35 °C. Solid lines are dual mode transport model fits with parameters given in Table 7.1.

Table 7.1: Dual mode transport parameters for carbon dioxide and methane in Matrimid® asymmetric hollow fiber membranes at 35 °C

Gas	Fiber State	D_{D_i} / L (cm/sec)	K_i	F_i
CO_2	Non-Annealed	6.2×10^{-4}	8.8	0.086
CO_2	Annealed	4.6×10^{-4}	10	0.082
CH_4	Non-Annealed	3.6×10^{-4}	29	0.014
CH_4	Annealed	1.8×10^{-4}	17	0.023

From examination of Figures 7.1 and 7.2, it is apparent that the pressure dependence of the carbon dioxide and methane permeances with a binary feed gas are

well described by the dual mode transport model. However, as discussed below, the dual mode model is not able to account for the entire reduction in permeance seen upon introduction of a highly-sorbing contaminant, such as toluene or n-heptane, to the feed gas. Applying Equation 7.2, the reduction in carbon dioxide permeance upon introduction of toluene to the feed stream is given as:

$$\frac{\left(\frac{P_{CO2}}{L}\right)^{3^o}}{\left(\frac{P_{CO2}}{L}\right)^{2^o}} = \frac{\left(1+\frac{F_{CO2}K_{CO2}}{1+b_{CO2}p_{CO2_2}+b_{CH4}p_{CH4_2}+b_{toluene}p_{toluene_2}}\right)}{\left(1+\frac{F_{CO2}K_{CO2}}{1+b_{CO2}p_{CO2_2}+b_{CH4}p_{CH4_2}}\right)}, \qquad (7.3)$$

where $\left(\frac{P_{CO2}}{L}\right)^{3^o}$ is the carbon dioxide permeance with a ternary feed gas containing toluene and $\left(\frac{P_{CO2}}{L}\right)^{2^o}$ is the carbon dioxide permeance with a binary feed gas free of toluene. For non-annealed Matrimid® fibers, substitution of the dual mode sorption parameters given in Chapter 5 and the dual mode transport parameters given in Table 7.1 into Equation 7.3 results in the prediction of only a 4% reduction in carbon dioxide permeance at 400 psia upon introduction of 293 ppm toluene to the feed gas; however, as described in Chapter 6, a 45% reduction in carbon dioxide permeance was observed experimentally with this level of toluene feed stream contamination.

It is interesting to determine the maximum possible reduction in carbon dioxide permeance, resulting solely from competitive sorption, as given by the dual mode transport model. The maximum reduction in permeance is achieved by evaluating Equation 7.3 in the limit of an infinite value for the contaminant affinity

constant or an infinite upstream contaminant partial pressure, whereby Equation 7.3 reduces to:

$$\frac{\left(\frac{P_{CO2}}{L}\right)^{3^o}}{\left(\frac{P_{CO2}}{L}\right)^{2^o}} = \left(1 + \frac{F_{CO2}K_{CO2}}{1 + b_{CO2}p_{CO2_2} + b_{CH4}p_{CH4_2}}\right)^{-1}. \qquad (7.4)$$

For non-annealed fibers, Equation 7.4 predicts the maximum possible reduction in carbon dioxide permeance, solely from competitive sorption, as 17%. For annealed fibers, Equation 7.4 predicts the maximum possible reduction in carbon dioxide permeance as 13%. As discussed in the previous chapter, much greater losses in the carbon dioxide permeance were observed experimentally upon introduction of highly-sorbing feed gas contaminants, which the simple dual mode transport model is not capable of capturing.

7.1.2 Fiber Compaction

The decrease in fiber performance during exposure to highly-sorbing feed stream contaminants has been hypothesized to result from compaction of the porous asymmetric hollow fiber membrane substructure [1]. Following this hypothesis, the modulus of the fiber substructure is believed to decrease substantially due to the large concentration of feed stream contaminant sorbed into the glassy polymer matrix. The combination of this decreased modulus and the large transmembrane pressure applied during operation results in compaction of the delicate, porous fiber substructure. This compacted substructure adds an increased resistance for gas transport across the membrane. In the case of thin-skin, defect-free asymmetric membranes the increased

resistance is capable of reducing the overall permeance and selectivity through the membrane [3].

Mathematically, the effect of an increased substructure resistance to gas transport may be examined using the resistance model developed by Henis and Tripodi [4]. This model applies Ohm's law by analogy to describe gas transport as shown below [5]:

$$\frac{Q_A}{A} = \frac{(P_A)(\Delta p_A)}{L}, \tag{7.5}$$

$$I = \frac{\Delta V}{R}, \tag{7.6}$$

where the molar gas flux, Q_A / A (molar flow rate/membrane area), is analogous to electrical current, I, and the partial pressure difference, Δp_A, across the membrane is analogous to the voltage difference, ΔV. From this model, the resistance to gas transport is given as:

$$R = \frac{L}{P_A}. \tag{7.7}$$

Clausi et al. [5] applied the Henis and Tripodi resistance model to study the impact of substructure resistance on the helium permeance and helium/nitrogen selectivity of Matrimid® asymmetric hollow fiber membranes. For the case of a defect-free asymmetric hollow fiber membrane, Clausi expresses the permeance of gas 'A' as two resistances in series:

$$\frac{P_A}{L} = \frac{1}{(L_{skin} / P_A) + R_{sub}}, \tag{7.8}$$

where P_A is the intrinsic permeability of gas 'A' in bulk Matrimid®, $\left(L_{skin} / P_A\right)$ is the skin layer resistance, and R_{sub} is the substructure resistance.

Applying Equation 7.8, the impact of substructure resistance on helium permeance and helium/nitrogen selectivity is shown in Table 7.2. In this example, a selective skin thickness, L_{skin}, of 250 nm was assumed and the substructure resistance was assumed to equal 10% of the skin layer resistance for helium. Values of 0.34 Ba and 26.30 Ba were used for the intrinsic permeability at 35 °C in bulk Matrimid® for nitrogen and helium, respectively [6].

Table 7.2: Predicted effect of substructure resistance on helium permeance and helium/nitrogen selectivity in Matrimid® asymmetric hollow fibers at 35 °C

Resistance	He/N_2 Selectivity	P_{He} / L (GPU)
No substructure resistance	105	77
With substructure resistance	95	70

The effect of substructure resistance, which leads to decreases in helium permeance and helium/nitrogen selectivity, is apparent from examination of Table 7.2. If fiber compaction was the cause of the significant loss of gas permeance and selectivity observed during the presence of highly-sorbing feed stream contaminants, one would expect to observe an equally significant loss of helium/nitrogen selectivity and helium permeance after contaminant exposure. In Tables 7.3 and 7.4, the helium permeance and helium/nitrogen selectivity are given for non-annealed fibers before and after a 5 day exposure to a 10/90 CO_2/CH_4 feed gas containing 293 ppm toluene and 505 ppm n-heptane, respectively, at 400 psia and 35 °C.

Table 7.3: Experimentally observed helium permeance and helium/nitrogen selectivity before and after exposure to a 10/90 CO_2/CH_4 feed gas containing 293 ppm toluene at 400 psia and 35 ^oC in non-annealed fibers

Fiber State	He/N_2 Selectivity	P_{He} / L (GPU)
Before exposure	100	65
After exposure	116	56

Table 7.4: Experimentally observed helium permeance and helium/nitrogen selectivity before and after exposure to a 10/90 CO_2/CH_4 feed gas containing 505 ppm n-heptane at 400 psia and 35 ^oC in non-annealed fibers

Fiber State	He/N_2 Selectivity	P_{He} / L (GPU)
Before exposure	110	69
After exposure	96	72

The changes in helium permeance and helium/nitrogen selectivity after exposure to toluene and n-heptane feed stream contamination, as shown in Tables 7.3 and 7.4, are not consistent with the predicted effects of substructure compaction shown in Table 7.2. Instead the data in Tables 7.3 and 7.4 show a very complex impact on helium permeance and helium/nitrogen selectivity after exposure to highly-sorbing feed stream contaminants. After exposure to 293 ppm toluene, the helium/nitrogen selectivity is actually increased by 16%, while the helium permeance is decreased by 14%. After exposure to 505 ppm n-heptane, the helium/nitrogen is decreased by 13%, while the helium permeance is slightly increased. These effects are most likely the result of subtle changes in the glassy state of the selective skin,

due to conditioning, rather than the result of changes in the fiber substructure. The overall much higher selectivity and lower permeance measured experimentally in asymmetric hollow fiber membranes (see Tables 7.3 and 7.4) than the predicted selectivity and permeance from intrinsic permeabilities (see Table 7.2) is the result of accelerated physical aging [7]. It is important to realize, however, that while compaction of the fiber substructure does not have a significant impact on membrane performance under the conditions studied in this work, at higher levels of feed stream contamination and transmembrane pressure fiber compaction may significantly impact performance.

7.2 Impact of Antiplasticization

In this section, the impact of antiplasticization and plasticization on membrane performance during exposure to highly-sorbing feed stream contaminants will be investigated. It will be shown that the combined effect of reductions in permeance from competitive sorption and antiplasticization account for the loss in membrane performance described in Chapter 6 for Matrimid® asymmetric hollow fiber membranes exposed to highly-sorbing feed stream contaminants.

7.2.1 Antiplasticization Model Development

As described in Chapter 2, antiplasticization occurs when sorption of a gas or vapor reduces the free volume of the polymer/vapor mixture relative to the free volume of the pure polymer [8-12]. A reduction in free volume is well correlated to a reduction in gas permeability [13]. It is hypothesized that the loss of permeance

experienced upon introduction of highly-sorbing feed stream contaminants is a direct result of antiplasticization. In this section, a model of antiplasticization will be developed that is capable of accounting for this loss in membrane performance during feed stream contamination.

The effect of antiplasticization on gas permeation is most readily captured through the use of so-called free volume models. The most simplistic of these models, has been previously shown in Chapter 2 [13]:

$$P_A = A_A \exp\left(\frac{-B_A}{FFV}\right), \tag{2.20}$$

where A_A and B_A are constant for a particular gas and *FFV* is the fractional free volume of the polymer. Table 7.5 provides values of A_A and B_A for carbon dioxide and methane correlated from a dataset of 105 polymers [13].

Table 7.5: Values of A_A and B_A for carbon dioxide and methane at 10 atm and 35 °C. $P_A = A_A \exp(-B_A / FFV)$ (Barrer) [13]

Parameter	CO_2	CH_4
A_A	1750	114
B_A	0.860	0.967

In Chapter 2, the fractional free volume of the polymer was defined as:

$$FFV = \frac{\hat{V}_g - \hat{V}_0}{\hat{V}_0}, \tag{2.21}$$

where $\hat{V}_g$ is the specific volume of the polymer in the glassy state and $\hat{V}_0$ is the occupied specific volume of the polymer chains. Typically $\hat{V}_0$ is calculated using Bondi's group contribution method where [14]:

$$\hat{V}_0 = 1.3\sum_{k=1}^{K}\left(\hat{V}_W\right)_k \; . \tag{7.9}$$

$\left(\hat{V}_W\right)_k$ are the specific van der Waals volumes of various groups in the polymer repeat structure. *K* is the total number of groups into which the repeat structure is divided. The factor 1.3 accounts for the packing density.

The free volume model described above is used to predict permeability for a given gas as the fractional free volume changes. Typically, the change in free volume is achieved by simply switching to a different polymer; therefore, application of the model described above allows for prediction of gas permeability in various polymers. In the case of antiplasticization, however, the polymer remains the same but its fractional free volume changes due to sorption of a diluent. In this case, the fractional free volume of the polymer/antiplasticizer mixture is dependent upon the mass uptake of antiplasticizer and can be written as [15]:

$$FFV_{mix} = \frac{\hat{V}_{mix}^{glass} - \left(\hat{V}_0\right)_{mix}}{\hat{V}_{mix}^{glass}}, \tag{7.10}$$

where $\hat{V}_{mix}^{glass}$ is the specific volume of the polymer/antiplasticizer mixture in the glassy state. By application of Equation 2.20, the permeability of gas *A* in the polymer/antiplasticizer mixture, $\left(P_A\right)_{mix}$, is therefore given as:

$$\left(P_A\right)_{mix} = A_A \exp\left[\frac{-B_A}{FFV_{mix}}\right] \quad . \tag{7.11}$$

The occupied volume of polymer/antiplasticizer mixture, $\left(\hat{V}_0\right)_{mix}$, is given as [15]:

$$\left(\hat{V}_0\right)_{mix} = 1.3\left[w_1 \sum_{j=1}^{J} \left(\hat{V}_W\right)_j + w_2 \sum_{k=1}^{K} \left(\hat{V}_W\right)_k \right] \tag{7.12}$$

where w_1 is the weight fraction of antiplasticizer and w_2 is the weight fraction of polymer in the polymer/antiplasticizer mixture.

Methods are available in the literature to calculate the specific volume of a polymer/antiplasticizer mixture in the glassy state, $\hat{V}_{mix}^{glass}$ [8, 12]. Ruiz-Treviño and Paul give the specific volume of any polymer/diluent mixture in the glassy state at temperature *T* as [12]:

$$\hat{V}_{mix}^{glass}(T) = w_1 \hat{V}_1^{liquid}(T) + w_2 \hat{V}_2^{liquid}(T) + \left(\frac{d\hat{V}_{mix}^{liquid}}{dT} - \frac{d\hat{V}_{mix}^{glass}}{dT} \right)\left(T_{g_{mix}} - T\right) \tag{7.13}$$

where $\hat{V}_1^{liquid}$ and $\hat{V}_2^{liquid}$ are the *equilibrium* specific volumes of the diluent and polymer, respectively, in the liquid state at temperature *T*; however, these volumes need not be physically attainable due to the glass transition. $\frac{d\hat{V}_{mix}^{liquid}}{dT}$ and $\frac{d\hat{V}_{mix}^{glass}}{dT}$ are the thermal expansion coefficients of the polymer/diluent mixture in the liquid and glassy states, respectively. Values of the thermal expansion coefficients of polymer/diluent mixtures are not common in the literature; therefore, Ruiz-Treviño and Paul make the following assumption [12]:

$$\left(\frac{d\hat{V}_{mix}^{liquid}}{dT} - \frac{d\hat{V}_{mix}^{glass}}{dT} \right) \approx \left(\frac{d\hat{V}_2^{liquid}}{dT} - \frac{d\hat{V}_2^{glass}}{dT} \right) \tag{7.14}$$

whereby, the thermal expansion coefficients in the liquid and glassy states for the mixture are equal to that of the pure polymer.

Several techniques exist to correlate and predict $T_{g_{mix}}$, the glass transition of a polymer/diluent mixture [16-19]. Ruiz-Treviño and Paul [12] make use of the Gordon-Taylor equation [19], which expresses $T_{g_{mix}}$ as:

$$T_{g_{mix}} = \frac{w_1 T_{g1} + \theta w_2 T_{g2}}{w_1 + \theta w_2}. \tag{7.15}$$

T_{g1} and T_{g2} are the glass transition temperatures of the pure diluent and polymer, respectively. θ is an adjustable correlation parameter.

It is important to note that only two assumptions were made in the derivation of Equation 7.13: volume additivity applies in the liquid state (i.e., $\hat{V}_{mix}^{liquid}(T) = w_1 \hat{V}_1^{liquid}(T) + w_2 \hat{V}_2^{liquid}(T)$) and that the polymer/diluent mixture has a linear volume-temperature relationship above and below its glass transition.

The effect of diluent sorption on the gas permeability is given by combing Equations 2.20 and 7.11 to yield:

$$\frac{(P_A)_{mix}}{P_A} = \exp\left[B_A \left(\frac{1}{FFV} - \frac{1}{FFV_{mix}} \right) \right]. \tag{7.16}$$

When the fractional free volume of the polymer/diluent mixture is less than the factional free volume of the pure polymer ($FFV_{mix} < FFV$), antiplasticization occurs, and the permeability in the mixture is less than the permeability in the pure polymer ($(P_A)_{mix} < P_A$). When the fractional free volume of the polymer/diluent mixture is greater than the fractional free volume of the pure polymer ($FFV_{mix} > FFV$), plasticization occurs, and the permeability in the mixture is greater than the permeability in the pure polymer ($(P_A)_{mix} > P_A$).

7.2.2 Antiplasticization Model Application

In this section the combined effect of competitive sorption and antiplasticization/plasticization are shown to account for the degradation in membrane performance observed in Chapter 6 during exposure to highly-sorbing feed stream contaminants. Mathematically, this combined effect is expressed as the sum of the reduction in permeance due to competitive sorption given by Equation 7.3 and the impact on permeance due to antiplasticization/plasticization given by Equation 7.16. The application of Equation 7.3 to calculate the impact of competitive sorption is straightforward with the use of the dual mode sorption parameters in Chapter 5 and the dual mode transport parameters in Table 7.1.

To the author's knowledge this is the first application of a relation such as Equation 7.16 to account for the effect of antiplasticization/plasticization from a component which was sorbed into the membrane from the feed stream. However, relations similar to Equation 7.16 have been used successfully in past work to account for the effect of antiplasticization/plasticization on gas permeability through polymers which were blended with high molecular weight additives [15, 20]. There are two key differences between these applications. Firstly, in the case of the polymer blends, the high molecular weight additive which acts as an antiplasticizer or plasticizer, depending on concentration, is well-mixed throughout the glassy polymer matrix. In the case of a diluent sorbed from the feed stream, a gradient in diluent concentration exists from the upstream to downstream side of the membrane. In this application, the diluent weight fraction, w_1, used in Equations 7.12, 7.13, and 7.15, is the average

diluent weight fraction across the membrane. Since the downstream side of the membrane is maintained under vacuum in these experiments, the average diluent weight fraction through the membrane is estimated as equal to half the diluent weight fraction at the upstream side of the membrane. Secondly, the past work on high molecular weight diluent/polymer mixtures was used to predict the pure gas permeability through the mixture. In this work, dissolved populations of carbon dioxide and methane exist in the polymer along with the dissolved population of highly-sorbing diluent (toluene or n-heptane). However, since the effect of the sorbed carbon dioxide and methane populations alone on the gas permeability was accounted for by the dual mode transport model, carbon dioxide and methane are assumed to have neither an antiplasticizing or plasticizing effect on gas permeability. In this analysis the highly-sorbing diluent, toluene or n-heptane, is treated as the only sorbed component capable of acting as an antiplasticizer or plasticizer.

For application of the model of antiplasticization/plasticization, described in the previous section, determination of several parameters must be made.
In Equation 7.13, the hypothetical equilibrium specific volume of the polymer in the liquid state, $\hat{V}_2^{liquid}$, may be calculated using the following expression [12]:

$$\hat{V}_2^{liquid} = \hat{V}_2^{glass} + \left(\frac{d\hat{V}_2^{glass}}{dT} - \frac{d\hat{V}_2^{liquid}}{dT} \right)\left(T_{g2} - T\right). \qquad (7.17)$$

where $\hat{V}_2^{glass}$ is the specific volume of the pure polymer in the glassy state. The difference in the thermal expansion coefficients of the polymer in the liquid state and glassy state is estimated using the following expression as suggested by Ruiz-Treviño and Paul [12]:

$$\left(\frac{d\hat{V}_2^{liquid}}{dT} - \frac{d\hat{V}_2^{glass}}{dT} \right) \approx 5.5 \times 10^{-4} \hat{V}_W , \qquad (7.18)$$

where $\hat{V}_W$ is the specific van der Waals volume of the polymer repeat unit. In application an adjustable parameter, α, has been added such that Equation 7.13 becomes:

$$\hat{V}_{mix}^{glass}(T) = w_1 \hat{V}_1^{liquid}(T) + w_2 \hat{V}_2^{liquid}(T) + \alpha\left(5.5 \times 10^{-4} \hat{V}_W\right)\left(T_{g_{mix}} - T\right). \qquad (7.19)$$

The two adjustable parameters, θ in Equation 7.15 and α in Equation 7.19, are different for carbon dioxide and methane. The difference in these parameters for carbon dioxide and methane ultimately results in a different fractional free volume in the diluent/polymer mixture for each gas. A similar assumption of effective free volumes, which are different for each gas in pure polymers, has been made previously by Park and Paul [13]. This assumption is supported by molecular simulations that indicate the size and shape of the gas molecule influence the amount of space accessible to the gas in the polymer [21].

The remaining parameters required for model application are known and given in Table 7.6.

Table 7.6: Parameters used to model antiplasticization/plasticization behavior in Matrimid® asymmetric hollow fiber membranes at 35 °C

Parameter	Value
$\left(\hat{V}_W\right)_{Matrimid}$ [22]	0.531 cm^3/g
$\left(\hat{V}_W\right)_{Toluene}$ [22]	0.645 cm^3/g
$\left(\hat{V}_W\right)_{n-hep\tan e}$ [22]	0.783 cm^3/g
$\hat{V}_{Matrimid}^{glass}$ [23]	0.807 cm^3/g
$\hat{V}_{Matrimid}^{liquid}$ *	0.727 cm^3/g
$\hat{V}_{Toluene}^{liquid}$ [24]	1.173 cm^3/g
$\hat{V}_{n-hep\tan e}^{liquid}$ [24]	1.490 cm^3/g
$\left(T_g\right)_{Matrimid}$ [23]	305 °C
$\left(T_g\right)_{Toluene}$ [25]	-156 °C

* calculated from Equation 7.17

7.2.2.1 Model Application During Toluene Exposure

In order to apply the model of antiplasticization/plasticization, developed above, during exposure to toluene feed stream contamination additional data points were collected beyond the two shown in Chapter 6 (i.e., 293 ppm and 544 ppm toluene). These additional data points were collected using an abbreviated form of the permeation protocol described in Chapter 6. The Matrimid® asymmetric hollow fiber membranes were simply pressurized with a 10/90 CO_2/CH_4 feed gas to 400 psia. A concentration of toluene was introduced to the feed stream at 400 psia and maintained for 3 days. After the initial changes in the carbon dioxide permeance and carbon dioxide/methane selectivity during the first 24 hours of toluene exposure, significant changes in membrane performance were not observed over the remainder of the abbreviated 3 day exposure period. For these data points, the hysteresis in transport properties upon depressurization was not investigated.

The observed reduction in carbon dioxide and methane permeance through Matrimid® asymmetric hollow fiber membranes upon introduction of toluene feed stream contamination is shown in Figures 7.3 and 7.4, respectively. In Figures 7.3 and 7.4, the permeance is normalized by the pre-exposure permeance at 400 psia and is plotted versus the average weight fraction of toluene sorbed into the membrane. The solid lines in Figures 7.3 and 7.4 represent the fit from the model developed in the previous section, which accounts for the effect of competitive sorption (Equation 7.3) and antiplasticization/plasticization (Equation 7.16).

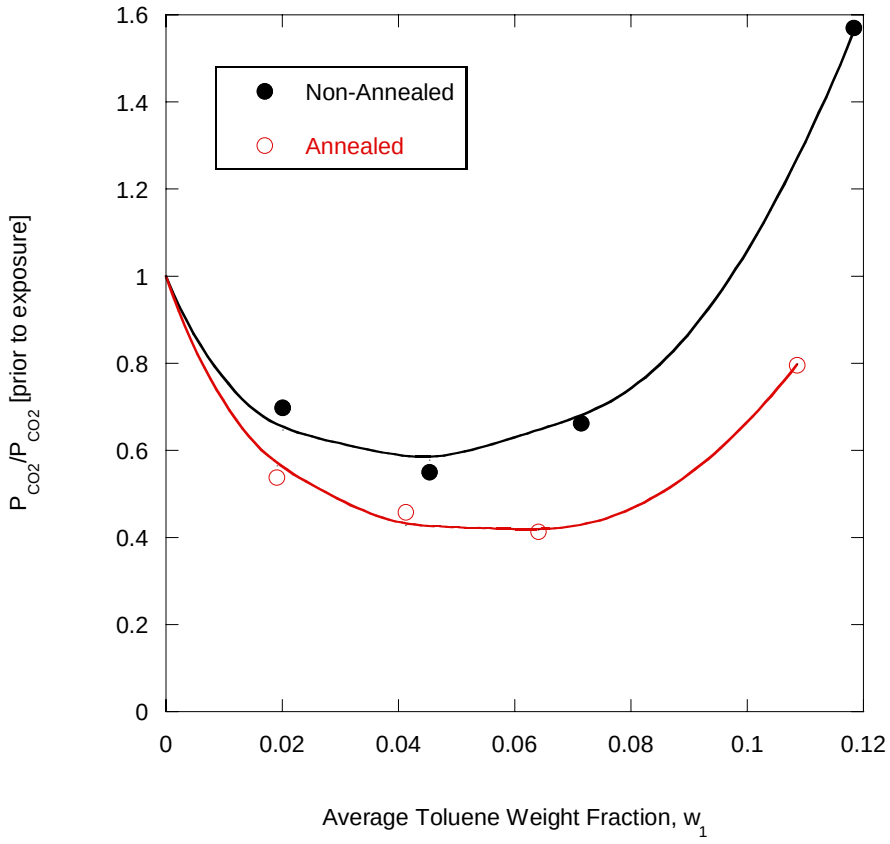

Figure 7.3: Effect of sorbed toluene weight fraction on carbon dioxide permeance in annealed and non-annealed Matrimid® asymmetric hollow fiber membranes at 35 °C. Solid lines are model fit.

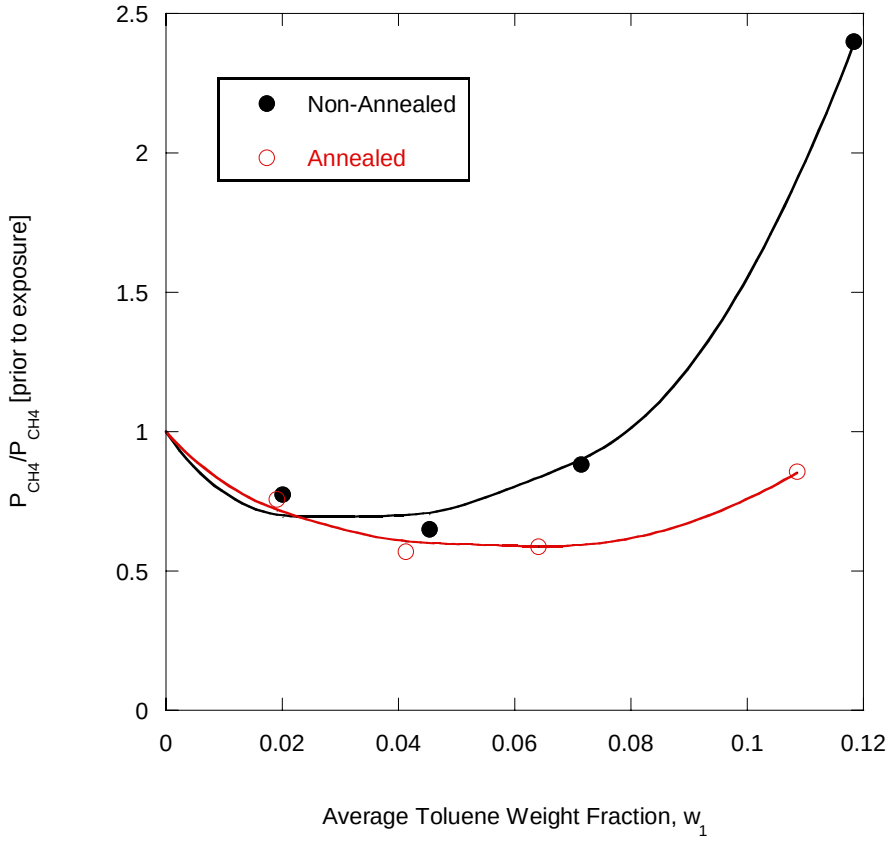

Figure 7.4: Effect of sorbed toluene weight fraction on methane permeance in annealed and non-annealed Matrimid® asymmetric hollow fiber membranes at 35 °C. Solid lines are model fit.

For reference, Table 7.7 lists the corresponding concentration and activity of toluene in the feed stream for the data points shown in Figures 7.3 and 7.4.

Table 7.7: Toluene feed stream compositions used in Figures 7.3 and 7.4

Toluene Feed Stream Composition		Average Sorbed Weight Fraction of Toluene, w_1	
Concentration (ppm)	Activity $\left(P_{toluene} / P_{toluene}^{sat}\right)$	Non-Annealed fibers	Annealed fibers
112	0.05	0.020	0.019
293	0.13	0.045	0.041
544	0.24	0.072	0.064
1224	0.54	0.118	0.109

From examination of Figures 7.3 and 7.4, the reduction in permeance for both carbon dioxide and methane is seen at low uptakes of toluene, which is a clear indication of antiplasticization. At high toluene weight fractions (high concentration of toluene in the feed stream), the permeance for both carbon dioxide and methane increases indicating plasticization. As anticipated from the discussion provided in Chapter 4, the plasticization response is not seen until higher toluene uptakes for annealed fibers compared to non-annealed fibers.

The values of the adjustable parameters, θ in Equation 7.15 and α in Equation 7.18, used in the model fits shown in Figures 7.3 and 7.4 are provided in Table 7.8. In all cases, the value of α is less than one indicating that the value of $\left(\frac{d\hat{V}_{mix}^{liquid}}{dT} - \frac{d\hat{V}_{mix}^{glass}}{dT}\right)$ is overestimated. The reason for this over prediction is most likely due to the failure of the assumptions implicit in Equations 7.14 and 7.18. At

the high concentration of dissolved diluent studied in this work, it is likely that the thermal expansion coefficient of the diluent/polymer mixture is not equal to that of the pure polymer. The values of θ given in Table 7.8 are similar to the values used by Ruiz-Treviño and Paul [12]. As stated previously, the difference in θ and α between carbon dioxide and methane indicate that a slightly different free volume is accessible to each gas inside the polymer.

Table 7.8: Adjustable parameters used in the model fits during toluene exposure shown in Figures 7.3 and 7.4

Gas	Non-Annealed		Annealed	
	θ	α	θ	α
CO_2	0.103	0.473	0.100	0.526
CH_4	0.107	0.445	0.152	0.643

7.2.2.2 Model Application During n-Heptane Exposure

Additional data points were collected for the performance of Matrimid® asymmetric hollow fiber membranes during exposure to n-heptane feed stream contamination beyond the two shown in Chapter 6 (i.e., 505 ppm and 2003 ppm toluene). These additional data points were collected using the same abbreviated permeation protocol described for toluene in the last section.

The observed reduction in carbon dioxide and methane permeance through Matrimid® asymmetric hollow fiber membranes upon introduction of n-heptane feed stream contamination is shown in Figures 7.5 and 7.6, respectively. In these figures, the permeance is normalized by the pre-exposure permeance at 400 psia and is plotted versus the average weight fraction of n-heptane sorbed into the membrane. The solid

lines in Figures 7.5 and 7.6 represent the fit from the model developed in the previously, which accounts for the effect of competitive sorption (Equation 7.3) and antiplasticization/plasticization (Equation 7.16).

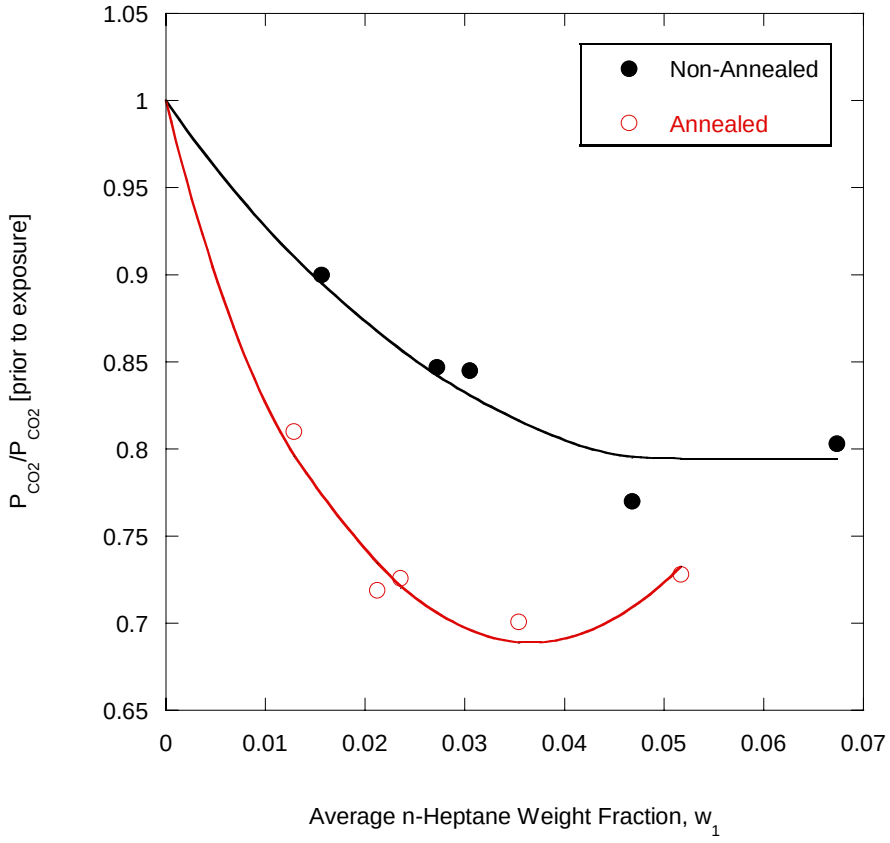

Figure 7.5: Effect of sorbed n-heptane weight fraction on carbon dioxide permeance in annealed and non-annealed Matrimid® asymmetric hollow fiber membranes at 35 °C. Solid lines are model fit.

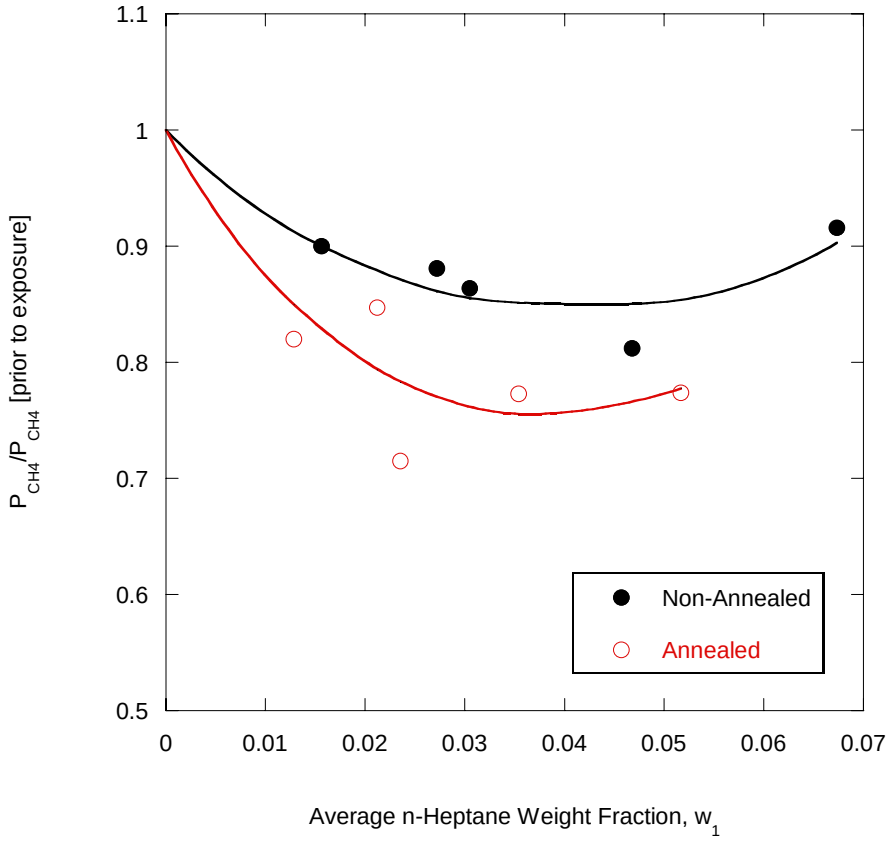

Figure 7.6: Effect of sorbed n-heptane weight fraction on methane permeance in annealed and non-annealed Matrimid® asymmetric hollow fiber membranes at 35 °C. Solid lines are model fit.

For reference, Table 7.9 lists the corresponding concentration and activity of n-heptane in the feed stream for the data points shown in Figures 7.5 and 7.6.

Table 7.9: n-Heptane feed stream compositions used in Figures 7.5 and 7.6

n-Heptane Feed Stream Composition		Average Sorbed Weight Fraction of n-Heptane, w_1	
Concentration (ppm)	Activity $\left(P_{toluene} / P_{toluene}^{sat}\right)$	Non-Annealed fibers	Annealed fibers
250	0.07	0.016	0.013
505	0.14	0.027	0.021
590	0.17	0.030	0.024
1108	0.31	0.047	0.035
2003	0.56	0.067	0.052

The values of the adjustable parameters, θ in Equation 7.15 and α in Equation 7.18, used in the model fits shown in Figures 7.5 and 7.6 are provided in Table 7.10. Unfortunately n-heptane is not a glass-forming liquid, so a glass transition temperature for use in Equation 7.15 is not available for n-heptane. In this situation, the hypothetical glass transition temperature of n-heptane in Equation 7.15, T_{g1}, is treated as an additional adjustable parameter. The value of the hypothetical glass transition temperature regressed from the data was -151 ^{o}C. This value is in the range of the glass transition temperatures reported for other seven carbon atom containing glass forming molecules [26, 27].

Table 7.10: Adjustable parameters used in the model fits during n-heptane exposure shown in Figures 7.5 and 7.6

Gas	Non-Annealed		Annealed	
	θ	α	θ	α
CO_2	0.245	1.11	0.126	0.683
CH_4	0.203	0.932	0.151	0.789

7.2.3 Discussion of Model Results

From investigation of the model results presented in the previous section for the performance of Matrimid® asymmetric hollow fiber membranes during exposure to toluene and n-heptane the following key conclusions may be made:

- A model which accounts for both the effect of competitive sorption and antiplasticization/plasticization on gas permeance is capable of describing the performance of Matrimid® asymmetric membranes in the presence of highly-sorbing feed stream contaminants.
- Annealing of Matrimid® asymmetric hollow fiber membranes increases the reduction in gas permeance due to antiplasticization. The greater reduction in segmental mobility due to antiplasticization in the case of annealed fibers may be the result of the initial segmental mobility, prior to contaminant sorption, being less than in non-annealed fibers. Therefore, the presence of an antiplasticizing penetrant has more of an effect on the mobility of the already hindered segment, in the case of annealed fibers, than on the mobility of an "unhindered" segment, in the case of non-annealed fibers.

- The variation in the adjustable parameters, θ and α, indicates that carbon dioxide and methane "sense" the effect of antiplasticization/plasticization slightly differently. This difference in behavior between carbon dioxide and methane behaviors can be rationalized using the concept of an effective free volume where differences in the shape and size of carbon dioxide and methane affect the amount of volume accessible to each gas. However, admittedly, some of the variation of the adjustable parameters is simply due to complexity in the physical situation that is not accounted for by the model.
- Speculatively, α and θ are both related to the contaminant-polymer interactions. In general, estimating the interaction energy between diluent molecules and polymer segments is extremely difficult for polar components such as those studied in this work. This is a problem that is commonly faced in development of advanced sorption models such as the Sanchez-Lacombe model [28, 29] and the nonequilibrium lattice fluid model [30]. Usually, in these situations a mixing rule based on the pure component interaction energies with a deviation variable is used to calculate the diluent-polymer interaction energy. The value of the deviation variable may be calculated from a single mixture data point. With further experimental measurements, it may be possible to develop mixing rules for the calculation of α and θ based on intrinsic thermodynamic properties of the contaminant and the polymer, such as the difference in solubility factors.

It is important to note that in future work this model may be extended to correlate membrane performance in the presence of multiple feed stream

contaminants. In this situation, Equation 7.15 maybe used to correlate the glass transition temperature of the mixture, $T_{g_{mix}}$, where T_{g1} is the hypothetical glass transition of the sorbed contaminant mixture and w_1 is the average weight fraction of all sorbed contaminants. It is expected that the performance during exposure to multiple contaminant will be a complex average of the performance during exposure to individual contaminants.

Examination of Figures 7.3-7.6 allows one to make an interesting suggestion regarding the industrial operation of gas separation membranes. Since reducing the concentration of highly-sorbing feed stream contaminants to zero is not practical in industrial operation, feed stream contaminants are usually reduced to the lowest concentration which is economically feasible. However, this may not be the best strategy for dealing with contaminants during industrial operation. From examination of Figures 7.3-7.6, an intermediate contaminant concentration exists where the permeance in the presence of the contaminant is the same as the permeance when no contaminant is present. For example, in Figure 7.3 for non-annealed fibers the carbon dioxide permeance with an average toluene weight fraction of 0.1 is approximately equal to the carbon dioxide permeance with no toluene uptake. This level of toluene uptake equates to a concentration of ~900 ppm toluene in the feed stream at 400 psia and 35 ^{o}C. For a slight sacrifice in selectivity, operating at this intermediate level of feed stream contamination would decrease the costs associated with the pre-treatment and obviate the significant reduction in permeance experienced at lower contaminant concentrations due to antiplasticization.

7.3 Summary

In this chapter, it was shown that neither competitive sorption nor fiber compaction fully account for the degradation in membrane performance experienced during exposure to highly-sorbing feed stream contaminants as described in Chapter 6. The dual mode transport model was used to show that competitive sorption only accounted for a small portion of the overall loss in membrane performance observed during feed stream contamination. A resistance model was used to show that significant compaction of the fiber substructure did not occur under the conditions which were tested in this work. It is important to realize, however, that substructure compaction is capable of greatly reducing membrane performance. At higher contaminant concentrations and transmembrane pressure differences than those studied in this work, fiber compaction may have a significant impact on membrane performance.

A free volume model was developed to account for the effects of antiplasticization and plasticization on membrane performance. It was shown that the combined contributions of competitive sorption and antiplasticization/plasticization account for the loss of membrane performance observed during feed stream contamination. When the glass transition of the feed stream contaminant is known, the model developed in this chapter is able to successfully correlate the permeance of a given gas at any concentration of feed stream contamination using only two adjustable parameters.

7.4 References

1. Al-Juaied, M., *Carbon Dioxide Removal from Natural Gas by Membranes in the Presence of Heavy Hydrocarbons and by Aqueous Diglycolamine/Morpholine*, in *Chemical Engineering*. 2004, The University of Texas: Austin, TX.

2. O'Brien, K.C., et al., "A new technique for the measurement of multicomponent gas transport through polymeric films," *Journal of Membrane Science*, **29**(3), 229 (1986).

3. Pinnau, I. and W.J. Koros, "Relationship between substructure resistance and gas separation properties of defect-free integrally skinned asymmetric membranes," *Industrial & Engineering Chemistry Research*, **30**(8), 1837 (1991).

4. Henis, J.M.S. and M.K. Tripodi, "Composite hollow fiber membranes for gas separation: the resistance model approach," *Journal of Membrane Science*, **8**(3), 233 (1981).

5. Clausi, D.T., S.A. McKelvey, and W.J. Koros, "Characterization of substructure resistance in asymmetric gas separation membranes," *Journal of Membrane Science*, **160**(1), 51 (1999).

6. Perry, J., *personal communication*. 2005.

7. Pfromm, P.H. and W.J. Koros, "Accelerated physical aging of thin glassy polymer films: evidence from gas transport measurements," *Polymer*, **36**(12), 2379 (1995).

8. Vrentas, J.S., J.L. Duda, and H.C. Ling, "Antiplasticization and volumetric behavior in glassy polymers," *Macromolecules*, **21**(5), 1470 (1988).

9. Jackson, W.J., Jr. and J.R. Caldwell, "Antiplasticizers for bisphenol polycarbonates," *Advances in Chemistry Series*, **No. 48**, 185 (1965).

10. Maeda, Y. and D.R. Paul, "Effect of antiplasticization on gas sorption and transport. I. Polysulfone," *Journal of Polymer Science, Part B: Polymer Physics*, **25**(5), 957 (1987).

11. Maeda, Y. and D.R. Paul, "Effect of antiplasticization on gas sorption and transport. II. Poly(phenylene oxide)," *Journal of Polymer Science, Part B: Polymer Physics*, **25**(5), 981 (1987).

12. Ruiz-Trevino, F.A. and D.R. Paul, "A quantitative model for the specific volume of polymer-diluent mixtures in the glassy state," *Journal of Polymer Science, Part B: Polymer Physics*, **36**(6), 1037 (1998).

13. Park, J.Y. and D.R. Paul, "Correlation and prediction of gas permeability in glassy polymer membrane materials via modified free volume based group contribution method," *Journal of Membrane Science*, **125**(1), 23 (1997).

14. Bondi, A., *Physical Properties of Molecular Crystals, Liquids, and Glasses*. 1968, New York: Wiley.

15. Maeda, Y. and D.R. Paul, "Effect of antiplasticization on gas sorption and transport. III. Free volume interpretation," *Journal of Polymer Science, Part B: Polymer Physics*, **25**(5), 1005 (1987).

16. Chow, T.S., "Molecular interpretation of glass transition temperature of polymer-diluent systems," *Macromolecules*, **13**(2), 362 (1980).

17. Condo, P.D., et al., "Glass transition behavior including retrograde vitrification of polymers with compressed fluid diluents," *Macromolecules*, **25**(23), 6119 (1992).

18. Couchman, P.R. and F.E. Karasz, "A classical thermodynamic discussion of the effect of composition on glass-transition temperatures," *Macromolecules*, **11**(1), 117 (1978).

19. Brekner, M.J., H.A. Schneider, and H.J. Cantow, "Approach to the composition dependence of the glass transition temperature of compatible polymer blends. 1," *Polymer*, **29**(1), 78 (1988).

20. Maeda, Y. and D.R. Paul, "Effect of antiplasticization on selectivity and productivity of gas separation membranes," *Journal of Membrane Science*, **30**(1), 1 (1987).

21. Gee, R.H. and R.H. Boyd, "Small penetrant diffusion in polybutadiene: a molecular dynamics simulation study," *Polymer*, **36**(7), 1435 (1995).

22. van Krevelen, D.W., *Properties of Polymers*. 3rd ed. 1990, New York: Elsevier.

23. Moore, T., *Effects of Materials, Processing, and Operating Conditions on the Morphology and Gas Transport Properties of Mixed Matrix Membranes*, in *Chemical Engineering*. 2004, The University of Texas: Austin, TX.

24. *http://webbook.nist.gov/chemistry/*. [cited August 30, 2005].

25. Yamamuro, O., et al., "Calorimetric Study of Glassy and Liquid Toluene and Ethylbenzene: Thermodynamic Approach to Spatial Heterogeneity in Glass-Forming Molecular Liquids," *Journal of Physical Chemistry B*, **102**(9), 1605 (1998).

26. Privalko, V.P., "Excess entropies and related quantities in glass-forming liquids," *Journal of Physical Chemistry*, **84**(24), 3307 (1980).

27. Angell, C.A., J.M. Sare, and E.J. Sare, "Glass transition temperatures for simple molecular liquids and their binary solutions," *Journal of Physical Chemistry*, **82**(24), 2622 (1978).

28. Sanchez, I.C. and R.H. Lacombe, "Statistical thermodynamics of polymer solutions," *Macromolecules*, **11**(6), 1145 (1978).

29. Sanchez, I.C. and P.A. Rodgers, "Solubility of gases in polymers," *Pure and Applied Chemistry*, **62**(11), 2107 (1990).

30. Doghieri, F. and G.C. Sarti, "Nonequilibrium Lattice Fluids: A Predictive Model for the Solubility in Glassy Polymers," *Macromolecules*, **29**(24), 7885 (1996).

CHAPTER 8

CONCLUSIONS AND RECOMMENDATIONS

8.1 Summary and Conclusions

The goal of this work, as detailed in Chapter 1, was to better understand the performance of Matrimid® asymmetric hollow fiber membranes operating in the presence of aggressive feed streams. The defect-free Matrimid® asymmetric hollow fiber membranes used in this work represent the current state-of-the-art in the gas separation membrane technology. A proper understanding of how these membranes perform in aggressive feed streams, such as those experienced in natural gas processing, is critical for the future utilization of membranes in even more aggressive conditions.

In Chapter 4, the sorption and permeation of carbon dioxide in Matrimid® asymmetric hollow fiber were studied. Two studies were conducted in an attempt to replicate the previous observations of greatly enhanced and age-dependent sorption of carbon dioxide [1]. Unfortunately, all attempts to replicate the anomalous carbon dioxide sorption were unsuccessful; however, it is believed that a small set of fiber spinning parameters could lead to anomalous sorption and ultimately have a significant impact on membrane performance. Permeation of carbon dioxide thorough Matrimid® asymmetric hollow fiber membranes was shown to be significantly age-dependent. The carbon dioxide permeance prior to plasticization and the carbon dioxide plasticization pressure both substantially decreased with increasing fiber "age". Thermal annealing was capable of reclaiming some of the

permeance lost to physical aging prior to plasticization. Furthermore, thermal annealing was shown to increase the carbon dioxide plasticization pressure in relatively "old" fibers. The complicated effects of thermal annealing on carbon dioxide permeation are likely the result of charge transfer complex formation.

In Chapter 5, the sorption of carbon dioxide, methane, toluene, and n-heptane in non-annealed and annealed Matrimid® asymmetric hollow fiber membranes was investigated. The equilibrium sorption isotherms for all penetrants, in both non-annealed and annealed membranes, were well-described by the dual mode sorption model. Thermal annealing of the fibers resulted in a significant decrease in the equilibrium sorption of all penetrants. Within the framework of the dual mode sorption model [2], the reduction in equilibrium sorption upon thermal annealing was correlated to a reduction of the Langmuir capacity constant, $C_H^{'}$. The Berens-Hopfenberg model [3] was used to analyze the transient sorption isotherms of toluene and n-heptane in Matrimid® asymmetric hollow fiber membranes. The range of transient sorption behaviors observed in this study was exceedingly complex. This complexity results from the interaction of concentration dependent phenomena such as antiplasticization/plasticization and history dependent phenomena such as the formation of charge transfer complexes.

In Chapter 6, the performance of Matrimid® asymmetric hollow fiber membranes during and after exposure to highly-sorbing feed stream contaminants was investigated. During exposure to low to intermediate concentrations of toluene and n-heptane in the feed stream, the carbon dioxide permeance and carbon dioxide/methane selectivity were reduced. The loss in carbon dioxide permeance or

membrane productivity was greater than the loss in carbon dioxide/methane selectivity. In general, annealed membranes experienced greater loss of performance during exposure to highly-sorbing contaminants than non-annealed membranes. After contaminant removal, upon depressurization the carbon dioxide permeance was increased and the carbon dioxide/methane selectivity was decreased in non-annealed membranes. This hysteresis was more apparent after toluene exposure than after exposure to n-heptane. Annealing of the fibers was found to greatly reduce the hysteresis.

In Chapter 7, the performance loss during feed stream contaminant exposure was analyzed. The effect of competitive sorption alone was shown to be too small to account for the loss in membrane performance observed in Chapter 6. A resistance model was used to show that compaction of the fiber substructure did not occur under conditions studied in this work. A free volume model based on the work of Ruiz-Treviño and Paul [4] was applied to account for antiplasticization and plasticization of the membrane during exposure to highly sorbing feed stream contaminants. Applying the model of Ruiz-Treviño and Paul with two adjustable parameters and accounting for the effect of competitive sorption allowed for successful correlation of membrane performance during feed stream contamination.

The following key conclusions can be drawn from this work:

- The carbon dioxide plasticization response of Matrimid® asymmetric hollow fiber membranes is highly age dependent. The carbon dioxide plasticization pressure was shown to substantially decrease with fiber "age". Industrially, this observation limits the shelf-life of thin-skin membranes.
- In general, exposure to highly sorbing feed stream contaminants results in two effects: a loss of membrane performance during contaminant exposure and a hysteresis in membrane performance upon removal of the feed stream contaminant. Obviously, both of these effects impact membrane performance in industrial application. Since the effect of feed stream contamination is often not accounted for during membrane development, membranes may perform much better in the laboratory than in the field. Furthermore, the hysteresis in membrane performance from feed stream upsets, which are common in industrial application, complicates plant control.
- The loss of membrane performance during exposure to highly sorbing feed stream contaminants is the result of the combined effects of competitive sorption and antiplasticization/plasticization. At all concentrations of feed stream contamination, competitive sorption decreases membrane performance. However, the effect of competitive sorption alone is not able to entirely account for the experimentally observed decrease in membrane performance during feed stream contamination. At low concentrations of feed stream contamination, the sorbed contaminant acts as an antiplasticizer, hindering segmental mobility, and thereby decreasing gas permeability. At higher

concentrations of feed stream contamination, the sorbed contaminant acts as a plasticizer, enabling segmental mobility, and thereby rapidly degrading membrane selectivity.

- Macroscopically, sub-T_g annealing of Matrimid® asymmetric hollow fiber membranes decreases sorption capacity, increases carbon dioxide plasticization resistance, and reduces hysteresis in membrane performance after exposure to feed stream contaminants. However, the effect of antiplasticization, which reduces membrane performance during exposure to feed stream contaminants, is increased in sub-T_g annealed membranes.
- Microscopically, sub-T_g annealing of Matrimid® asymmetric hollow fiber membranes reduces the fractional free volume and induces formation of charge transfer complexes. The loss of fractional free volume is correlated by a reduction in equilibrium sorption capacity and a corresponding reduction of the Langmuir capacity constant, C_H', in the dual mode sorption model. Formation of charge transfer complexes increases intra and inter chain interactions, which limits the effects of plasticization and conditioning on membrane performance.
- In this work, a difference between physical aging at ambient temperature and sub-T_g annealing at 220 ^oC was observed. Traditionally, sub-T_g annealing is assumed to only accelerate the rate of physical aging by introducing more segmental mobility to the polymer. However, in this work, it is apparent that the gas transport properties are vastly different between a fiber that was aged at ambient temperature for a long period of time and a fiber that underwent

thermal annealing at 220 ^{o}C. This difference in gas transport properties was rationalized by the formation of charge transfer complexes in the sub-T_g annealed fibers, which are not present in fibers that were simply aged at ambient temperature. It was shown in this work that the formation of charge transfer complexes in sub-T_g annealed fibers have significant and often non-intuitive effects on membrane performance.

8.2 Recommendations

Listed below are several recommendations for future areas of investigation based on the findings presented in this work.

- Fluorescence spectroscopy should be used to correlate the degree of charge transfer complex formation to gas transport properties for various annealing treatments. This work would best be conducted on solvent cast Matrimid® films where the thermal and processing histories are more easily controlled than in the asymmetric hollow fiber morphology.
- The effects of physical aging and sub-T_g annealing on carbon dioxide plasticization in the mixed gas environment should be studied. There is recent evidence which suggests plasticization is suppressed in the mixed gas environment due to competitive sorption [5]. It would be industrially beneficial to know if the age dependency of the carbon dioxide plasticization pressure is also suppressed in the mixed gas case.
- Investigations of membrane performance during exposure to feed stream contamination at higher pressures, higher temperatures, and with more

contaminants should be pursued. These conditions would more closely resemble the actual feed streams experienced during industrial usage.

- The effect of other contaminants besides toluene and n-heptane should be studied. With more experimental data a clearer understanding of the physical significance of the adjustable parameters, α and θ, would be gained. Speculatively, α and θ are both related to the contaminant-polymer interactions. In general, estimating the interaction energy between diluent molecules and polymer segments is extremely difficult for polar components such as those studied in this work. This is a problem that is commonly faced in development of advanced sorption models such as the Sanchez-Lacombe model and the nonequilibrium lattice fluid model. Usually, in these situations a mixing rule based on the pure component interaction energies with a deviation variable is used to calculate the diluent-polymer interaction energy. The value of the deviation variable may be calculated from a single mixture data point. With further experimental measurements, it may be possible to develop mixing rules for the calculation of α and θ based on intrinsic thermodynamic properties of the contaminant and the polymer, such as the difference in solubility factors.
- The evidence of antiplasticization/plasticization from membrane performance shown in this work should be collaborated with mechanical testing data. Antiplasticization results in a decreased T_g and an increased modulus, while plasticization results in a decreased T_g and a decreased modulus [6]. Dynamic mechanical analysis of Matrimid® asymmetric hollow fibers in the presence of

the contaminant vapor would, therefore, confirm the cause of the degraded membrane performance during contaminant exposure as antiplasticization/plasticization. However, it is important to stress the experimental difficulty in obtaining these measurements, since they ideally are made in the presence of the vapor. Furthermore, antiplasticization, as sensed by the gas transport measurements made in this work, occurs in the selective skin of the fiber, while mechanical measurements would be dominated by effects occurring in the fiber substructure. It is not entirely clear that the selective skin and fiber substructure would demonstrate equivalent behaviors.

- Positron annihilation lifetime spectroscopy (PALS) is a technique capable of determining the free volume distribution of glassy polymers. It would be interesting to use PALS to determine the change in the free volume distribution upon thermal annealing and upon exposure to feed stream contaminants. Unfortunately, PALS is not feasible in Matrimid® due to a quenching effect, but PALS may be used in other materials, including non-BTDA containing polyimides.
- The performance of *defect-free* Matrimid® asymmetric hollow fiber membranes in the presence of aggressive feed streams was investigated in this work. Current commercially available asymmetric hollow fiber membranes are intrinsically defective; however, they are post-treated via a "caulking" technique to repair pinhole defects formed in the selective skin. In this case, the performance of commercial fibers in aggressive feed streams is dependent not only on the properties of the polymer used to form the membrane but also

on the properties of the material used to "caulk" the membrane. It would be industrially interesting to study how highly-sorbing feed stream contaminants affect the performance of these repaired membranes compared to their effect on *defect-free* membranes.

8.3 References

1. Madden, W.C., D. Punsalan, and W.J. Koros, "Age dependent CO2 sorption in Matrimid asymmetric hollow fiber membranes," *Polymer*, **46**(15), 5433 (2005).

2. Vieth, W.R., J.M. Howell, and J.H. Hsieh, "Dual sorption theory," *Journal of Membrane Science*, **1**(2), 177 (1976).

3. Berens, A.R. and H.B. Hopfenberg, "Diffusion and relaxation in glassy polymer powders. 2. Separation of diffusion and relaxation parameters," *Polymer*, **19**(5), 489 (1978).

4. Ruiz-Trevino, F.A. and D.R. Paul, "A quantitative model for the specific volume of polymer-diluent mixtures in the glassy state," *Journal of Polymer Science, Part B: Polymer Physics*, **36**(6), 1037 (1998).

5. Visser, T., G.H. Koops, and M. Wessling, "On the subtle balance between competitive sorption and plasticization effects in asymmetric hollow fiber gas separation membranes," *Journal of Membrane Science*, **252**(1-2), 265 (2005).

6. Maeda, Y. and D.R. Paul, "Effect of antiplasticization on gas sorption and transport. III. Free volume interpretation," *Journal of Polymer Science, Part B: Polymer Physics*, **25**(5), 1005 (1987).

APPENDIX A

SPARGER DESIGN AND OPERATION

A.1 Design

A gas sparger system was designed to allow for the mixing of feed streams with higher concentrations of solvents than those available for purchase from AirGas®. A schematic representation of the sparger system is given in Figure A.1. The main components of the sparger system are two mass flow controllers (Brooks Instrument Model 5850E), a 2-micron media grade sintered metal filter (Mott Model 6065020-020), a demister, and a helical element static mixer (Koflo Stratos Series 250). The flow of carrier gas from the cylinder is controlled by the two mass flow controllers. One mass flow controller sends gas through the sintered metal filter which is submerged in solvent. The gas bubbles through the liquid solvent and then passes through a demister. The demister is fabricated from a ½" stainless steel tubing packed with stainless steel wool. The demister removes any entrained solvent droplets from the wet gas stream. After passing through the demister, the wet gas is mixed with dry gas (from the cylinder) by passing both streams through the static mixer. By adjusting the flow rate of the wet gas and dry gas via the mass flow controllers, a feed gas containing a specified activity of solvent may be mixed. Care must be taken when operating at high solvent activities to avoid subsequent condensation in the feed gas supply lines.

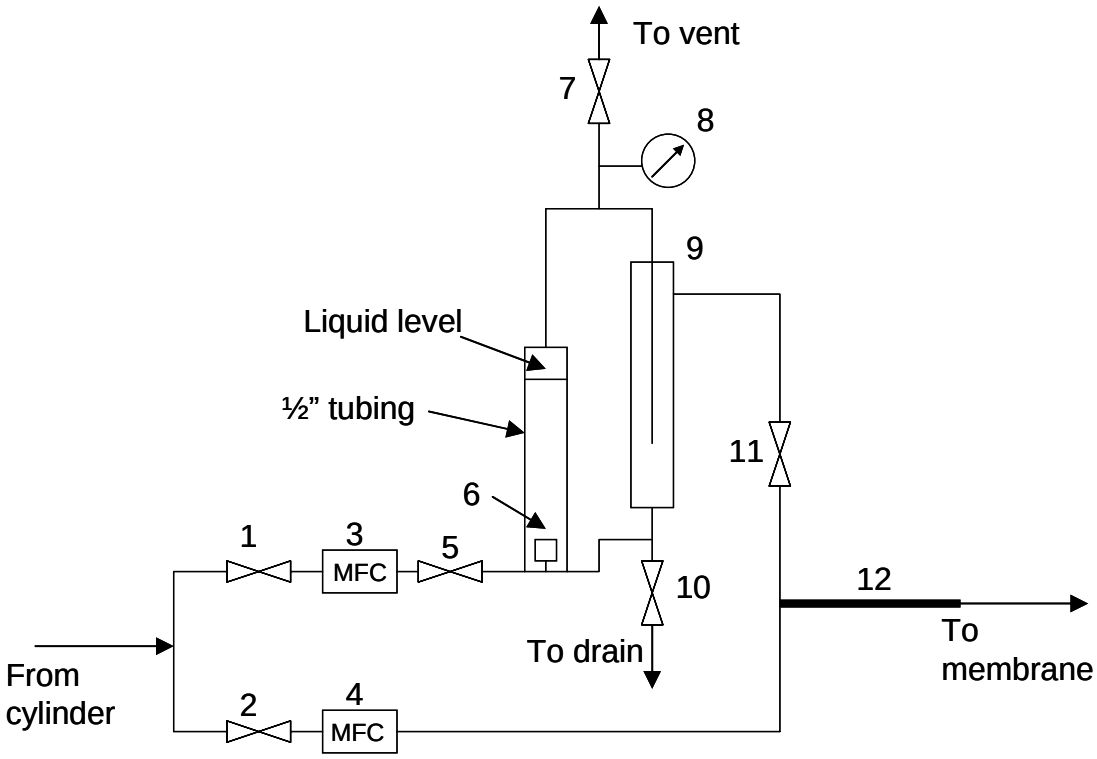

Figure A.1: Schematic of the sparger system. 1. Wet gas supply valve, 2. Dry gas supply valve, 3. Wet gas mass flow controller, 4. Dry gas mass flow controller, 5. Mass flow controller protection valve, 6. Sparger, 7. Vent valve, 8. Wet gas pressure transducer, 9. Demister, 10. Drain valve, 11. Wet gas bypass valve, 12. Static mixer.

A.2 Operation

In all experiments conducted in this work a nominally 10/90% carbon dioxide/ methane mixture from AirGas® is used as a carrier gas. Toluene and n-heptane were used as solvents and were supplied by Aldrich and Arcos, respectively. Solvent is loaded into the sparger by breaking the Swagelok® connection at the top of the ½" stainless steel tubing. Solvent is then squirted directly into the tubing via a Nalgene® squirt bottle. The sparger is filled to the top of the ½" tubing and will hold approximately 100 ml of liquid.

The experiments conducted in this work, pressurize the membrane with dry gas. Once a certain feed pressure is reach, wet gas is mixed into the feed stream. At the start of operation, valves 1 and 2 are open and valve 11 is closed. The dry gas mass flow controller is adjusted to provide the desired feed pressure. The wet gas mass flow controller is set to a low flowrate (~5 sccm) to allow for slow pressurization of the wet gas side of the sparger. After the membrane is pressurized to the desire feed pressure, wet gas may be mixed into the feed by opening valve 11. It is important that before opening valve 11 the pressure in the wet gas side has built up to a level that is close to that of the dry gas side. A large pressure difference between the two sides of the sparger system could potentially allow for carryover of liquid toluene to the membrane when valve 11 is opened. After mixing in wet gas at a low flow rate, the wet gas flow rate can be adjusted upward and the dry gas flow rate reduced via the mass flow controllers to achieve the desired solvent concentration and feed pressure.

After completion of the permeation run, the mass flow controllers can be turned off and the carrier gas cylinder turned off. It is important to shut valve 5 to preclude the possibility of solvent flooding the mass flow controller. The sparger can then be vented by opening valve 7 and drained of any remaining liquid solvent by opening valve 10. After draining, the sparger is cleaned by purging at the maximum flow rate of 200 sccm through each mass flow controller for 24 hours.

The concentration of solvent outputted from the sparger system is determined by sampling with a gas chromatograph (Hewlett-Packard 5890). The gas chromatograph is equipped with a HayeSep® Q packed column and a thermal

conductivity detector. Even at a gas chromatograph oven temperature of 200 ^{o}C the retention time of n-heptane and toluene are extremely long, 25 and 27 minutes, respectively. A capillary column would perform this separation more quickly, however, the HayeSep® Q column is also used for the separation of carbon dioxide and methane in the permeate.

The concentration of solvent detected by the gas chromatograph was calibrated to a single point using mixed gases supplied by AirGas® (Cylinders 2 and 3 in Table 3.2). The sample loop pressure of the gas chromatograph was monitored using a MKS Baratron® 25000 torr transducer. Injections of gas samples from cylinders 2 and 3 were made at various pressures and the response was determined to be linear. The response versus sample loop pressure is shown in Figure A.2 for toluene and in Figure A.3 for n-heptane.

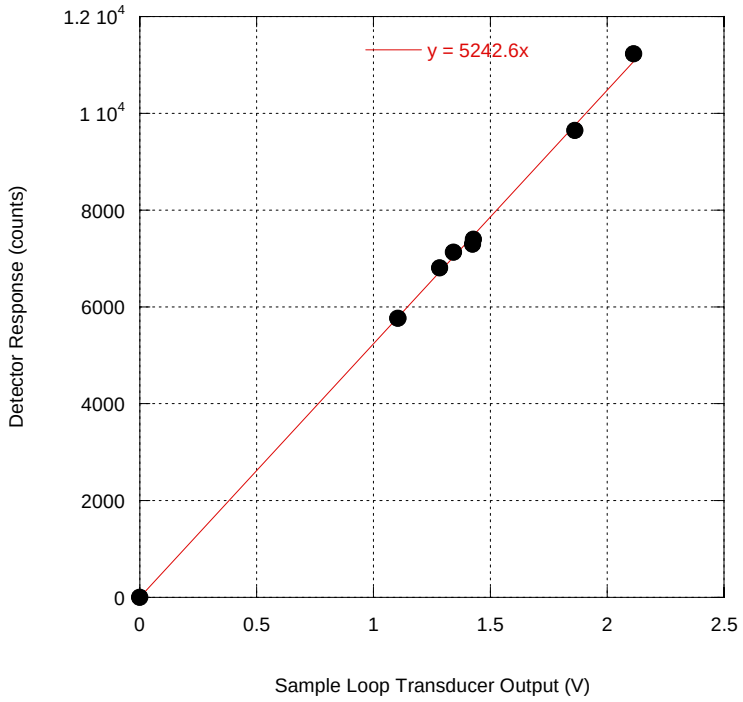

Figure A.2: Gas chromatograph detector response to toluene

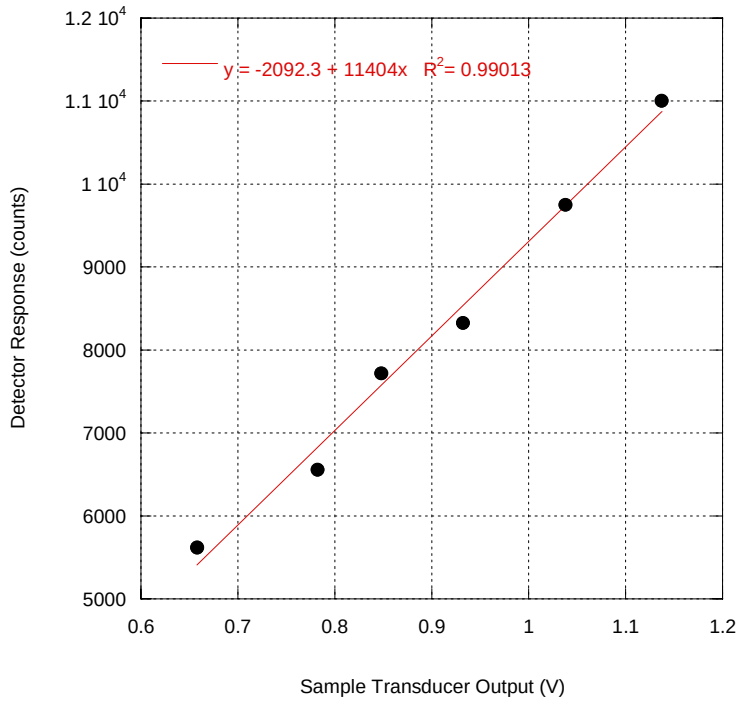

Figure A.3: Gas chromatograph detector response to n-heptane

The concentration of toluene in the sample stream can then be calculated as the following:

$$\text{toluene concentration} = \frac{293}{5242.6} * \frac{\text{Detector Response}}{\text{Sample Loop Pressure}}, \qquad \text{(A.1)}$$

where toluene concentration is given in units of parts-per-million. Similarly, the concentration of n-heptane is given by:

$$\text{n} - \text{heptane concentration} = \frac{505 * \text{Dectector Response}}{11404 * \text{Sample Loop Pressure} - 2092.3}. \qquad \text{(A.2)}$$

APPENDIX B

HOLLOW FIBER MODULE PREPARATION [1, 2]

Hollow fiber modules are required for permeation testing of asymmetric hollow fibers. The module serves as the interface between the permeation system (gas cylinder, tubing, valves, etc.) and the polymeric membrane.

B.1 Module Preparation

This appendix lists off the Parts, Procedure and Notes for constructing a double-ended hollow-fiber module for laboratory-scale experiments. This design has been used in a number of prior studies and is reported in work by Djoekita [3]. The table below lists the main parts needed to make a hollow fiber module.

Table B.1: Parts required for manufacture of double-ended lab-scale permeator

Name	Manufacturer	Notes
Ferrules	Swagelok®	Brass or Stainless Steel
Nut	Swagelok®	Brass or Stainless Steel
Female Adapter	Swagelok®	Brass or Stainless Steel
Male Adapter	Swagelok®	Brass or Stainless Steel
Tee	Swagelok®	Brass or Stainless Steel
Metal Tubing	Swagelok®	Brass or Stainless Steel
Cap	Swagelok®	Brass or Stainless Steel
Plug	Swagelok®	Brass or Stainless Steel
ID Tag		
Tygon Tubing	Fisher Scientific	
"5 Minute" Epoxy	GC Electronics or Devcon	

A 'blank' module is first prepared. Fibers are then put into the module and the ends sealed with Teflon tape and epoxy. Finally, the module is prepared to be put into the permeation testing system.

1. **The "Blank" Module**
    a. Stainless Steel (S.S.) Parts.
        i. Cut an 11.5cm piece of ¼" S.S. tubing.
        ii. Bore out the ends with a ¼" countersink tool used as the bit in a drill press.
        iii. Test the ends for burrs with a Q-tip.
        iv. Add a S.S. nut, ferrule and tee to each end.
    b. Brass Parts
        i. Attach a Brass nut and ferrule to a Brass female ¼" NPT adapter.
        ii. Attach the S.S. tee from step 1a(iv) to the Brass nut on the female adapter.
        iii. Repeat steps (i) and (ii) for the other end of the module. Both ends should be identical.
    c. Attach an ID tag to the S.S. tubing.

2. **Adding the Hollow Fibers.**
    a. Separate out nominally 25 1-meter long hollow fibers from the main hank of fibers. More fibers leads to less variability between modules, but any number can be used.
    b. Recount the fibers.
    c. Tie a 2-ft. long string to the middle of the 25 fibers.

d. Slide the string through the Blank Module, pulling the fibers through as well. (NOTE: Be careful and slow while pulling the fibers through - they break easily.)
e. Cut the string so that only ~3 inches remain.
f. Tape the other, non-tied, end of the fibers together with Scotch tape so that they can easily be threaded through ¼" tubing.
g. Slide the fibers so that equal length sections extend from each end of the module.
h. For particularly fragile fibers, it is often helpful to simply tape the ends together and then use tape to attach the fibers to the string before pulling the fibers through the module. This avoids the need for the fibers to remain intact while bending sharply to fit through the module bore.

3. Sealing the Module.

a. Pack a Teflon® tape "worm" into one of the Female Adapters and around the fibers. Be careful not to crush the fibers, yet still assure a good seal between the fibers and the brass wall of the female adapter. (A "worm" is a 5-cm long roll made up of ~16 layers of Teflon® tape.)
b. Put a 1-cm piece of 3/16" Tygon® Tubing onto a Brass Male ¼" NPT Adapter.
c. Add a 1:1 ratio of the GC electronics epoxy Hardener and Resin into a disposable container. Mix for 30 seconds. (NOTE: Once mixed, the epoxy becomes 'unworkable' after 2 minutes.) (Stycast® brand epoxy may be used as well, see notes.)

d. Pour the epoxy into the Brass Female Adapter, filling it slightly beyond the top.
e. Slide the fibers through the Brass Male Adapter and Tygon tubing piece. Screw the Male Adapter into the Female Adapter until the epoxy fills the Tygon tubing piece.
f. Wait ~10 minutes, then flip the module and repeat steps 3a-e for the other end of the module.

4. Prepare the Module for Permeation Tests

a. Once the epoxy has fully cured (30 minuites after mixing for the GC Electronics '5 minute' epoxy.), break off the Tygon tubing piece by tapping it on the countertop or striking sharply with a hammer. The fibers should be all open, with an encapsulating seal of epoxy around them.
b. Put a Brass nut and ferrule on the Male Adapter on each end of the module.
c. Put a Plug into one end of the module, and a Cap on the nearest Tee fitting, and a Port connecter on the furthest Tee fitting.

The GC Electronics '5 minute' epoxy may be used for general purpose modules. It is easy to use, inexpensive and cures quickly (within 30 minutes). For a more durable seal, Stycast® 2651 from Emerson & Cuming, Billerica, MA may be used. Stycast has excellent adhesion to a wide range of substrates, lower viscosity to fully encapsulate the fibers, high tensile strength (> 6500 psi) after curing for high-pressure applications and a high upper temperature tolerance (130°C). However, Stycast requires 24 hrs to cure at room temperature, is somewhat more difficult to use and mix, and is slightly more expensive.

B.2 References

1. Carruthers, S.B., *Integral Skin Formation in Hollow Fiber Membranes for Gas Separations*, in *Chemical Engineering*. 2001, University of Texas: Austin.

2. Wallace, D.W., *Crosslinked Hollow Fiber Membranes for Natural Gas Purification and Their Manufacture from Novel Polymers*, in *Chemical Engineering*. 2004, The University of Texas: Austin, TX.

3. Djoekita, G., D.Q. Vu, and W.J. Koros, "Pervaporative introduction of organic vapors into high-pressure gas feeds," *Journal of Applied Polymer Science*, **80**(2), 311 (2001).

APPENDIX C

TRANSIENT SORPTION DATA

C.1 Toluene Sorption in Non-Annealed Fibers

Table C.1: Transient sorption of toluene in Matrimid® asymmetric hollow fiber membranes at 35 °C. Activity change of 0.0 to 0.07.

$Time^{1/2}$ ($min^{1/2}$)	M_t/M_f
0.00	0.000
1.00	0.065
1.73	0.082
2.24	0.098
3.46	0.151
4.58	0.206
6.00	0.275
7.81	0.376
9.27	0.442
10.15	0.485
11.22	0.524
12.17	0.561
12.96	0.590
13.93	0.627
14.63	0.653
15.68	0.693
16.73	0.726
17.69	0.760
18.52	0.786
19.31	0.808
20.05	0.828
20.78	0.846
21.56	0.862
22.16	0.872
23.13	0.888
24.39	0.901
37.60	0.992
38.03	0.996
38.39	1.000

Table C.2: Transient sorption of toluene in Matrimid® asymmetric hollow fiber membranes at 35 °C. Activity change of 0.07 to 0.18.

$Time^{1/2}$ ($min^{1/2}$)	M_t/M_f
0.00	0.000
1.00	0.030
1.41	0.044
1.73	0.058
2.00	0.068
2.24	0.076
2.45	0.085
2.65	0.092
2.83	0.099
3.00	0.106
3.16	0.113
4.24	0.154
4.90	0.178
5.29	0.191
5.48	0.198
7.75	0.282
9.06	0.342
10.30	0.387
11.92	0.445
12.81	0.477
14.28	0.525
15.39	0.557
17.26	0.609
18.52	0.640
20.07	0.676
20.45	0.682
20.88	0.693
21.38	0.703
23.26	0.740
23.85	0.748
36.96	0.938
37.78	0.944
39.28	0.959
40.25	0.969
41.13	0.975
43.79	1.000

Table C.3: Transient sorption of toluene in Matrimid® asymmetric hollow fiber membranes at 35 °C. Activity change of 0.18 to 0.28.

$Time^{1/2}$ ($min^{1/2}$)	M_t/M_f
0.00	0.000
1.00	0.034
1.41	0.051
1.73	0.065
2.00	0.075
2.24	0.085
2.45	0.095
2.65	0.103
2.83	0.109
3.00	0.113
3.16	0.120
4.58	0.165
5.74	0.193
6.48	0.209
7.75	0.237
9.49	0.277
11.14	0.319
12.37	0.349
13.19	0.369
14.70	0.406
15.26	0.421
16.34	0.448
16.73	0.459
31.19	0.745
32.16	0.759
33.27	0.774
33.76	0.781
34.21	0.786
36.85	0.816
39.60	0.848
49.07	0.927
55.24	0.967
61.49	1.000

Table C.4: Transient sorption of toluene in Matrimid® asymmetric hollow fiber membranes at 35 °C. Activity change of 0.28 to 0.41.

$Time^{1/2}$ ($min^{1/2}$)	M_t/M_f
0.00	0.000
1.00	0.056
1.41	0.081
1.73	0.101
2.00	0.118
2.24	0.134
2.45	0.148
2.65	0.160
2.83	0.168
3.00	0.178
3.16	0.183
5.48	0.245
7.62	0.279
9.70	0.311
10.82	0.328
13.00	0.365
15.10	0.400
17.00	0.435
18.73	0.465
20.66	0.504
21.33	0.514
24.64	0.573
27.11	0.615
37.52	0.771
40.12	0.806
43.45	0.843
53.22	0.931
58.86	0.965
65.47	1.000

Table C.5: Transient sorption of toluene in Matrimid® asymmetric hollow fiber membranes at 35 °C. Activity change of 0.41 to 0.51.

$Time^{1/2}$ ($min^{1/2}$)	Mt/Mf
0.00	0.000
1.00	0.149
1.41	0.202
1.73	0.227
2.00	0.234
2.24	0.242
2.45	0.244
4.80	0.267
8.43	0.301
15.97	0.379
21.93	0.453
24.86	0.493
37.58	0.661
44.07	0.739
54.53	0.853
57.63	0.878
60.61	0.903
66.90	0.949
75.79	1.000

Table C.6: Transient sorption of toluene in Matrimid® asymmetric hollow fiber membranes at 35 °C. Activity change of 0.51 to 0.61.

$Time^{1/2}$ ($min^{1/2}$)	M_t/M_f
0.00	0.000
1.00	0.253
1.41	0.272
2.00	0.276
4.90	0.299
7.75	0.324
9.38	0.342
12.61	0.369
15.87	0.400
18.71	0.425
20.00	0.440
21.07	0.452
37.76	0.639
40.67	0.664
42.25	0.683
53.88	0.797
58.03	0.828
65.76	0.886
102.03	0.996
108.43	1.000

Table C.7: Transient sorption of toluene in Matrimid® asymmetric hollow fiber membranes at 35 °C. Activity change of 0.61 to 0.67.

$Time^{1/2}$ ($min^{1/2}$)	M_t/M_f
0.00	0.00
1.00	0.54
1.41	0.57
5.00	0.59
7.75	0.64
12.33	0.67
19.10	0.70
35.04	0.83
51.29	0.93
65.48	1.00
75.50	1.00
92.78	1.00

Table C.8: Transient sorption of toluene in Matrimid® asymmetric hollow fiber membranes at 35 °C. Activity change of 0.67 to 0.78.

$Time^{1/2}$ ($min^{1/2}$)	M_t/M_f
0.00	0.00
1.41	0.41
1.73	0.46
4.58	0.48
14.28	0.60
35.61	0.79
52.84	0.90
64.04	0.94
76.75	0.97
85.33	0.99
99.25	1.00

Table C.9: Transient sorption of toluene in Matrimid® asymmetric hollow fiber membranes at 35 °C. Activity change of 0.78 to 0.85.

$Time^{1/2}$ ($min^{1/2}$)	M_t/M_f
0.00	0.000
1.73	0.636
7.94	0.733
13.93	0.802
35.65	0.911
56.13	0.988
66.23	1.000

C.2 Toluene Sorption in Annealed Fibers

Table C.10: Transient sorption of toluene in annealed Matrimid® asymmetric hollow fiber membranes at 35 °C. Activity change of 0.0 to 0.05.

$Time^{1/2}$ ($min^{1/2}$)	M_t/M_f
0.00	0.000
1.41	0.062
1.73	0.099
2.00	0.156
2.24	0.188
2.45	0.218
3.87	0.354
5.39	0.477
7.07	0.600
7.94	0.654
9.17	0.718
10.86	0.796
12.29	0.852
13.15	0.876
35.76	0.990
52.14	1.000

Table C.11: Transient sorption of toluene in annealed Matrimid® asymmetric hollow fiber membranes at 35 °C. Activity change of 0.05 to 0.10.

$Time^{1/2}$ ($min^{1/2}$)	M_t/M_f
0.00	0.000
1.00	0.104
1.41	0.149
1.73	0.187
2.00	0.222
2.24	0.244
4.24	0.364
6.00	0.440
7.28	0.481
8.49	0.516
9.11	0.532
13.30	0.620
38.43	0.877
68.18	0.987
75.99	1.000

Table C.12: Transient sorption of toluene in annealed Matrimid® asymmetric hollow fiber membranes at 35 °C. Activity change of 0.10 to 0.17.

$Time^{1/2}$ ($min^{1/2}$)	M_t/M_f
0.00	0.000
1.00	0.102
1.41	0.142
1.73	0.180
2.00	0.212
2.24	0.228
2.65	0.245
3.16	0.285
4.47	0.344
7.94	0.414
9.80	0.441
11.53	0.470
12.81	0.492
13.64	0.508
14.42	0.519
16.19	0.543
20.05	0.602
35.69	0.785
37.83	0.801
40.47	0.817
52.31	0.895
55.68	0.909
65.77	0.957
100.35	1.000

Table C.13: Transient sorption of toluene in annealed Matrimid® asymmetric hollow fiber membranes at 35 °C. Activity change of 0.17 to 0.24.

$Time^{1/2}$ ($min^{1/2}$)	M_t/M_f
0.00	0.000
1.00	0.120
1.41	0.173
1.73	0.209
2.00	0.244
2.24	0.271
4.24	0.382
6.71	0.440
10.44	0.476
11.83	0.498
15.23	0.511
37.18	0.698
40.09	0.724
52.32	0.800
107.26	1.000

Table C.14: Transient sorption of toluene in annealed Matrimid® asymmetric hollow fiber membranes at 35 °C. Activity change of 0.24 to 0.34.

$Time^{1/2}$ ($min^{1/2}$)	M_t/M_f
0.00	0.000
1.00	0.146
1.41	0.222
1.73	0.262
2.00	0.285
2.24	0.307
2.45	0.320
3.46	0.380
5.39	0.421
6.93	0.446
11.31	0.499
13.49	0.529
15.87	0.559
37.76	0.829
39.95	0.846
52.52	0.947
55.78	0.970
64.98	1.000

Table C.15: Transient sorption of toluene in annealed Matrimid® asymmetric hollow fiber membranes at 35 °C. Activity change of 0.34 to 0.39.

$Time^{1/2}$ ($min^{1/2}$)	M_t/M_f
0.00	0.000
1.41	0.159
1.73	0.192
2.00	0.222
2.24	0.230
3.61	0.259
5.48	0.287
7.14	0.308
10.34	0.339
15.17	0.397
38.99	0.715
54.45	0.864
65.69	0.931
76.55	0.967
93.42	1.000

Table C.16: Transient sorption of toluene in annealed Matrimid® asymmetric hollow fiber membranes at 35 °C. Activity change of 0.39 to 0.53.

$Time^{1/2}$ ($min^{1/2}$)	M_t/M_f
0.00	0.000
1.00	0.450
1.41	0.566
1.73	0.609
3.61	0.638
6.08	0.666
7.81	0.684
10.95	0.716
17.64	0.775
19.10	0.781
37.09	0.916
40.64	0.934
45.49	0.966
53.24	1.000

Table C.17: Transient sorption of toluene in annealed Matrimid® asymmetric hollow fiber membranes at 35 °C. Activity change of 0.53 to 0.70.

$Time^{1/2}$ ($min^{1/2}$)	M_t/M_f
0.00	0.00
1.00	0.01
1.41	0.07
1.73	0.09
2.00	0.10
2.65	0.10
4.80	0.11
6.48	0.14
7.21	0.15
9.00	0.19
9.85	0.20
10.68	0.22
12.41	0.27
13.08	0.28
15.36	0.34
17.32	0.40
18.14	0.43
37.13	0.89
37.97	0.90
40.02	0.91
41.79	0.93
41.95	0.93
51.92	0.95
55.24	0.98
64.94	1.00

Table C.18: Transient sorption of toluene in annealed Matrimid® asymmetric hollow fiber membranes at 35 °C. Activity change of 0.70 to 0.84.

$Time^{1/2}$ ($min^{1/2}$)	M_t/M_f
0.00	0.000
2.24	0.356
5.20	0.375
7.48	0.392
8.77	0.396
9.43	0.401
10.63	0.413
12.25	0.431
14.00	0.448
14.83	0.468
15.17	0.489
16.00	0.501
16.49	0.517
36.03	0.913
37.66	0.923
39.53	0.934
41.39	0.939
52.35	1.000

C.3 n-Heptane Sorption in Non-Annealed Fibers

Table C.19: Transient sorption of n-heptane in Matrimid® asymmetric hollow fiber membranes at 35 °C. Activity change of 0.0 to 0.09.

$Time^{1/2}$ ($min^{1/2}$)	M_t/M_f
0.00	0.000
1.00	0.014
1.41	0.026
1.73	0.034
2.83	0.064
3.87	0.099
5.92	0.181
7.62	0.260
9.11	0.332
10.63	0.406
11.49	0.442
14.18	0.554
16.79	0.652
18.33	0.707
35.83	0.948
39.48	0.958
53.30	1.000

Table C.20: Transient sorption of n-heptane in Matrimid® asymmetric hollow fiber membranes at 35 °C. Activity change of 0.09 to 0.18.

$Time^{1/2}$ ($min^{1/2}$)	M_t/M_f
0.00	0.000
1.00	0.044
1.41	0.081
4.58	0.236
5.92	0.294
7.81	0.371
9.59	0.413
11.09	0.455
13.38	0.486
14.53	0.506
16.58	0.538
35.03	0.761
37.47	0.779
39.10	0.803
53.04	0.919
56.05	0.945
65.41	1.000

Table C.21: Transient sorption of n-heptane in Matrimid® asymmetric hollow fiber membranes at 35 °C. Activity change of 0.18 to 0.29.

$Time^{1/2}$ ($min^{1/2}$)	M_t/M_f
0.00	0.000
1.00	0.061
1.41	0.083
1.73	0.109
2.24	0.131
2.65	0.155
4.80	0.255
5.74	0.282
7.94	0.313
10.58	0.335
13.53	0.362
16.34	0.376
22.02	0.422
36.84	0.568
53.75	0.701
67.56	0.803
78.26	0.893
85.55	0.927
99.23	1.000

Table C.22: Transient sorption of n-heptane in Matrimid® asymmetric hollow fiber membranes at 35 °C. Activity change of 0.29 to 0.39.

$Time^{1/2}$ ($min^{1/2}$)	M_t/M_f
0.00	0.000
1.00	0.110
1.41	0.164
1.73	0.205
3.74	0.374
6.71	0.452
12.33	0.489
17.52	0.511
21.10	0.521
37.63	0.630
55.19	0.758
66.81	0.868
76.24	0.954
80.42	0.973
85.41	1.000

Table C.23: Transient sorption of n-heptane in Matrimid® asymmetric hollow fiber membranes at 35 °C. Activity change of 0.39 to 0.50.

$Time^{1/2}$ ($min^{1/2}$)	M_t/M_f
0.00	0.000
1.00	0.158
1.41	0.227
2.00	0.288
2.45	0.327
4.00	0.442
6.86	0.504
9.54	0.515
17.29	0.538
24.92	0.585
37.74	0.662
54.61	0.765
66.57	0.850
77.09	0.938
85.76	1.000

Table C.24: Transient sorption of n-heptane in Matrimid® asymmetric hollow fiber membranes at 35 °C. Activity change of 0.50 to 0.66.

$Time^{1/2}$ ($min^{1/2}$)	M_t/M_f
0.00	0.000
1.41	0.153
1.73	0.202
2.24	0.310
3.16	0.397
5.39	0.475
9.27	0.495
12.33	0.510
36.36	0.616
39.37	0.635
66.88	0.808
74.42	0.847
85.22	0.919
100.09	1.000

Table C.25: Transient sorption of n-heptane in Matrimid® asymmetric hollow fiber membranes at 35 °C. Activity change of 0.66 to 0.83.

$Time^{1/2}$ ($min^{1/2}$)	M_t/M_f
0.00	0.000
1.41	0.395
2.65	0.579
3.00	0.638
4.24	0.746
5.48	0.806
10.82	0.862
15.56	0.870
37.23	0.907
42.50	0.926
52.53	0.948
57.16	0.963
67.30	0.983
75.29	1.000

C.3 n-Heptane Sorption in Annealed Fibers

Table C.26: Transient sorption of n-heptane in annealed Matrimid® asymmetric hollow fiber membranes at 35 °C. Activity change of 0.0 to 0.10.

$Time^{1/2}$ ($min^{1/2}$)	M_t/M_f
0.00	0.000
1.41	0.078
1.73	0.111
2.24	0.153
3.74	0.324
6.24	0.609
7.42	0.709
7.87	0.741
9.27	0.803
10.95	0.838
12.17	0.854
15.00	0.876
37.70	0.954
40.29	0.959
51.79	0.980
63.97	1.000

Table C.27: Transient sorption of n-heptane in annealed Matrimid® asymmetric hollow fiber membranes at 35 °C. Activity change of 0.10 to 0.21.

$Time^{1/2}$ ($min^{1/2}$)	M_t/M_f
0.00	0.000
1.00	0.231
1.73	0.315
3.61	0.496
7.07	0.562
8.72	0.581
12.37	0.623
15.65	0.654
21.02	0.708
37.05	0.827
41.79	0.869
54.07	0.938
66.17	1.000

Table C.28: Transient sorption of n-heptane in annealed Matrimid® asymmetric hollow fiber membranes at 35 °C. Activity change of 0.21 to 0.30.

$Time^{1/2}$ ($min^{1/2}$)	M_t/M_f
0.00	0.000
1.00	0.218
1.41	0.282
1.73	0.361
2.45	0.421
5.00	0.480
13.49	0.535
20.37	0.589
36.46	0.718
53.91	0.842
65.57	0.911
75.35	0.975
77.89	0.990
83.83	1.000

Table C.29: Transient sorption of n-heptane in annealed Matrimid® asymmetric hollow fiber membranes at 35 °C. Activity change of 0.30 to 0.38.

$Time^{1/2}$ ($min^{1/2}$)	M_t/M_f
0.00	0.000
1.00	0.256
1.41	0.339
1.73	0.405
2.00	0.435
2.83	0.470
4.00	0.500
6.63	0.512
13.86	0.542
18.68	0.571
39.80	0.673
43.70	0.702
53.96	0.768
66.95	0.851
77.99	0.923
87.48	0.976
93.82	1.000

Table C.30: Transient sorption of n-heptane in annealed Matrimid® asymmetric hollow fiber membranes at 35 °C. Activity change of 0.38 to 0.51.

$Time^{1/2}$ ($min^{1/2}$)	M_t/M_f
0.00	0.000
1.00	0.264
1.41	0.359
1.73	0.407
2.00	0.442
2.65	0.485
6.56	0.524
12.73	0.541
36.01	0.623
42.28	0.654
54.86	0.719
65.38	0.779
76.03	0.883
84.22	0.913
93.36	0.961
100.13	1.000

Table C.31: Transient sorption of n-heptane in annealed Matrimid® asymmetric hollow fiber membranes at 35 °C. Activity change of 0.51 to 0.67.

$Time^{1/2}$ ($min^{1/2}$)	M_t/M_f
0.00	0.000
1.00	0.363
1.41	0.470
1.73	0.530
2.00	0.580
4.69	0.634
12.81	0.670
19.13	0.688
35.55	0.738
53.50	0.830
65.31	0.878
69.17	0.902
75.79	0.929
93.19	0.982
100.48	1.000

Table C.32: Transient sorption of n-heptane in annealed Matrimid® asymmetric hollow fiber membranes at 35 °C. Activity change of 0.67 to 0.80.

$Time^{1/2}$ ($min^{1/2}$)	M_t/M_f
0.00	0.000
1.00	0.333
1.41	0.505
1.73	0.614
2.00	0.701
2.24	0.770
2.45	0.815
2.65	0.852
2.83	0.881
37.42	0.905
51.72	0.915
65.48	0.968
77.30	1.000

VITA

William Clark Madden was born on December 11, 1977 to Betty Watters Cater and William Calvin Madden in Anniston, Alabama. He received a Bachelor of Science with Honors in Chemical Engineering from The University of Texas in May 2001. In November 2005, he fulfilled the requirements for a Doctorate of Philosophy in Chemical Engineering from the Georgia Institute of Technology. In February 2006, he joined Solvay Advanced Polymers of Alpharetta, GA as a research engineer.